



TECHNISCHE  
UNIVERSITÄT  
WIEN  
Vienna University of Technology



DIPLOMARBEIT

# An Apparatus for precisely measuring the surface tension of ultra-pure water

zur Erlangung des akademischen Grades

**Diplom-Ingenieur**

im Rahmen des Studiums

**Masterstudium Technische Physik**

eingereicht von

**Alexander Syböck**

Matrikelnummer 01528536

ausgeführt am Institut für Angewandte Physik  
der Fakultät für Physik der Technischen Universität Wien

Betreuung

Betreuer/in: Univ.Prof.in Dipl.-Ing.in.Dr.in techn. Dr.in h.c. Dlrke Diebold

Mitwirkung: Proj.-Ass. Dr.phil. Paul Ryan

Wien, 08.04.2025

\_\_\_\_\_  
(Unterschrift Verfasser/in)

\_\_\_\_\_  
(Unterschrift Betreuer/in)

# Surface Tension of ultra-pure Water in its Pure Vapor

Masterthesis

Alexander Syböck\*  
Matrikelnummer:01528536

September 10, 2024

## 1 Abstract

The thermodynamic properties of water are likely the most studied of any liquid. In particular, this is true for its surface tension, where there exists a number of techniques to measure it under and number of different conditions (different gases, temperatures etc.). But none of these prior measurements were undertaken with truly clean water as they were measured in some kind of gaseous atmosphere and in a majority of the cases, with normal air. This leads to contamination of the water through particles in the air and gases that make up the atmosphere itself. The exact influence of these contaminations on surface tension measurements is still not fully known. For this reason, the goal of this master's thesis was to create a drop of water as clean as possible in its own pure-water vapour and to measure the surface tension of this clean water drop with pendant drop tensiometry. In this way, surface tension measurements can be achieved free of the influence of contaminants and other gas phase species. This goal was achieved in part; the instrument was successfully built and initial surface tension measurements of the first water drops in their pure-vapour were undertaken. This thesis will discuss the instrument design and construction as well as the initial surface tension measurements.

## Contents

<b>1 Abstract</b>	<b>1</b>
<b>2 Introduction</b>	<b>3</b>
<b>3 Theory</b>	<b>7</b>
3.1 Vapour Pressure of Water . . . . .	7
3.2 Surface Tension - Molecular Level . . . . .	7

---

\*e-mail: alexander.syboeck@gmx.at

3.3	Surface Tension - Thermodynamics	9
3.4	Surface Tension - general	12
3.5	Techniques for measuring surface tension	12
3.5.1	Wilhelmy Plate Method	12
3.5.2	Capillary Rise Method	14
3.5.3	Pendant Drop Method	16
3.6	Pendant Drop Tensiometry	16
3.6.1	Theory	16
3.7	fitting	19
3.7.1	Input values and parameters for calculation	19
3.7.2	canny edge detection	20
3.7.3	fitting script	20
<b>4</b>	<b>Experimental Methods</b>	<b>22</b>
4.1	Experimental Parameters to be controlled	22
4.2	The Experimental Chamber Design	22
4.2.1	General Design	22
4.2.2	Cold Finger	26
4.2.3	schematics	31
4.2.4	Materials	35
4.2.5	Cryo-trap	36
4.2.6	Measures against vibrations	41
4.2.7	Environmental Box	42
4.3	The Drop Chamber Assembly	43
4.3.1	Assembly of the Cold finger	43
4.3.2	UHV Part Cleaning procedure	55
4.3.3	Assembly of Chamber	58
4.3.4	Water Cleaning procedure	58
4.4	Execution	59
4.4.1	Getting the Instrument Ready	59
4.4.2	Running an Experiment	59
4.5	Supporting Measurements	60
4.5.1	Diode Calibrations	60
4.6	Optics	65
4.6.1	Telecentric Lensing	65
4.6.2	Experiment to estimate Fresnel Diffraction effects.	66
<b>5</b>	<b>Results and Discussion</b>	<b>71</b>
5.1	Drop creation	71
5.2	Water surface tension in its pure vapour	72
<b>6</b>	<b>Summary and Outlook</b>	<b>84</b>
<b>7</b>	<b>Appendix</b>	<b>87</b>
7.1	Diode Calibration Data	87
7.2	Diode Costume Curve Data	91

7.3 Disolution Measurement . . . . .	95
--------------------------------------	----

## 2 Introduction

The surface tension of water is an important measurement for a variety of processes in nature. For example trees use capillary rise to transport water from their roots up to their leaves [5], surface tension plays a big role in the formation of clouds [7] and raindrops for meteorology. Surface tension even plays a role for the very beginning of life as a recent studies suggests that it is used during the development of embryos to achieve left-right symmetry in zebra-fish [22]. But water's surface tension is also a critical parameter for human developed technologies, from everyday technologies people have at home like inkjet printers where printing quality and speed depend on exact knowledge of, among other things, the surface tension of ink [9] to more "high tech" developments like "lab-on-a-chip" technologies where microfluidics, that are strongly influenced by surface tension, are an important field for transport of fluid [?]Microfluid).

Besides the importance of this property of water, there is still some uncertainty with respect to explanations of certain water-gas interfacial phenomena. This is best seen by observing the great number of water surface tension studies in the literature as shown in figure 2.0.1 [20]. The graph shows a collection of values for the surface tension plotted vs temperature and while each individual study claims rather small errors, the fitted line shows a statistical spread of  $\pm 0.4$  mN/m which corresponds to almost 0.5% at 25 °C. One explanation for this big statistical spread across the studies could be that each of the studies had different environmental conditions e.g. different amounts or kinds of contaminants, different humidities or different gas phase concentrations. Since all of these prior experimental studies featured here were undertaken in air or under some other gas environment, even if one started with clean water, gas phase species will end up contaminating the water

In particular, these contaminant potentially effect water interfacial phenomena such as the Jones-Ray effect [24]. The Jones-Ray effect can be visualized in a plot of a change in surface tension vs salt concentration (figure 2.0.2). It can be observed that while we expect the surface tension of water to increase with an increasing salt concentration (dotted line in figure 2.0.2) in reality we observe that for low concentrations of salt the surface tension first decreases before the increasing effect starts to dominate. While some studies claim this is due to contaminants in the water [24], others claim it is not [17] and to date, no consensus exists for an explanation to the Jones-Ray effect.

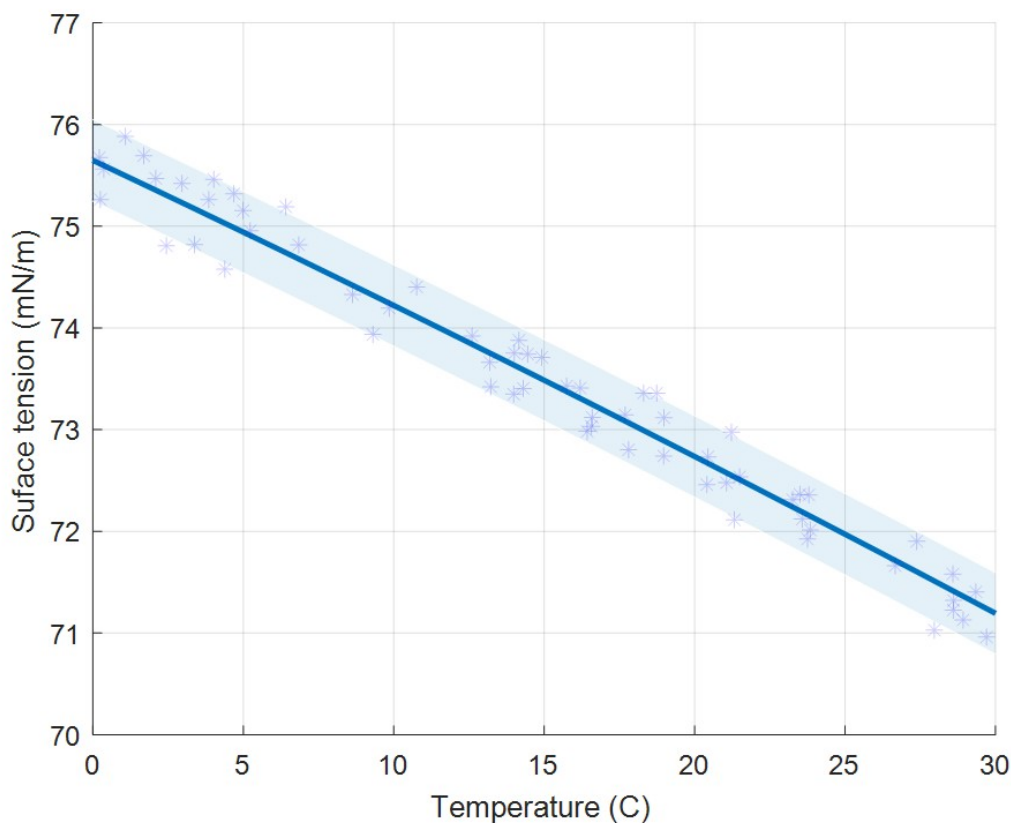


**Figure 2.0.1:** The surface tension of the water-air interface vs temperature. This graph shows a collection of values for the surface tension of water taken from historic literature with each point representing one study. While each study individually claims small errors, taken together there is a large statistical spread. Since all of these studies were done in air, different amounts or kinds of contamination could be one reason for this behavior. [20]

More generally, contaminants are known to affect water-solid interfacial phenomena as well and while such phenomena are not of central importance to this work, they provide a nice example of the effects of contaminants. Figure 2.0.3 shows a graph of the contact angle of water with graphite measured repeatedly over time in air. While graphite has a low contact angle when freshly prepared (time closer to zero) and is thus hydrophilic, it can be seen that the surface becomes more and more hydrophobic the longer the sample is exposed to air. It is argued that this is a clear consequence of contamination and has led to prevalent assumptions that graphite is hydrophobic when in fact the clean surface is not. Such apparent hydrophobicity has also been observed on other surfaces, such as cerium oxide [14]. ????. Is this source correct?

With these motivations in mind, in particular the potential effects of contaminants and other gas phase species on surface tension measurements, the goal of this thesis is to build a machine that is able to measure the surface tension of pure water in its pure vapour, thereby removing the effects of contaminants and other gas phase species from the experiment. To achieve such surface tension measurements, we have built a

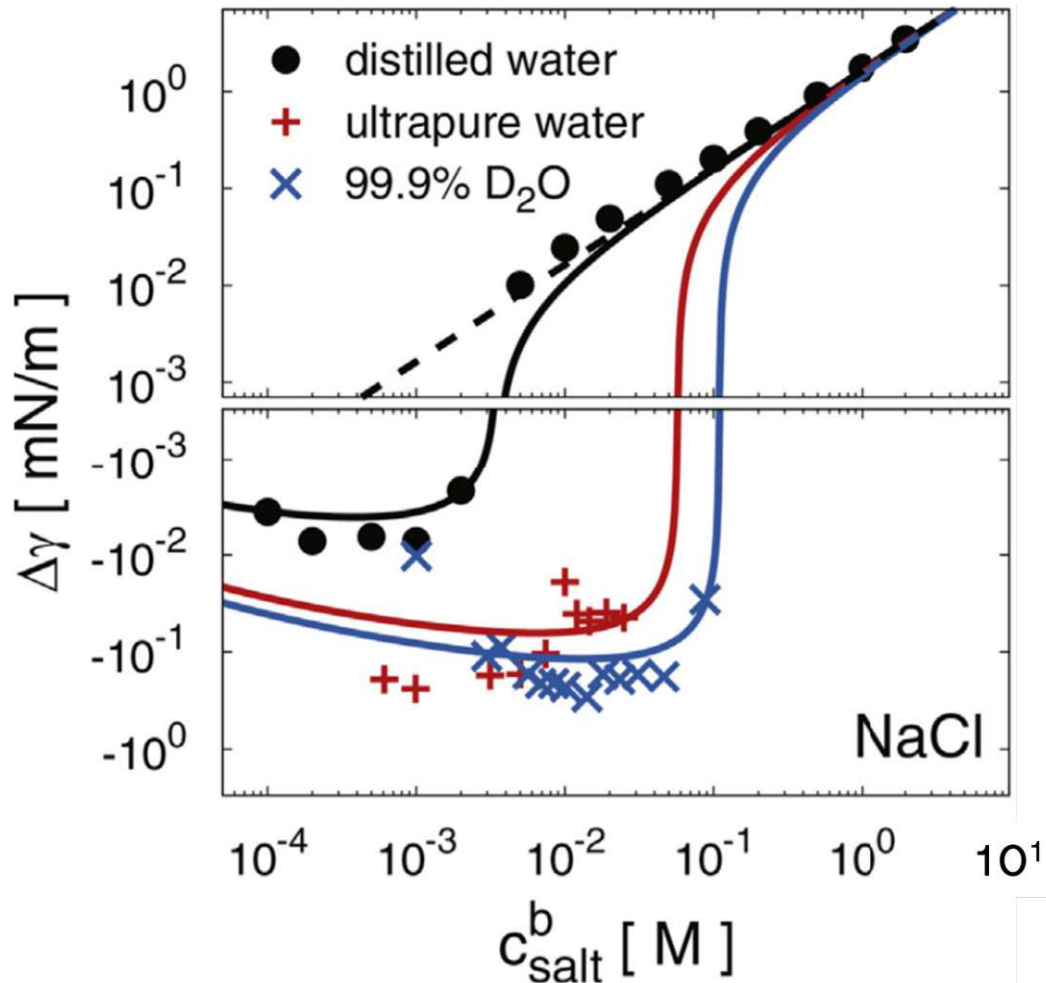


**Figure 2.0.2:** The surface tension of salt solutions vs salt concentration. The dotted line shows the expected linear increase while the fitted lines to the measured data points shows a slight drop in surface tension before the increase starts to dominate. This behavior is called the Jones-Ray effect and it is unknown what causes it. While some studies claim it's due to contaminants others say it is not. [24]

dedicated setup.

For the machine we chose the pendant drop tensiometry method where an image of a pendant drop is used to calculate the surface tension from the drops shape. To control contamination levels this drop will be created inside a ultra high vacuum (UHV) chamber via condensation on a coldfinger tip. The coldfinger design is based on previous machines built in the institute [2].

In the end, the instrument was successfully constructed and initial measurements of pure-water in its pure-vapour were undertaken. The details of the design and construction of the instrument will be outlined in this thesis along with the initial results, their analysis and interpretation. In short, we find that the surface tension of water in its pure-vapour is higher than previous measurements. We can explain this as being due to the absence of contaminants and/ or gas phase species in our pure-water measurements.

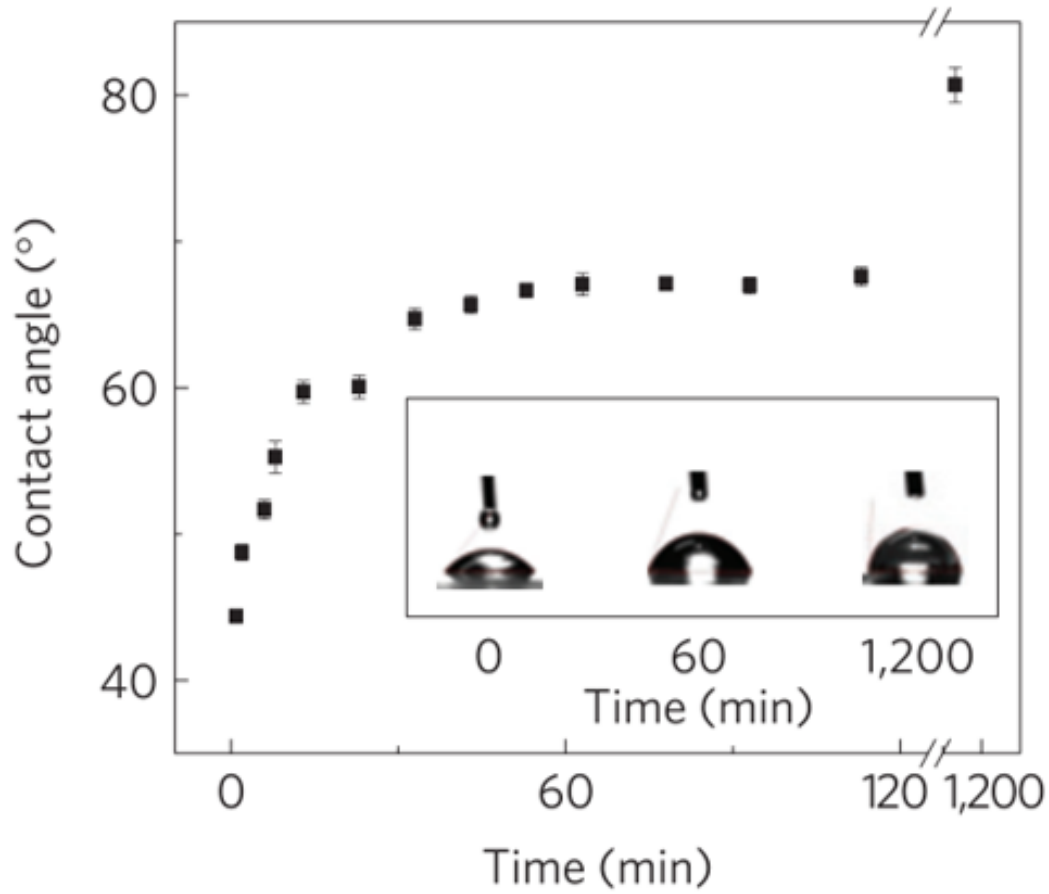


**Figure 2.0.3:** The graph shows the contact angle of water with graphite and how it changes over a time period that the sample spends in air. On a freshly prepared sample the graphite is hydrophilic while turning increasingly hydrophobic the longer the sample is exposed to air. This might be due to contaminants from the air collecting on the surface. [14]

The implications of this result are provided further in the discussion.

## 3 Theory

In this section we will go over the theory for some concepts and techniques used in the experiments. Firstly, we will discuss the thermodynamics utilised to grow the ultra clean water drop. In particular, focusing on a discussion about the vapour pressure of water. This is followed by a discussion of the behavior of fluid surfaces on a thermodynamic and also microscopic level showing how the concept of surface tension fundamentally arises. Moreover, we will have a look at the available techniques for surface tension measurements, ultimately providing the reasons why we choose pendant drop tensiometry as our experimental method.

### 3.1 Vapour Pressure of Water

The vapour pressure of a fluid is a threshold below which all particles have enough kinetic energy to exit the fluids bulk through the surface and go to the vapour phase. This goes on until either all the liquid is evaporated or the pressure in the system gets high enough to increase the rate at which slower particles enter the liquid phase to create an equilibrium with the ones exiting. The exact pressure at which this equilibrium between exiting (evaporating) and entering (condensing) particles is achieved depends on the temperature. The combination of pressure and temperature define the liquid gas phase transition line (vapour pressure line) of fluids.

Our experiments take place on and closely around this transition line. After pumping the chamber to UHV and opening the water reservoir valve the water will evaporate until vapour pressure is reached in the chamber. We can then grow a drop by condensing water at the desired spot from the vapour phase while at the same time evaporating water from liquid to vapour phase in the reservoir to keep the pressure constant. This process is how we transport water from the reservoir to the cold finger Tip until we equilibrate the temperatures to be able to take measurements of the drop in equilibrium state. This is also the reason why temperature control is so important in this experiment. We not only want the ability to find the exact position in the phase diagram we are in but also want to have good control over where water will condense. If for any reason a different spot of the chamber is colder than the Coldfinger tip, water will condense there and growing a drop becomes impossible. To give an idea of the order of magnitude of this pressure our experiments typically take place around room temperature of 20 °C which translates to a vapour pressure of 22.66 mbar.

### 3.2 Surface Tension - Molecular Level

In this section we want to ask the question "what is surface tension?" and to investigate this we first have to think about what a surface is. In our daily use sense, a surface is the border between 2 different phases. In the case of this thesis it will be the border between liquid water and water vapour. The description of the behavior of this border depends on the length scales we talk about. On a molecular level the surface is not a well defined sharp line but rather a steady transition between the bulk of one phase to the bulk of another. The thickness of this transition is of the order of magnitude of roughly 100 nm. In our experiment we use a drop that's 6 mm in diameter and we aim for a resolution

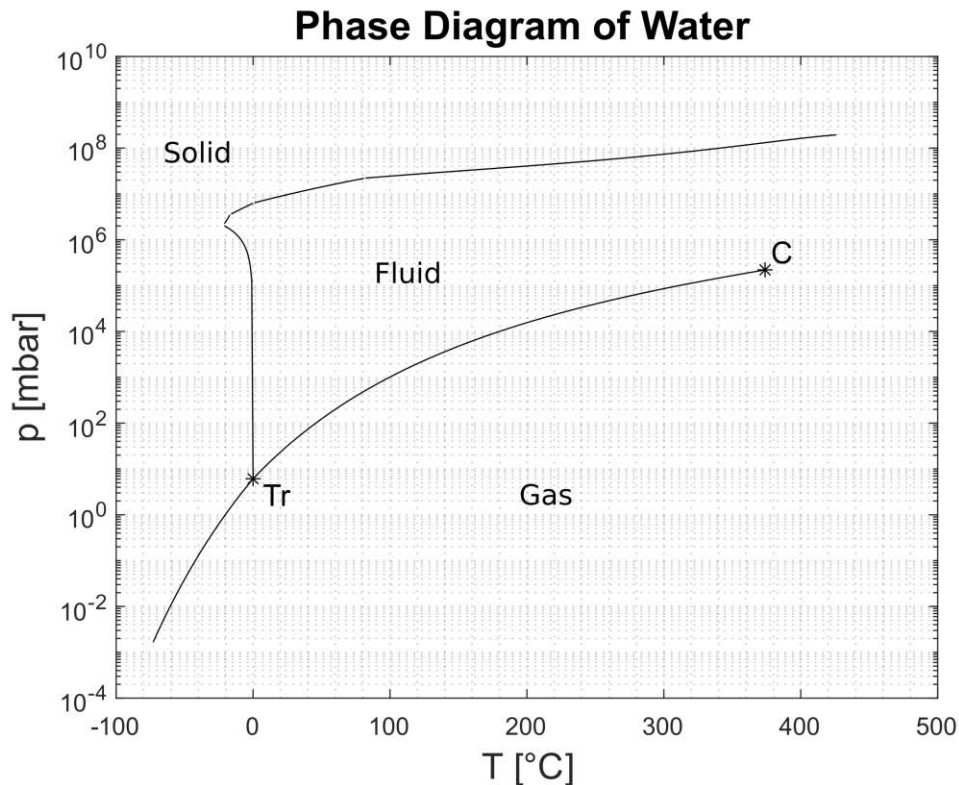


**Figure 3.1.4:** This figure shows the phase diagram of water. Our experiments take place on the transition line between gas and fluid phase in between the triple point marked with "Tr" and the critical point marked with "C".

of the order of  $100 \mu\text{m}$ . This means for our purposes we can assume the surface to be a sharp line that separates the liquid from the vapour phase in our instrument which saves us some complications. However we still take a look at the mechanism that are at play at the length scale of molecules at a surface loosely.

???? source for 100nm

Molecules in the bulk of a liquid have bond partners fully satisfied while molecules on the surface are lacking bond partners on one side. This means in the bulk molecules are more strongly bound than on the surface. To increase the surface area we need to increase the number of molecules at the surface and these molecules will have to come from the bulk. In turn, pulling a molecule from the bulk to the surface will require breaking a few bonding partners in the process. This breaking of bonds needs energy which is the surface energy increase we observe as surface tension. The calculations for this will be shown in the following chapter [3.3](#). On this level we can also argue why contaminants (solutes) like ions or surfactants would increase surface tension. When adding a solute it can distribute in three different ways.

1) Even distribution

A solute evenly distributing in the fluid means its density distribution across the surface is equal to the distribution of the liquid. This means the needed energy to pull a molecule from the bulk to the surface is also equal with or without the solute and so the

surface tension does not change with the added ion.

### 2) Collect at the surface (positive surface excess)

In some cases the density distribution of a solute in our liquid is higher at the surface than in the bulk. This can be the case if you add sodium dodecyl sulfate (SDS) to water, for example. The SDS Structure is made up of a long neutral carbon tail with a sulfate group at one end that is negatively charged. The negatively charged end likes to be bound by water molecules while the carbon tail does not. This causes the SDS molecules to collect on the surface in a way so that the charged end is bound to water molecules "under" the surface while the carbon end sticks out. This is energetically the most favourable for the carbon tail. This produces a surface excess of the SDS at the water-gas interface. This gives water something to bind to at the interface thus reducing the energy cost of getting a water molecule from the bulk to the surface which leads to a reduced surface tension.

### 3) Repelled from the surface(negative surface excess)

Due to the dielectric constant of water when ions are added the image charge to the positive ions (Na) is also positive. This leads to a repelling force for the ions from the surface. More specifically, with it this there are stronger binding energies for the bulk water which leads to an increase in the energy needed to pull a particle from the bulk to the surface. In turn, this causes an increase in surface tension. Another way to look at it would be that on top of the usual energy cost there is an electric potential to overcome thus increasing the total energy cost for a water molecule to go from the bulk to the surface.???? source

In the end, undertaking surface tension measurements in ambient conditions, where organic contaminants and other gases are present, could lead to lower measured surface tension values. The mechanism of such a decreased surface tension would be via "2) Collected at the surface" as described above.

## 3.3 Surface Tension - Thermodynamics

In this section we want to describe the thermodynamic behavior of a surface and for this we do a thought experiment. We imagine a horizontal tube that's filled half with water and half with water vapour. On the right it has an opening with a piston that has two springs attached to it to keep it in position and to fix its inclination and on the left there are two smaller openings with pistons positioned in a way so that both pistons are only in contact with one phase of the water each and with the surface of the water being in contact with a bit of wall in between the pistons. Outside there is no pressure and we will call the liquid water phase  $\alpha$  and the vapour water phase  $\beta$ . To simplify this, we will also ignore any absorption effects on the tube walls.

We can now read the pressure in each of the phases by looking at the force applied to the left pistons and dividing it by the pistons surface area. So  $p_\alpha = \frac{F_\alpha}{A_{Piston\alpha}}$  and  $p_\beta = \frac{F_\beta}{A_{Piston\beta}}$ . On the right side on the other hand the equation does not work like this. Instead we find that the force acting on our Springs is equal to the surface times the pressure of the phase in contact with it added for each phase but minus the contact area

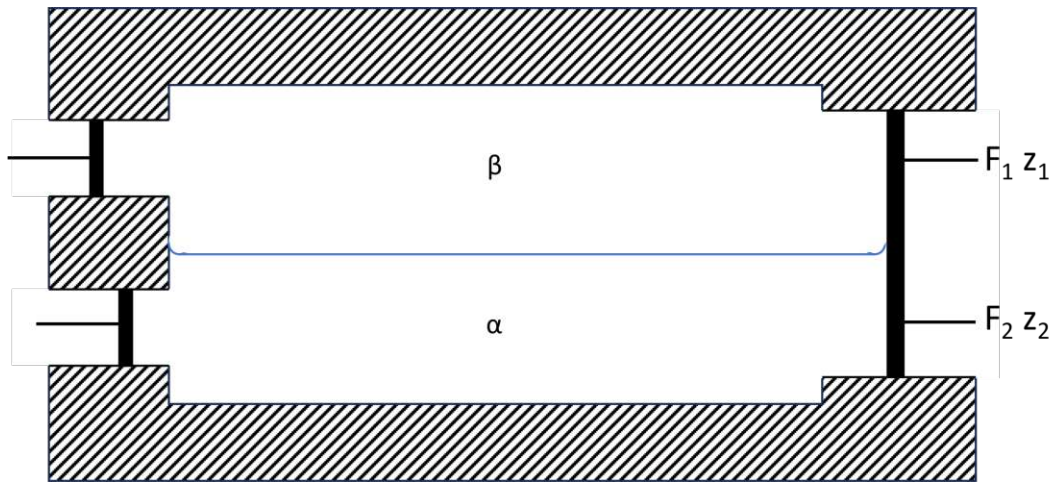
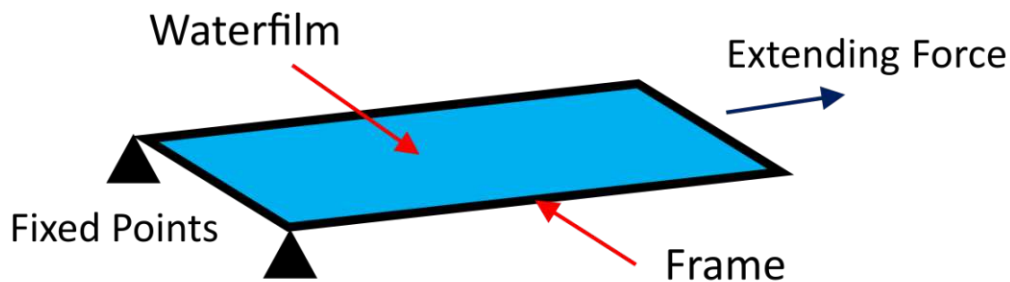


Figure 3.3.5

with the surface in between the phases. This means while the bulk of each of the phases is "pushing" with the pressure we can read from the left pistons the surface in between the phases is not. If we now decide to compress the insides of this tube by pushing the right piston in and keeping the left piston where it is, while also changing the right piston's inclination to keep the contact area with both phases identical, we find that the work done is not just equal to the pressure times the change in volume but instead also has a term that describes the change in surface area of the surface in between the phases.

$$dW = -pdV + \sigma dA$$



**Figure 3.3.6:** Representation of an experiment that shows the concept of surface tension on a mechanical example. A thin water film is spanned in a frame that is extended by a force in one direction which leads to an increase in the water film's surface  $dA$  according to the work  $dW$  put into the system by the extending force. This is a first simple example that showcases that an increase in surface area needs energy and this energy can be seen as a resistance against a surface area increase that can be described as a tension.

With the work due to changing the surface area being proportional to a parameter  $\sigma$  that describes the resistance of the surface against a change in area. This resistance

is what we call surface tension. To define this resistance, we will first look at a simple mechanical example. If we look at a square frame that has a thin water film spanned in it as can be seen in figure 3.3.6 and we apply a force  $F$  parallel to that film's surface we can extend the length  $L$  of the square in one direction and get the mechanical work  $dW = Fdx$  while the surface area grows according to  $dA = 2Ldx$  where the factor two is due to both sides of the film growing. With surface tension being the work necessary to extend the surface we get  $\sigma = \frac{dW}{dA} = \frac{F}{2L}$ . This means the surface tension as the unit of  $\frac{N}{m}$  however due to the low strength of this tension typically  $\frac{mN}{m}$  is used. To investigate where this resistance comes from we need to take a look at the thermodynamics. Let's go back to our thought experiment and the compression we did in it. If the compression is done adiabatic so we assume no heat exchange with the outside the work done on the system equals the increase of the energy in the system.

So

$$dU = dW$$

which means

$$dU = -p(dV)_S + \sigma(dA)_s$$

or

$$p = -\left(\frac{\delta U}{\delta V}\right)_{S,A,n}, \quad \sigma = \left(\frac{\delta U}{\delta A}\right)_{S,V,n} \quad (1)$$

where the constant  $n$  means that the number of components in the system is constant during the compression.  $S$  stands for the entropy and  $A$  and  $V$  are constant parameters representing volume and surface area. It should be mentioned that in this case the temperature in the device would rise which has influence on the absorption of the water on the walls but as said in the beginning we will ignore them.

If we do the compression isothermal on the other hand the work done on the system depends on the change in the Helmholtz free energy.

$$dF = -p(dV)_T + \sigma(dA)_T$$

or

$$p = -\left(\frac{\delta F}{\delta V}\right)_{T,A,n}, \quad \sigma = \left(\frac{\delta F}{\delta A}\right)_{T,V,n} \quad (2)$$

This means the reason for this resistance against area change is a result of the surface energy but it depends on external constraints which energy is manipulated. In practice changes in surface area are usually done in fixed temperature as is our drop, so for our intents it can be said in conclusion that the surface tension is the rate of increase of the Helmholtz free energy with the surface area. [21]

Substance	Temperature[°C]	Surface Tension [mN/m]
Mercury	20	465
Water	20	72.75
Ethanol	20	22.36
Hexane	20	18.22

**Table 1:** Different values for surface Tension. [12] [10] [8] [26]

### 3.4 Surface Tension - general

Now lets look at how strong of a force surface tension actually is by looking at a few typical values.

While surface tension is almost always positive as a negative value would cause spontaneous surface growth there is one case of negative surface tension. When alkali metals get in contact with water its well known that the behavior can be describes as an explosion. Looking at the early stages of this with a high speed camera you can see that the metal is repelled as many thin metal spikes. This happens due to a release of electrons from the metal into the water which causes the leftover positive charges to repel each other. This means in this case the energy of a surface atom is lower than the energy of a bulk atom which pushes the atoms from the bulk to the surface forming surface area maximizing structures. This can be interpreted as the opposite of normal "positive" surface tension behavior and therefore as negative surface tension. [15]

### 3.5 Techniques for measuring surface tension

To measure the surface tension of any substance a large number of methods are available. In this section a few of these methods will be presented. While the most common methods are the wilhelmy plate method and the the capillary rise method, we have chosen to utilize the pendant drop method for our measurements. Arguments for this choice will be provided.

#### 3.5.1 Wilhelmy Plate Method

In this method a thin plate a few cm in size that is attached to a balance is dipped about half in a fluid. The material is chosen so that the fluid wets its surface completely with a contact angle close to 0. In this way, the fluid climbs up the plate and the surface tension force vector acts vertical down into the fluid. By measuring the force required to pull the plate out of the liquid, the liquid surface tension can be measured. The surface tension is calculated using

$$\sigma = \frac{F}{l \cos(\theta)}$$

where  $\sigma$  is the surface tension,  $F$  the force measured,  $\theta$  the contact angle and  $l$  the length of the borderline between wetted and not wetted areas on the plate which equates to 2 times the plates width plus 2 times the plates thickness  $l = 2 * w + 2 * t$ .

Due to the large size of the wetted area, this method can be robust against disturbant factors. But since we want to experiment in a UHV chamber some problems occur.

The plate is usually mounted movable to be able to lower it into the fluid or lift it back out which require custom made movable parts which is more work and harder to keep leak tight and clean than other options that were considered. Another problem is measuring the temperature. Ideally we want to measure the temperature as close to the contact surface as possible but this would be very difficult with this method. A diode could be placed inside the plate but the wiring would be a considerable challenge while manipulating the temperature of the plate would be an even bigger one. Also this method only offers an absolute value of the surface tension under the assumption of a 0 degree contact angle between the fluid and the plate. This 0 degree contact angle is very hard to achieve and later verify during the experiment. Lastly another big problem of this method is contamination control even aside from the movable parts. A big water body is required for this method to work and keeping contamination levels low gets more and more difficult the bigger the amount of water gets one has to handle. Also the plate is in contact with the water and even for materials with high resistance against corrosion some particles will enter the water from the material it is in contact with which means we have a contamination source directly at the site we take data from. [13]

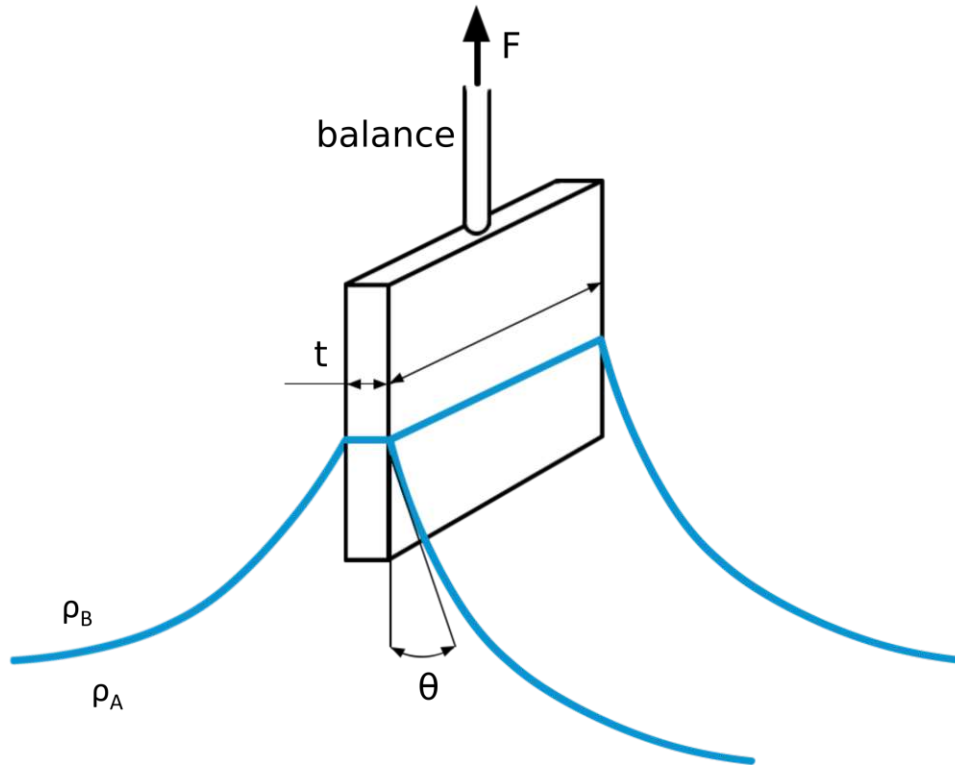


**Figure 3.5.7:** Schematic of the wilhelmy plate method. The plate is dipped into a fluid and then lifted a bit so that the fluid climbs up the sides. The plate material has to be chosen for the fluid to wet its surface for this to work. The force applied onto the plate into the bulk of the fluid is then measure by a balance and acts as measure for the surface tension. An absolute value can only be achieved under the assumption of a 0 degree contact angle which is hard to achieve experimentally. Also building a device in a UHV setting has many challenges that can be avoided with other methods. [13]

### 3.5.2 Capillary Rise Method

If one sticks a capillary of diameter  $r$  into a bulk of a fluid, the fluid will rise above the reservoirs zero level inside the capillary. This happens due to a balance of cohesive forces like surface tension and adhesive forces in between the fluid and the capillaries walls. The height  $h$  of this rise is therefore dependant on the surface tension  $\sigma$ , the contact angle between the fluid and the wall  $\theta$ , the density of the fluid  $\rho$ , the radius of the capillary  $r$  and the applied force fields constant which in most cases will be the gravitational field constant  $g$ . The formula to it can be defined as

$$h = 2 \sigma \frac{\cos(\theta)}{\rho g r}$$

This means if we measure the height and know the contact angle for the chosen fluid and capillary material we can calculate the surface tension using

$$\sigma = \frac{h \rho g r}{2 \cos(\theta)}$$

This method requires no movable parts but offers very low flexibility. In a UHV chamber setting we would be limited to a single diameter size or would need to design the machine in a way to be able to exchange them. This would not be possible without venting the chamber followed by a new bake out for each exchange. Also precise temperature measurements and control would be difficult to achieve. Infrastructure for this could be placed around the capillary but this would make the exchange of capillaries much more difficult and while reading the height precisely is already difficult optically it would become even worse with temperature control infrastructure around the capillary. Additionally this method also needs data on the contact angle between the fluid and the capillaries material which is difficult to measure in the experiment itself. One could measure it beforehand but then would have to trust it is also true for the experiment which is a source of error. Even more problematic is the fact, for very accurate measurements, the meniscus shape and the volume of water in the meniscus need to be modelled. These are tricky to determine and, ultimately, many studies utilising this technique rely on correction factors rendering the measurements non-absolute. Lastly another downside of this method is the high contact area compared to the volume of water. Even the most corrosion resistant materials release some amount of particles into the water when in contact for extended periods of time so we want to minimize contact of the water to any materials as much as possible. This method does not fit that demand. [6]

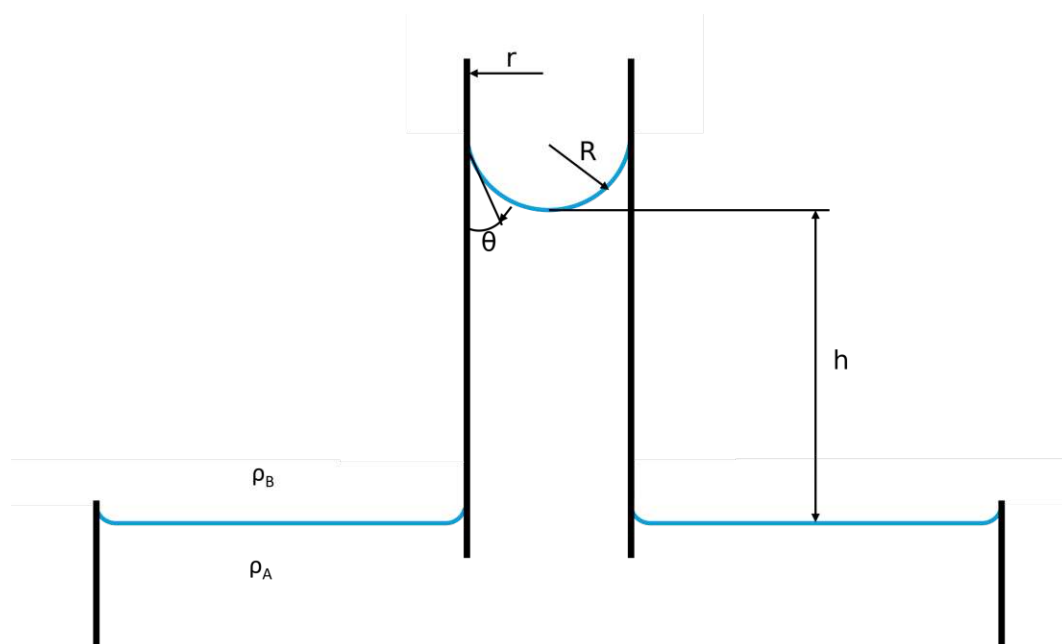


**Figure 3.5.8:** A schematic of the capillary rise method. The height of the rise is used as a measure for surface tension. The main problem with this method is the low flexibility in combination with high difficulties to achieve precise results. In a UHV chamber exchanging the capillary for a different size would mean venting the chamber or having multiple set build at the same time which also multiplies the needed infrastructure for temperature control and measuring.

### 3.5.3 Pendant Drop Method

The pendant drop method is described in detail in the following sections. It was chosen since it is the best suited for use in a UHV chamber and there is previous experience with cold fingers and water drops in UHV available in the institute. It requires no movable parts neither to grow the drop nor to undertake the measurements and offers the possibility to get an absolute value for surface tension. It is also the most compact method with the best options for temperature control. The drop hangs from a tip that can have diodes and infrastructure for controlling the temperature inside without having to deal with wiring or moving parts inside the experimental chamber. Additionally this method has most utility for further experimentation. A sample holder can easily be added below the cold finger tip to be able to do contact angle measurements in this clean environment for example.

## 3.6 Pendant Drop Tensiometry

### 3.6.1 Theory

Pendant drop tensiometry is a method to calculate the surface tension of a liquid drop from its measured curvature in equilibrium state together with the current pressure and the gravitational acceleration.

The necessary calculation stems from the young Laplace equation which describes the

difference between the pressure inside and outside a boundary surface which in our case is the drops surface and can be defined as

$$\gamma\left(\frac{1}{R_1} + \frac{1}{R_2}\right) = \Delta P_0 = P_{in} - P_{out} \quad (3)$$

where

$R_1, R_2$  are the principle radii of curvature

$\Delta P$  is the Laplace pressure across the interface

$P_{in}$  is the pressure inside the drop

$P_{out}$  is the pressure outside

It is true for a perfect spherical drop which would translate to infinite surface tension. In reality however gravity alters the shape of the drop from a sphere to more of a "pear" shape. Under the conditions of gravity, we alter equation 3 to get the pressure of a singular point in the apex of the drop as part of a theoretical spherical drop and equate that to the hydrostatic pressure due to gravity. The altered equation is

$$\gamma\left(\frac{1}{R_1} + \frac{1}{R_2}\right) = \Delta P = \Delta P_0 \pm \Delta \rho g z \quad (4)$$

where  $\Delta P_0$  is a calculable reference change in pressure at any point on the surface. The choice of the reference point defines the sign in the equation. The second term  $\Delta \rho g z$  describes the hydrostatic pressure due to gravity. The density is described as  $\Delta \rho$  since the medium outside the drop counteracts the gravitational pull with buoyancy forces. This term is made of the hydrostatic pressure  $\rho g h$  where  $h$  is the height of the water pillar above the point we look at and the buoyancy of the drop in the vapour around it which is equal to  $\rho V_{apour} g V$ . Due to cylindrical symmetry, this can be simplified to a 1 dimensional  $\rho V_{apour} g h$  where again  $h$  is the height of the drop. Additionally since we describe the pressure relative to a reference point we can replace the height by a distance to this reference point so we replace the  $h$  with a  $z$  which gives us the term  $\rho g z - \rho V_{apour} g z = \Delta \rho g z$ .

Equation 4 is true for the whole drop and in theory, any reference point can be selected for  $\Delta P_0$ . However, it is generally decided to use the apex as a reference point. By using a small number of data points at the bottom of the drop we can fit a theoretical spherical drop to the apex curvature in which the two principal radii end up equal to each other. In this case we replace  $\pm$  in equation 4 with a - since going up from the apex, the hydrostatic pressure decreases and therefore the pressure has to shrink compared to the reference point at the bottom. The resulting equation can only be solved numerically for finite surface tension values.

To get the surface tension we look at a parameterised version of this equation in the form of a set of differential equations in terms of the arc length of the drops curvature.

$$\frac{d\varphi}{ds} = 2 - \text{Bo} \bar{z} - \frac{\sin(\varphi)}{\bar{r}}$$

$$\frac{d\bar{r}}{ds} = \cos(\varphi)$$

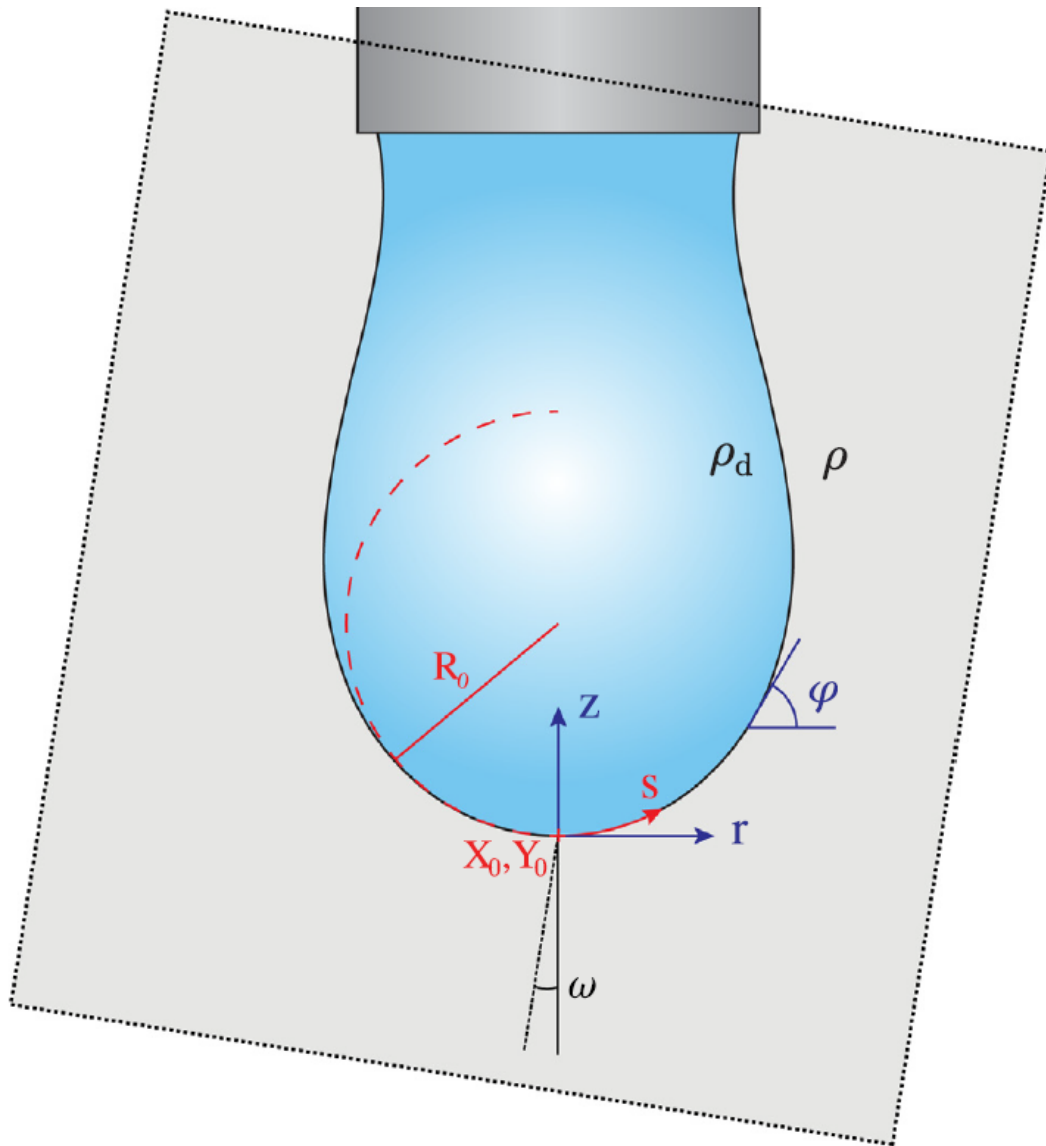


**Figure 3.6.9:** Pendant drop with its coordinates and relevant entities.  $R_0$  is the radius of a theoretical spherical drop that has the drops apex curvature. Since we assume cylindrical symmetry our coordinate system can be simplified to a 2D one with  $z$  being the vertical and  $r$  the horizontal coordinate.  $s$  being the arc length and  $\varphi$  describes the drops curvature via an angle between the horizontal  $r$  coordinate and a tangent to the drops surface in that point.  $\rho_d$  is the density inside the drop while  $\rho$  describes the density of the atmosphere around it.

$$\frac{dz}{ds} = \sin(\varphi)$$

where

$\varphi$  is the angle between the horizontal  $\bar{r}$  base vector and a tangent to the drops curvature

$\bar{z}$  is your vertical distance to the apex scaled by the radius of the theoretical sphere ( $R_0$ ) inside the drop to a dimensionless entity

$\bar{r}$  is the radius at the current  $\bar{z}$  value and also scaled by ( $R_0$ ) to a dimensionless value

$\bar{s}$  is the arc length which is also scaled to ( $R_0$ ) to be a dimensionless entity

and  $Bo$  is a dimensionless parameter that describes the drops shape that is described with

$$Bo = \frac{\Delta\rho g R_0^2}{\gamma}$$

The boundary conditions come from the apex as a reference point and equate to  $r = 0, z = 0, \varphi = 0, s = 0$ .

$Bo$  is central to the pendant drop tensiometry method. Determining  $Bo$  from a drop shape, and measuring or calculating the other parameters, allows us to directly retrieve the surface tension of the imaged interface. In this equation for  $Bo$  we can also see why a precise value for the gravitational acceleration is so important. Without any force field altering the shape of the drop we would have to set  $g$  to zero in the above equation. This results in the bond number equating to zero which describes a perfectly spherical drop with infinite surface tension. For the differential equation, a bond number of zero would mean we lose any dependency on  $\bar{z}$  which leads to a constant  $\bar{r}$ ,  $\bar{s}$  and  $\varphi$  which also describes a spherical drop with no possibility to calculate a finite surface tension value from.

[3](#) [1](#)

### 3.7 fitting

In this section we describe the script that turns an image of a drop into a surface tension value. We discuss the inputs the script needs and how we acquire it followed by an explanation of our edge detection method. Lastly we will discuss how the script itself is structured and which steps are taken in which order.

#### 3.7.1 Input values and parameters for calculation

The exact value of the gravitational acceleration varies around the globe based on a few different factors. The main factors are position on the globe, height, density of the ground below and density above. There are maps available that include alot of this data but in the end we opted for a colaboration with the austrian "Bundesamt für Eich- und Vermessungswesen". They used a CG-5 autogravometer to take some relative measurements in our laboratory and an official reference point nearby that in combination with the absolute measurement they have from their building gave us a value for the gravitaional acceleration of  $g = 9.80841169 \frac{m}{s^2}$ .

The pressure and density values are in part measured and in part calculated. The experimental chamber has an absolute pressure gauge that tells us the pressure in the chamber. This is not only used as our pressure value but from it we can also calculate the vapour density using the ideal gas equation  $\rho = \frac{p}{R \cdot T}$  where  $p$  is the pressure in the experimental chamber,  $R$  the general gas constant of water and  $T$  the temperature we measure on the chamber. For the drop we calculate the density from the temperature we

measure in the cold finger tip. Additionally we use the vapour pressure in the chamber to calculate the temperature as a check.

### 3.7.2 canny edge detection

In our fitting process an important step is to find the drop's edge in the picture. For this we use a canny edge detection algorithm that can be simplified to 3 steps.

1. Smoothing the picture. Noise is a problem for most edge detection algorithms as it can cause random edges to be found. To reduce the influence of noise, the Canny edge detection algorithm first applies a Gaussian smoothing kernel to the image.
2. Finding intensity gradients in the picture. Strong changes in neighboring pixels intensity are good potential places for edges. Finding these points in the image is achieved by applying a Laplacian kernel to the image.
3. Suppress non-maximal values. To create thinner edges positions that are not the maximum in their local environment are thrown away.
4. Finally, to find subpixel locations, local splines are fitted to three points at a time. Due to the large number of data points and the subsequent low curvature of the drop shape, such a procedure is valid.

### 3.7.3 fitting script

The goal of the fitting procedure is to extract a drop profile from an image followed by fitting the Young-Laplace equation to this drop profile. Subsequently, the Bond number and drop apex radius can be fitted and finally the surface tension value calculated using the methods described in section [3.6](#). To achieve this, the fitting script executes the following steps. More detailed explanations to each are found in sections [3.6](#), [3.7.1](#), [3.7.2](#) and below this list.

1. Rotate the Image

Using the tips sides for reference we make sure the real apex of the physical drop is also the lowest point in the picture.

2. Edge Detection

We find the edge of the drop in the picture using canny edge detection with sub pixel interpolation

3. Transform Data

In our pictures the origin is on the top left. Switching the picture to data in Matlab it is interpreted with the origin on the bottom left. So the data view of our drop is a mirrored image of the picture view. To fix this we first minus the maximum y value from all y values. This moves the apex on the horizontal origin line. Then we switch the sign of all y values which flips the drop back to the upright orientation.

4. Fit the Circle

Next we fit a circle using the bottom  $\frac{1}{60}$  of the drops data points which gives us the drops initial radius guess and the x position of the apex.

5. Transform Data

Again we move the apex by subtraction its x position from all x values. After this step we have an upright oriented drop with its apex in the 0,0 coordinate.

6. Remove repeat Values

Some of the data points are available twice. To streamline the fitting process we remove

such values

#### 7. Transform half of the Data.

Since the drops necks as a slight s shape we may have x values that appear twice. each time with differing y values. Since this might cause problems in the fitting process we decided to use y as the independent variable. To avoid y values showing up twice due to the drops symmetry we transform half of the drop down. So each y value that corresponds to a negative x value is flipped to a negative as well.

#### 8. Fitting and confidence intervals

The fitting can also be spread in a few steps

8.1. Find the arch length of the drop. This means the full length from the bottom left to the top right.

8.2. Initial Guess for the drop shape.

As initial parameters we use the Radius we got from the circle fitting and a surface tension of  $73 \frac{N}{m}$ . This will have to be changed for measurements at different temperatures but is for now in use. Also the values for pressure, density and gravity from section 3.6 are input here. To solve the necessary equations the "ode15s" function of Matlab is used.

8.3. Scale

The previous step outputs a Drop shape in the form of a dimensionless Bond number. So to be able to compare it to our picture we scale it to the Drop Radius from the circle fitting. SO now we have the drops data from the canny edge detection and fit data available to us. We just are missing a way to compare them properly.

8.4. Remove repeating values

8.5. Interpolation.

To be able to compare the actual data to the fit we already prepare the data in a way to be able to us y values as our independent variable. So we take the actual drops y values and interpolate x values of the fitted drop ti them. Doing this we end up with 2 Drops. One were we have real y-values vs real x-values and one were we have real y-values vs fitted x-values. This fitted drop gives us a new Bond number that is used in the next step.

8.6. Residual

Buy subtracting the 2 drops from each other we get the Residual. Its a dataset that describes how much they differ from each other. The smaller it is the closer our fit is to the real image. To reduce it we use the Matlab algorithm "levenberg-Marquardt" that alters the parameters of the fitting to get a as small as possible Residual. This is repeated 2 times.

8.7. Confidence and prediction intervals

The confidence interval tells us how likely it is that our fitting coefficients lie within the prediction bounds we defined. So assuming our fitting coefficients accuracy is normal distributed we can define an upper and a lower bound for them as our prediction interval on the normal distribution. A confidence of 95 % would then mean we are 95 % certain that our coefficients are within that interval.

????discuss details with paul again 8.2 to 8.3 do we use a bnd number as input or just a surface tension? does the radius get into it in 8.2? of no how does the calculation work? why 2 fits?

## 4 Experimental Methods

In this section we will discuss how the pure water drop will be created. More specifically, for both accurate surface tension measurements with pendant drop tensiometry and successful creation of a hanging pendant drop, a number of parameters require precise control. Which parameters these are will firstly be discussed. Following this, the general and specific design of the instrument (names the “Drop Chamber”) is outlined, with discussions on how the instrument was designed around the control of these specific parameters. Finally, a section is provided for how the instrument was built together with a section that describes how an experiment is executed on the machine.

### 4.1 Experimental Parameters to be controlled

The primary goal of this work is to undertake extremely clean surface tension measurements of water. This requires having very good control of the environmental composition of both the liquid and gas phase water. To achieve this, all of our surface tensions measurements will be undertaken in a dedicated ultra-high vacuum (UHV) chamber: the Drop Chamber. Using UHV standard cleaning procedures, such as 150 degree C bake-outs, pressures as low as  $10^{-10}$  mbar can be reached ensuring no organic contaminants and only trace amounts of water and H<sub>2</sub> are present in the system [28].

For any surface tension measurements, accurate control of the temperature is required. Not only does the surface tension strongly depend on temperature ( $0.15 \frac{mN}{m} K$ ) [20] but our drop creation method requires precise control of the liquid drop temperature as it forms. More specifically, the drop creation is via condensation onto a metal tip from a pure-water vapour phase and so this requires holding the temperature of this metal tip lower than a liquid water reservoir. Additionally, for the surface tension measurement using pendant drop tensiometry, we need to measure the pressure in the chamber to know the density difference between the liquid and gas phases accurately (LINK TO EQUATION). Therefore, we not only need a system that can reach UHV as a cleaning step but also for the ability to measure the pressure accurately. The pressure measurement also allows us to be confident that the vapour phase is a pure-water vapour phase when its pressure corresponds to that of pure-water. Finally, for pendant drop tensiometry measurements, an image of the drop must be taken and the distances within this image must be known to micron precision. Thus great care must be taken with the optical setup of the instrument. Cleanliness, temperature, pressure and the instrument optics are the main guiding parameters to be controlled in the instrument design. The following sections will outline the specific design features of the instrument and included discussions on how these parameters are controlled in each case.

### 4.2 The Experimental Chamber Design

#### 4.2.1 General Design

With all the above considerations combined the pendant drop method was chosen as the best option for our surface tension measurements. To prevent contamination, the water drop would be created inside a UHV chamber termed the experimental chamber. The chamber would be cleaned, baked and pumped to UHV removing all trace organic

contaminants form the system. The general procedure of drop creation is shown in figure 4.2.11. The extremely clean UHV chamber is exposed to a pure-water vapour from a pure-water reservoir (figure 4.2.11b). A metal “cold finger” inside the chamber is cooled causing water to condense onto the tip of the cold finger (figure 4.2.11c) until a large hanging pendant drop is formed (figure 4.2.11d). Once the maximum drop size is reached, the cold finger temperature is brought into equilibrium with pure-water reservoir temperature causing the drop to stabilize in size and shape.

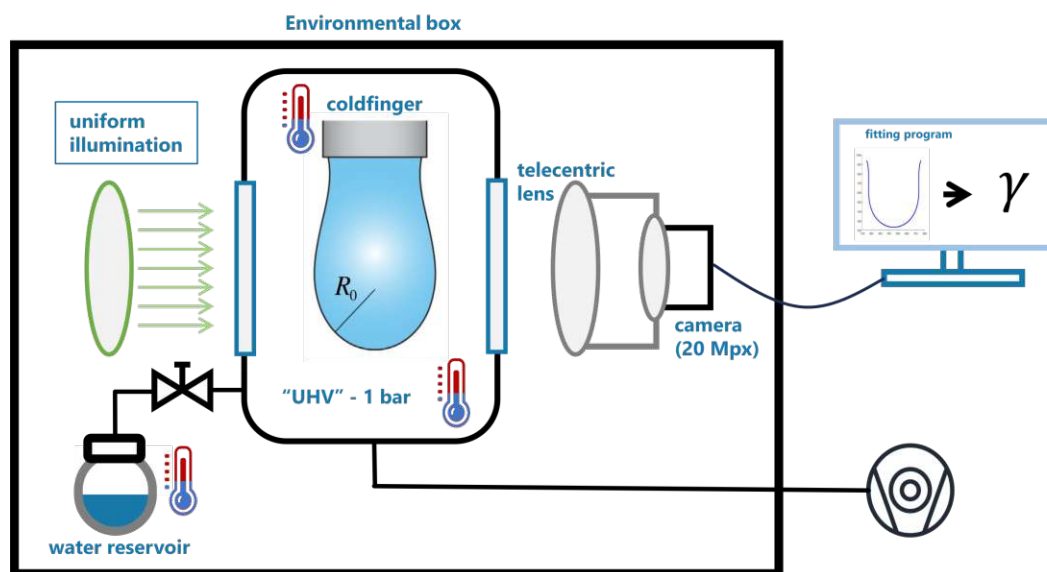


**Figure 4.2.10:** Schematic representation of the design principle. Water is evaporated into a UHV chamber. Precise control over the temperature of the water reservoir and the cold finger allow a drop to grow. At its maximum possible volume the system is equilibrated and a picture of the drop is taken. The surface tension can then be calculated with a fit to the drops shape and radius, the pressure in the chamber and the gravitational acceleration.

The temperature of the system is controlled at multiple important points in the system. The drops temperature is controlled via the mentioned cold finger on which it grows. The cold finger has hollow insides to make place for 2 heating elements and a capillary that supplies liquid nitrogen. With this combination of cooling and counter heating we can control the temperature of the tip and therefore of the drop very precisely. Second for the reservoir we have a shroud that has channels through which a heat exchanger can pump oil to control the reservoir temperature. This good control over the temperature of the cold finger tip and the reservoir fuel the condensation process that we use to transport water from the reservoir to the cold finger and back. Lastly the whole experimental chamber is inside an environmental box. The box is connected to a second heat exchanger and allows us to control the temperature of the experimental chambers walls. This broadens the available temperature range of the system since it allows us to stop the walls from heating the drop or water condensing on the walls instead of the cold finger during attempts of experimenting with temperatures higher or lower than room temperature.

The image of the drop the chamber is equipped with 2 windows that allow for a camera with a telecentric lens and a back illuminator to be mounted to it. Both are also inside the environmental box. The images then are taken to our fitting script that extracts the drops shape and calculate the surface tension from it. A schematic of the design can be found in figure [4.2.10](#).

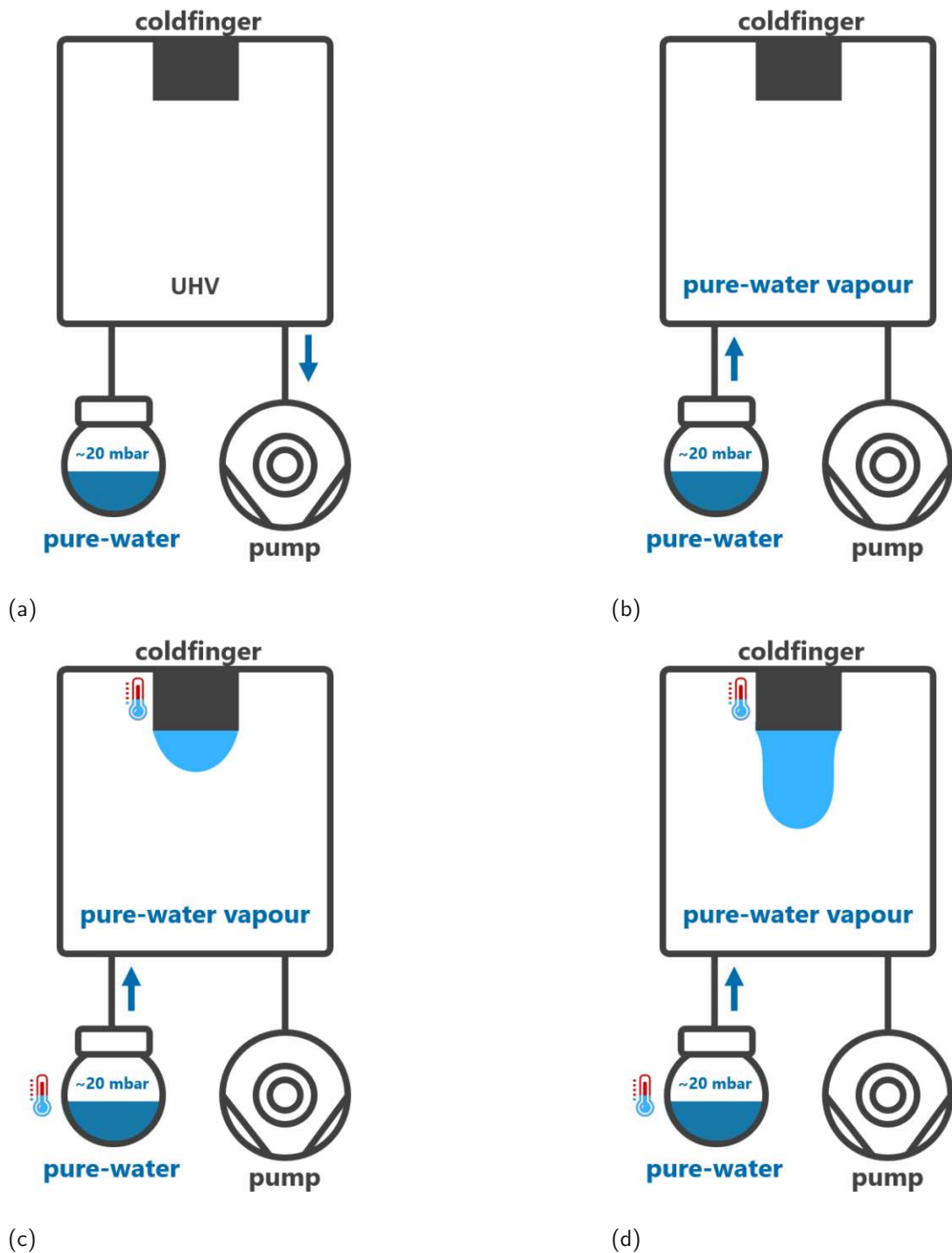


**Figure 4.2.11:** This figure shows the concept of our drop creation process. The experimental chamber undergoes a complete UHV cleaning and pumping procedure (a). After this a valve to the reservoir is opened and water from it evaporates into the experimental chamber (b). By controlling the temperature of the cold finger and the reservoir precisely and independently of each other, water condenses on the cold finger (c) until it reaches the maximal possible drop volume (d) at which point we equilibrate the system in preparation for data acquisition.

### 4.2.2 Cold Finger

The cold finger is not only the anchor from which the drop grows in the chamber but also contains all necessary infrastructure to control its temperature. A schematic representation can be found in figure 4.2.12 that includes all functional parts for this to work and a more detailed view including all peripheral parts is displayed in figure ???. A PID loop from a Lakeshore model 336 temperature controller controls resistant wire heating which in a combination with cooling by liquid nitrogen allows for very precise temperature control of the tip. The tip temperature is measured very accurately ( $\pm 35$  mK) with a silicon diode

The cold finger is located above the experimental chamber with the cold finger tip as the only part that reaches into the chamber. On the bottom surface of the tip the water is condensed to form a drop. This tip is precisely machined and measure to an outer diameter of  $6 \pm 0.001$  mm. The tip is internally hollow to allow for the heating and cooling elements to be placed inside. The bottom thickness of the tip is just 0.5 mm so as to bring the temperature controlled parts as close as possible to the actual drop. In the same vain, the side walls of the tip are only 0.3 mm thick to reduce the thermal load from other parts of the cold finger. The temperature control system consist of a liquid nitrogen reservoir at the very top of the structure that has a leak valve inside through which a capillary allows the fluid to flow down into a cylindrical copper heat exchanger at the end of the tip that we will call "tip heater" as it is referred to in figure 4.2.12. From the tip heater, it flows back up through the piece and out an exhaust. This flow of liquid nitrogen/ cold nitrogen gas provides the cooling power and is facilitated by a venturi pump. For the heating power, current is run through electrically resistant manganin wires ( $\sim 50 \Omega$ , max current 0.15 A) which are wrapped around the end of the tip heater. For better overall control of the temperature, an additional heating source termed the "counter heater" ( $\sim 50 \Omega$ , max current 0.15 A) is placed higher in the cold finger at the same level as the connection point between the cold finger tip and the experimental chamber. Both heating sources are equipped with a silicon diode to measure their temperature with our model 336 Lakeshore controller. In total there are two temperature measurements from the cold finger: the "tip" temperature measured on the tip heater and a "counter heating" temperature measured at the other heating source, both are shown in figure 4.2.12 and referred to as "Counter Diode" and "Tip Diode".

The wires for the diodes and heating are bundled in a packages of four wires for each of the diodes and a package of two wires for each heaters and run through the outside of the spine in the cold finger insulation volume up to a DIN feed through from which it is connected to the Lakeshore. The liquid nitrogen reservoir is also thermally insulated with the reservoir insulation volume. Both insulation volumes are in static vacuum. Both heater elements are spring loaded for improved thermal contact. The tip heaters spring is called "Spring A" in figure 4.2.14 and uses a ledge in the neck to apply 4 kg of force on the spine that is connected to the tip heater at its bottom. "Spring B" corresponds to the counter heater and also uses a ledge in the neck and the counter

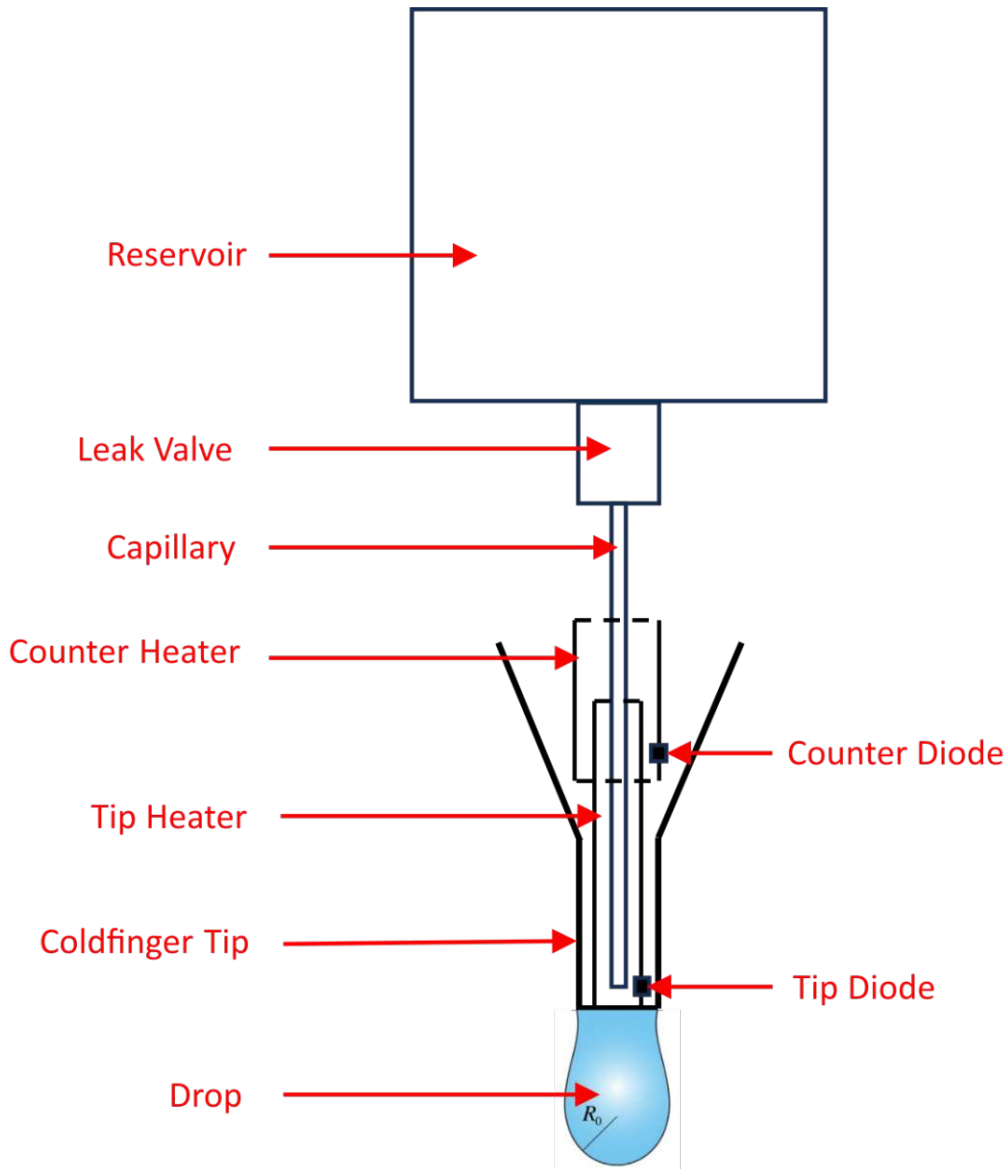


**Figure 4.2.12:** A schematic not to scale representation of all important parts of the cold finger. The reservoir is on top and nitrogen can flow down to the cold finger tip through the capillary. Two heaters equipped with a diode each counter heat to regulate the temperature of the drop that's hanging on the bottom surface of the cold finger tip inside the experimental chamber. The thicker lines of the cold finger tip represent the walls that separate the experimental chamber from the "outside".

heater adaptor to press it in position. Another noteworthy design point is the position of the counter heater. It is on a level with the contact point between the cold finger tip and the experimental chamber and is positioned that way to stop heat transfer from the chamber walls up to the liquid nitrogen reservoir and limit water condensation on the very top of the cold finger tip since water flowing down from there could disturb the experiments. For the same reason there are 3 zirconium balls placed in slots around

the tip heater. While we want very good thermal contact and heat transition with the bottom surface of the cold finger tip ideally we don't want water to condense on the sides. That's why the tip heater is smaller in diameter than the space it is placed in. The zirconia balls then center it and try to isolate the side walls against the tip heaters temperature. Details about assembly can be found in chapter [4.3](#).

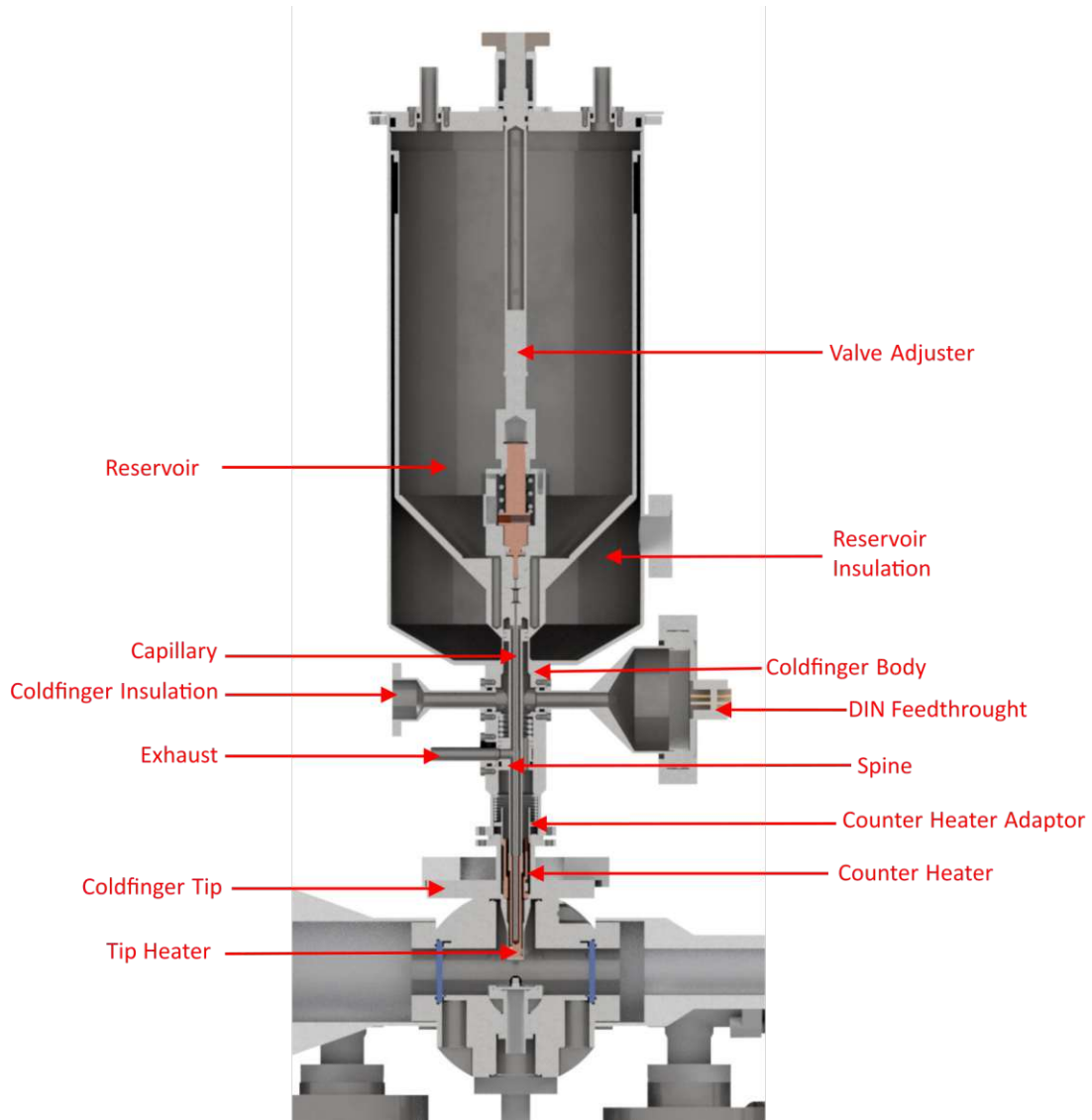


**Figure 4.2.13:** This figure shows a render of the cut in half cold finger and shows all relevant parts names as they are referred to in this thesis.

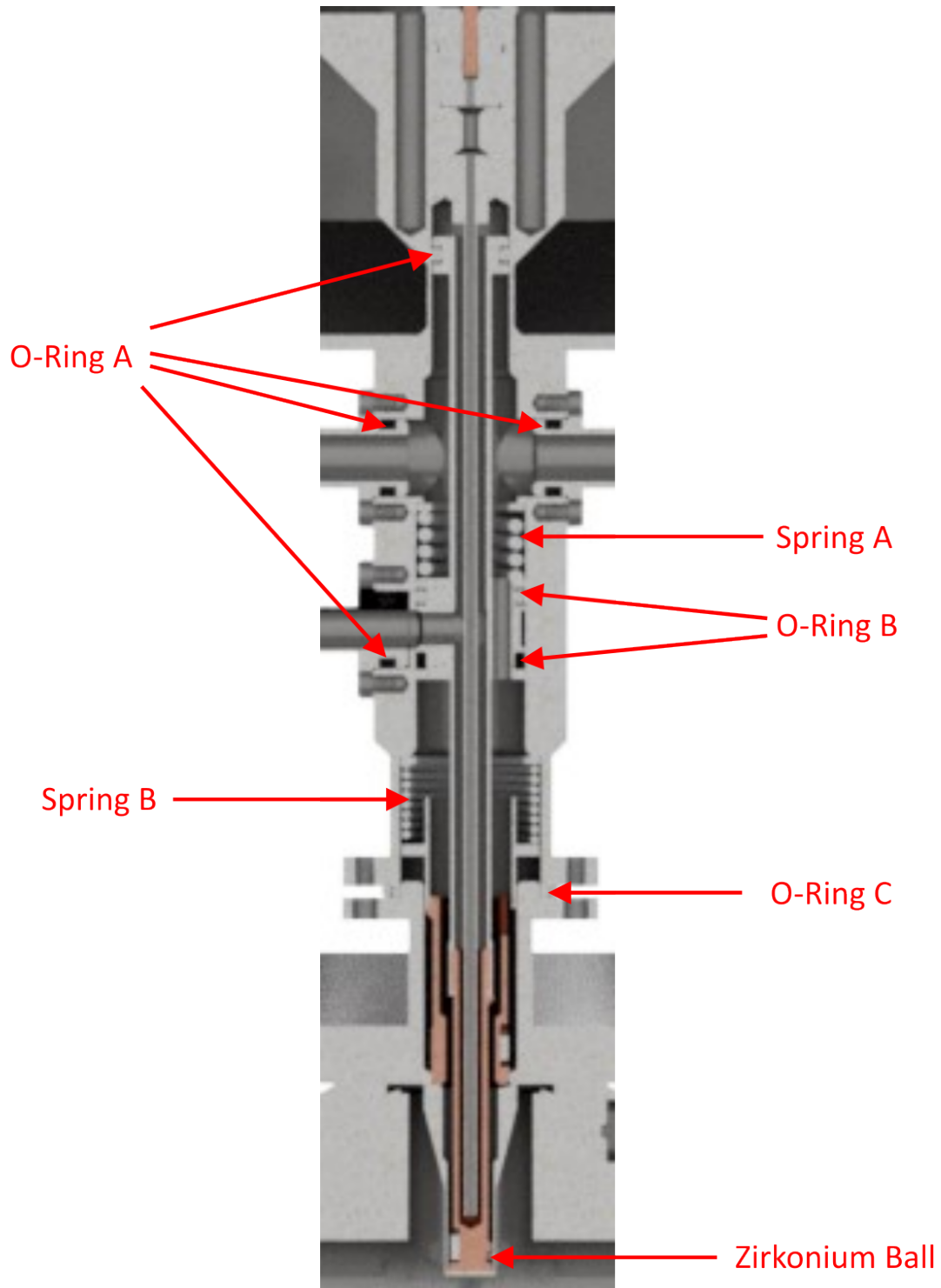


**Figure 4.2.14:** This picture shows a close up of the cold finger below the liquid nitrogen reservoir and points out the rest of the named parts as they are referred to in this thesis.

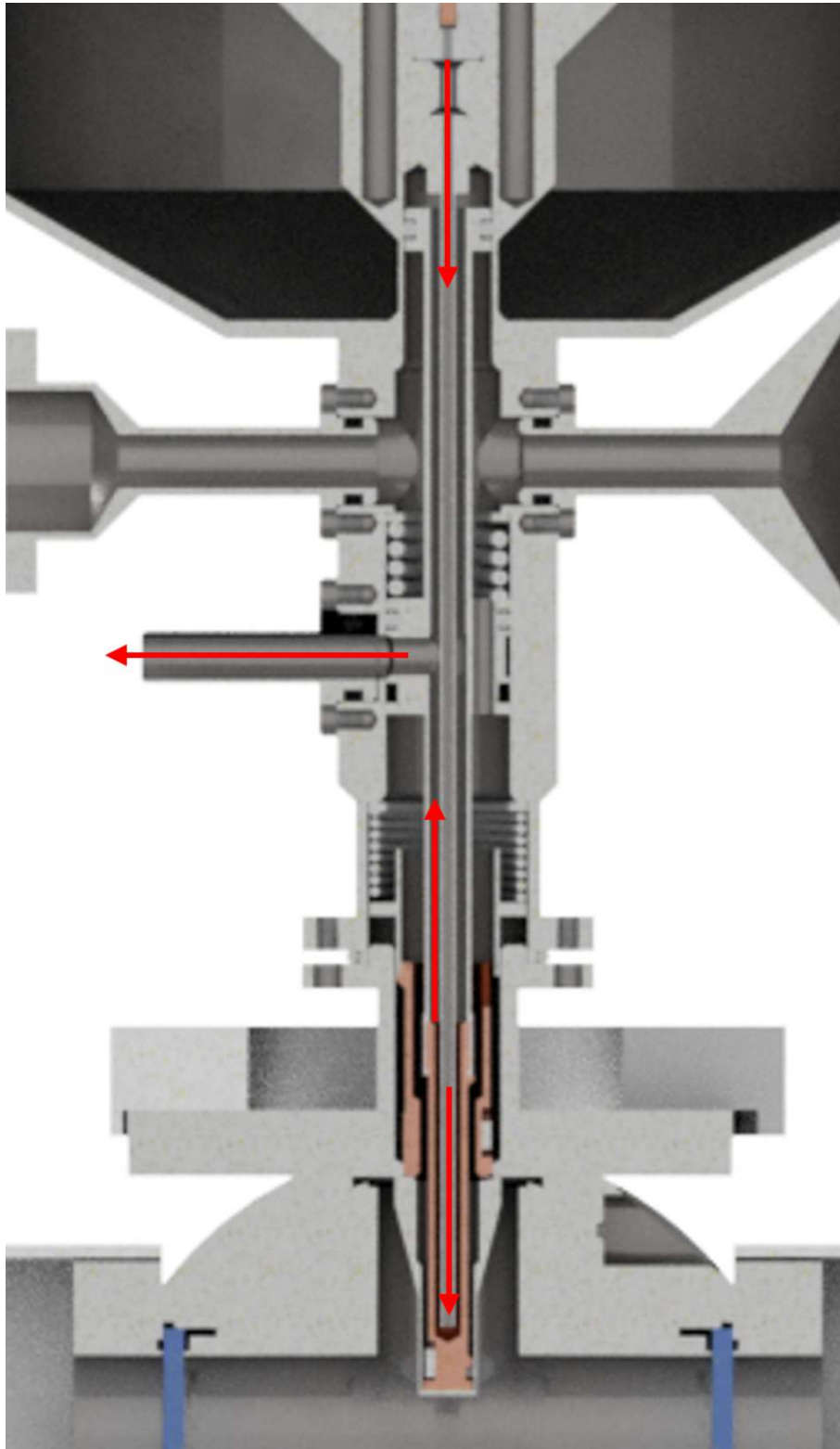


**Figure 4.2.15:** Representation of the nitrogen flow through the System. Its coming from the reservoir on top and goes down to the tip heater through a capillary tube. Then back up through the volume around the capillary inside the spine until it reaches the exhaust. This flow is fueled by a venturi pump that is connected to the exhaust.

### 4.2.3 schematics

This chapter shows schematics for the vacuum system, the optical system and electronic connections as overviews over the machine.

Figure 4.2.16 shows a schematic representation of the optical system. A uniform light source is used as back illumination. The mirror represents the periscope that is needed to fit the light into the environmental box. The telecentric lens and the camera on the opposite side acquire images for the drop shape fitting. Sapphire windows allow a look into the chamber without adding to much contamination due to the contact with the water vapour. The light ray hitting the cold finger instead of reaching the lens shows how the field of view is designed to have a bit of the cold finger in the picture. The idea was to use this precisely measured part to verify the optical systems calibration. However in the end the calibration was done with other more precise methods.

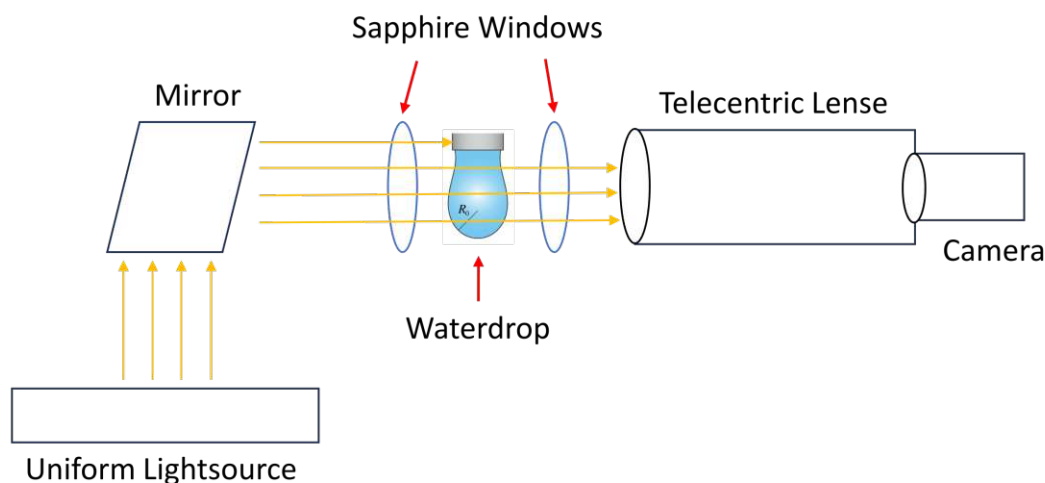


**Figure 4.2.16:** This figure shows a schematic representation of the optical system.

Figure 4.2.17 shows the vacuum scheme. Were on the right one finds the pumping chamber that has the pumps, a pressure gauge, a transfer arm, a gate valve to introduce samples to the system, a gate valve to the experimental chamber and a connection for venting the system connected to it. Left of it one can see the experimental chamber. It is pumped via the pumping chamber but has a gate valve to close it off during experimentation. Between the two chambers there is a cryo-trap that is cooled with liquid nitrogen to catch any particles that could travel from one side to the other by freezing them to its walls when the gate valve is open. The whole experimental chamber is inside the environmental box while the pumping chamber is outside. Also inside the box on the bottom of the experimental chamber are the windows that are insulated by a small volume that also is pumped to vacuum by a scroll pump. This volume and the experimental chamber are sealed off against each other. On top of the experimental chamber there is the cold finger, cold finger insulation and the liquid nitrogen reservoir insulation. The insulation is pumped by a scroll pump and then closed with an angle valve to be kept at static vacuum while the scroll pump is used to also pump the cold finger insulation to a static vacuum. This is done to reduce vibrations from pumping

during experimentation. Also connected to the cold finger is a venturi pump that fuels the liquid nitrogen flow for the temperature control system.

In the electronic schematic in figure [4.2.18](#) all electronic connections in the lab are represented. Green lines show LAN connections between the PC and all devices that are controlled with it. At the bottom there is the camera that is powered buy an injector and at the top two LAN switches that connect to both chillers, the Lakeshore, the Pfeiffer MaxiGauge and the massspectrometer. The Pfeiffer Maxigauge is connected to all but one of the pressure gauges. These connections are shown in orange. The blue lines show the connections between the Lakeshore and the diodes that measure temperature. The diodes are shown with the their serial numbers and the positions in the system. The fifth connection to the Lakeshore is to the Baratron controller and from there to the Baratron gauge. This is the pressure gauge for the experimental chamber and the cable is a costume made one to be able to read the 10V output signal from the gauge with the Lakeshore where a costum curve translates it to a pressure that can be read with the computer or on the Lakeshores display. On the top left there is the turbo pump and its controller. It can currently not be controlled with the computer and is therefore not connected to any other device electronically.

The schematic in figure [4.2.19](#) shows the connection of the back illumination. The light is powered by a power supply while a 0-10V source controls the lights brightness. To work the lights power supply and the 0-10V sources negative pole have to be connected electrically.

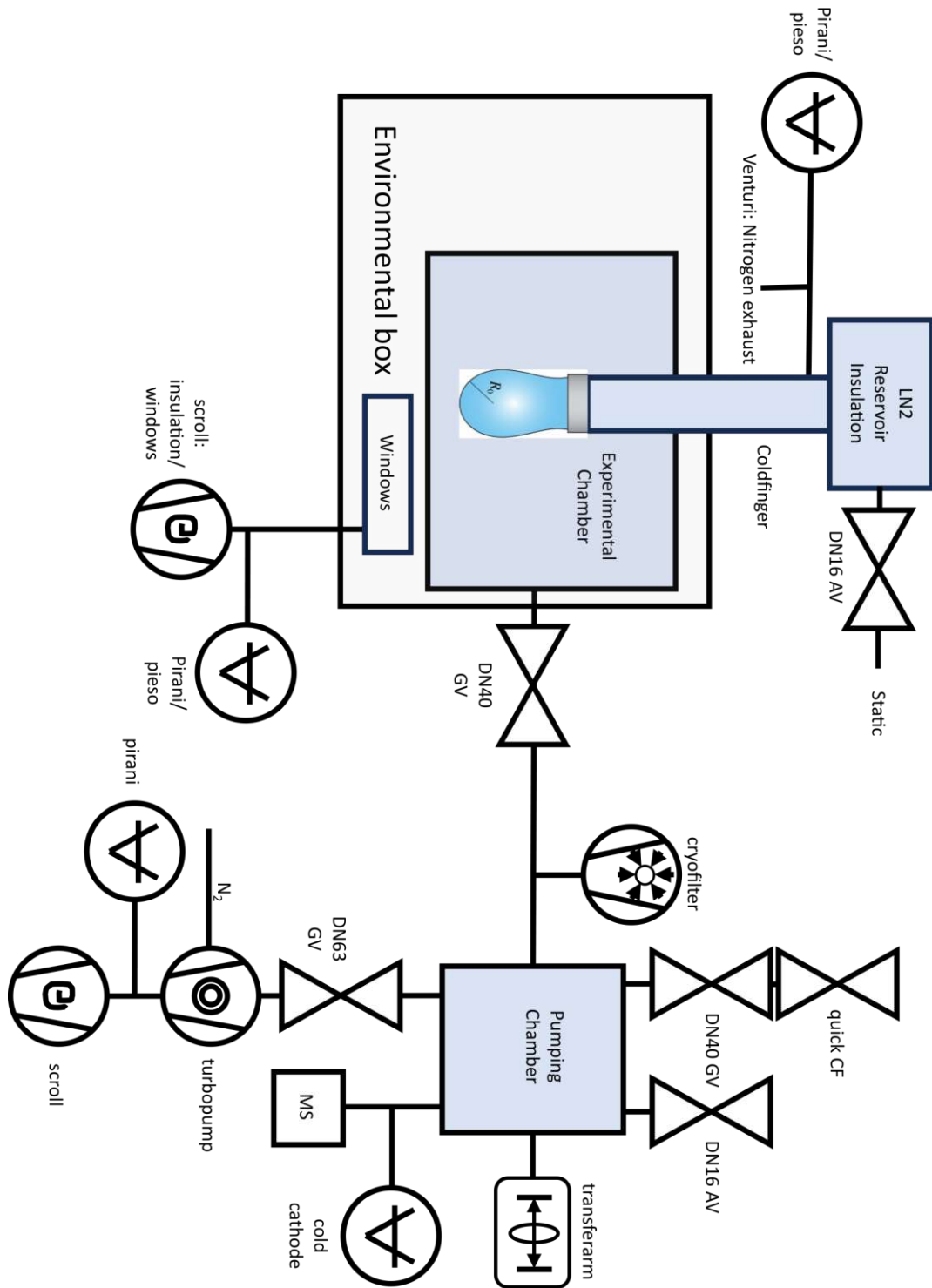


Figure 4.2.17: This figure shows the vacuum scheme.

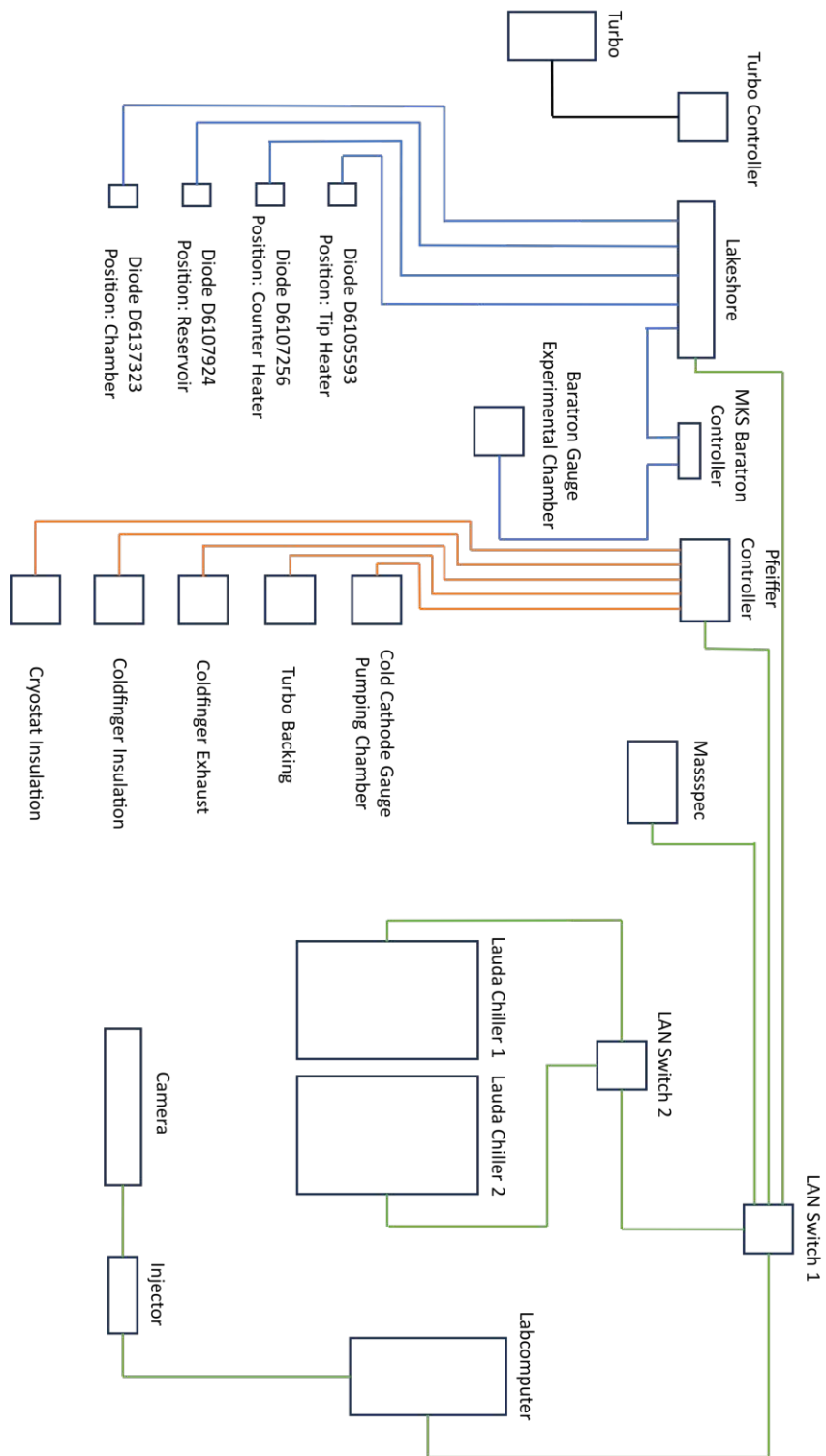
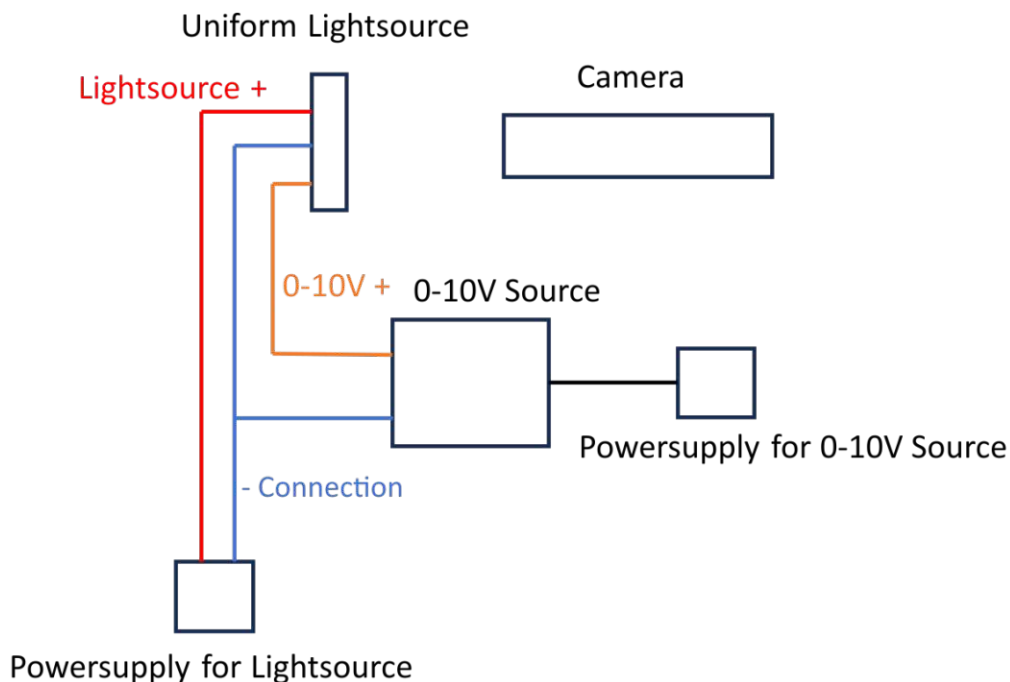


Figure 4.2.18: This figure shows the electronic scheme.



**Figure 4.2.19:** This schematic shows the connection of the back illumination.

#### 4.2.4 Materials

The materials used for the experimental chamber are a potential source of contamination. Everything that gets in contact with the water corrodes at different rates. Therefore we made sure to use materials where this effect is as small as possible. In the end it was possible to reduce the number of Materials that are exposed to water down to four namely:

- gold
- FKM (Viton)
- sapphire
- 316LN stainless steel

Stainless steel is necessary for the walls of the vacuum chamber. Sapphire was used for the windows of the optical system and Viton is needed to seal them. Gold is used for the UHV gaskets. Copper reacts strongly with water so instead of the usual copper gaskets gold plated ones were used. For the cold finger tip, 316 LN stainless steel is also used. It is known that pure-water corrodes even stainless steel. As such, we undertook an dissolution experiments as discussed in apendix [7.3](#). With these experiments we showed that while Fe species are found in pure-water exposed to 316 LN, these are typically on the order of 10 ppb and so very unlikely to affect the surface tension measurements [\[18\]](#). This is much less dissolution than other stainless steels such as 304.

### 4.2.5 Cryo-trap

To further improve the cleanliness of the instrument, a custom cryo-trap was design and produced. The cryo trap is placed at the connection between the pumping chamber and the experimental chamber. It has a cylindrical reservoir for liquid nitrogen that sits inside the tube that connects to the experimental chamber's gate valve. Through its centre is a cylindrical hole for the transfer am to be able to transfer sample plates in and out of the experimental chamber. When filled with liquid Nitrogen the reservoirs walls reach temperatures of  $-140\text{ }^{\circ}\text{C}$  and gas phase species/ contaminants that could pass from the Pumping to the experimental chamber instead adsorb to its walls. This is to avoid contamination of the experimental chamber during transferring processes or while pumping the Experimental Chamber to UHV. The temperature of the cryo trap would stay below  $-140\text{ }^{\circ}\text{C}$  for 3.5 h hours and reached  $-100\text{ }^{\circ}\text{C}$  only after 5 h after which we stopped the experiment. A schematic cut through the middle of the cryo trap can be seen in figure [4.2.20](#).

To test the cryo trap we fixed a thermocouple wire with a screw to a threaded hole in the cryo trap and used a feed through to be able to pump the chamber to UHV during the test run. The cryo trap then was filled with liquid nitrogen, given some time to cool down and filled again fully before we started noting the temperature and the pressure value in the experimental chamber every 10 minutes. The pressure values were taken without a bake out so they are not representative for the systems capabilities but should gather data on the effects of the cryo trap on the pressure due to particles freezing to its walls. Table [2](#) shows the data taken in this test with figures [4.2.21](#), [4.2.22](#) showing the Temperature, pressure in the pumping chamber and pressure in the experimental chamber plotted against time passed.

Time [min]	Temp (°C)	P [mbar]
0	22	1.16E-06
10	-143	2.11E-07
20	-143	1.89E-07
30	-143	1.78E-07
40	-143	1.68E-07
50	-143	1.60E-07
60	-143	1.52E-07
70	-142	1.47E-07
80	-142	1.40E-07
90	-142	1.35E-07
100	-142	1.31E-07
110	-142	1.26E-07
120	-142	1.22E-07
130	-141	1.20E-07
140	-141	1.16E-07
150	-141	1.14E-07
160	-141	1.11E-07
170	-141	1.08E-07
180	-141	1.06E-07
190	-140	1.03E-07
200	-140	1.02E-07
210	-140	1.00E-07
220	-139	9.87E-08
230	-136	9.62E-08
245	-129	9.45E-08
260	-127	9.35E-08
270	-124	9.21E-08
280	-120	9.07E-08
290	-116	9.07E-08
300	-112	9.35E-08
310	-109	1.08E-07

**Table 2:** Data from the cryo trap test. Fully filled with liquid nitrogen we measured the cryo trap to stay below  $-140^{\circ}\text{C}$  for 3h and below  $-100^{\circ}\text{C}$  for over 5h with a minimum temperature of  $-143^{\circ}\text{C}$  at the start. Also in the table are the pressure values in the experimental chamber that show the pressure reducing effects of the cryo trap due to particles freezing to the cryo traps walls.

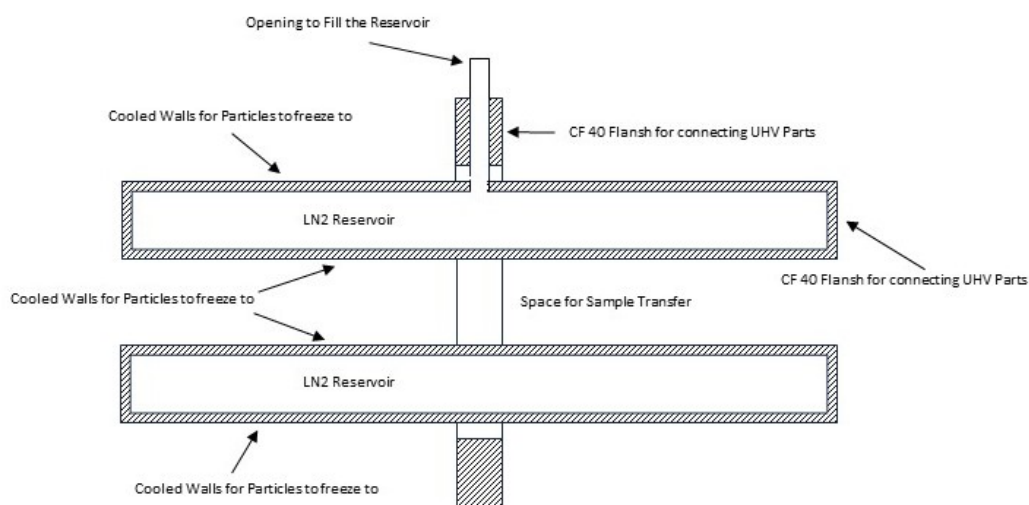


**Figure 4.2.20:** The cryo trap is placed between the experimental and the pumping chamber. It has a liquid nitrogen reservoir to cool its walls for particles to freeze stuck to them. This is to stop particles to travel from the pumping chamber to the experimental chamber and potentially contaminate our experiment when the gate valve is opened during pumping or sample transfer. The figure shows a schematic version of it. The ring in the middle is to connect to standard UHV parts. The reservoir is a double walled cylinder that still allows sample transfer through the cryo trap thanks to the opening through the middle. Tests showed that one filling of the cryo trap keeps it below  $-140\text{ }^{\circ}\text{C}$  for 3.5 h and below  $-100\text{ }^{\circ}\text{C}$  for 5 h.

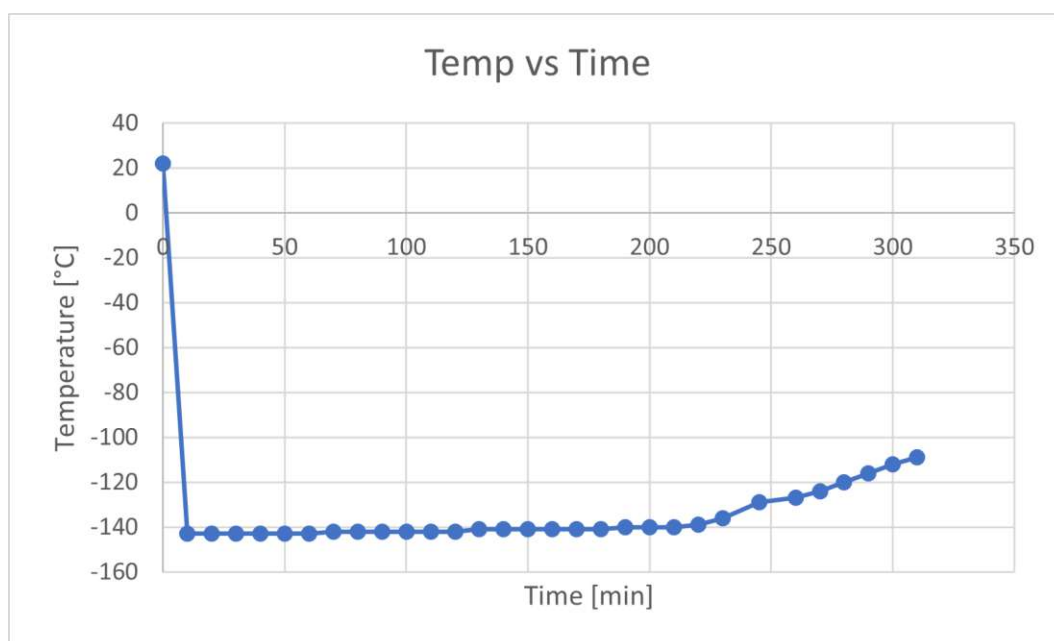


**Figure 4.2.21:** Temperature of the cryo trap plotted against time passed. The cryo trap was cooled with liquid nitrogen until the temperature stopped falling and then fully filled before we started noting the temperature every 10 minutes. The system stayed below  $-100\text{ }^{\circ}\text{C}$  for 5h after which the experiment was stopped.

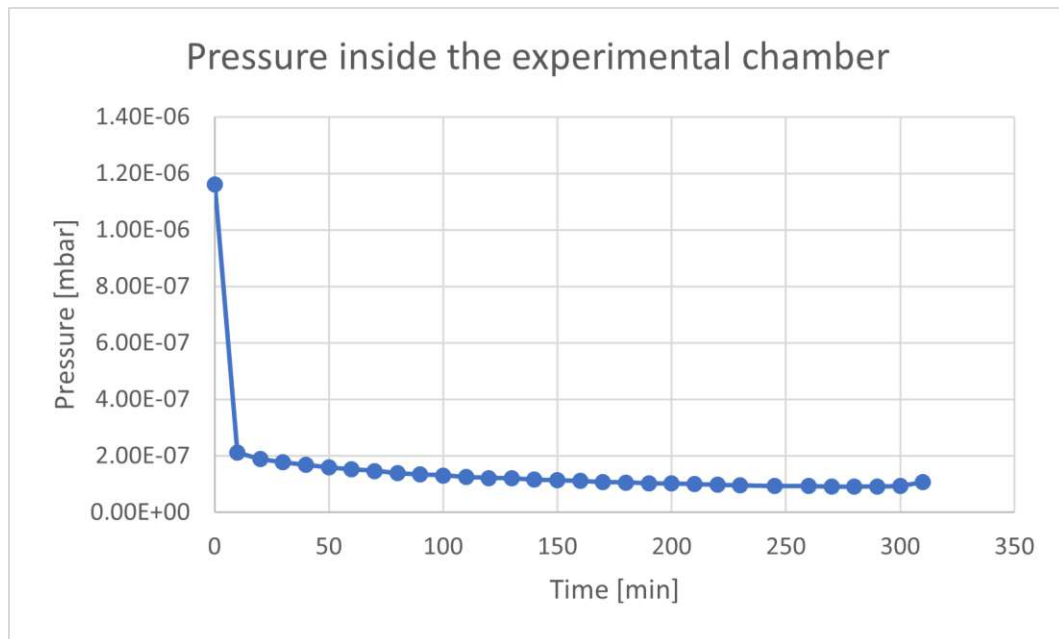


**Figure 4.2.22:** Pressure in the experimental chamber plotted against time passed. The cryo trap was cooled with liquid nitrogen until the temperature stopped falling and then fully filled before we started noting the pressure every 10 minutes. While the pumps stayed on during the 5 h period the experiment took place in, it is visible that between the very first data point that was taken at room temperature and the second that was taken 10 minutes later at  $-143$  °C there is a pressure reducing effect due to particles freezing to the cryo traps walls taking place.

#### 4.2.6 Measures against vibrations

Vibrations play a big role in the precision of the instrument. For an oscillating drop the edge detection is less accurate the more the drop moves. Therefore we had to take care to reduce vibrations from reaching the drop as much as possible. First off the instrument, the pumps and the chillers are placed on metal plates on vibration damping foam (Sylomer SR18). Second the KF hoses for the Pumping are connected to vibration damping weights in between the instrument and the scroll pumps. These weights consist of a tube with KF40 connectors on both sides that is welded onto a big block of metal and are placed on plates and damping foam as well.

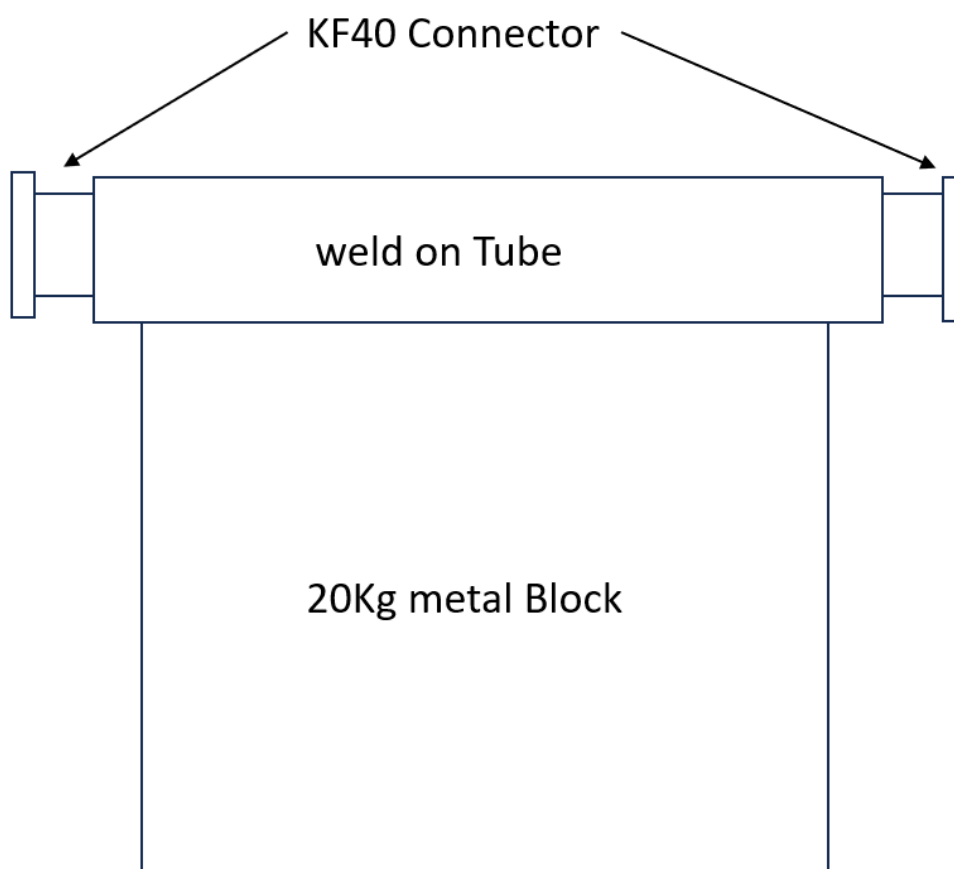


**Figure 4.2.23:** Schematic of a vibration damper. It contains of a big piece of metal that weights roughly 20 kg and has a tube welded on its top. The tube has a KF40 connector on both sides and is placed in between a scroll pump and the instrument to stop vibrations from the scroll pump from transfer to the instrument via the hoses. Additionally the damper is placed on a metal plate that rests on vibration damping foam to also reduce vibration transmission via the floor.

In operation additionally the turbo pump that is connected to the pumping chamber and its backing scroll pumps are shut off and the liquid nitrogen reservoir of the cold finger is filled and given time to cool before starting the measurements to reduce vibrations

from boiling nitrogen.

#### 4.2.7 Environmental Box

The distillation of water from the pure-water reservoir to the cold finger tip works by cooling the cold finger tip with respect to the reservoir. Water will evaporate at the warmer spot and condense at cooler spots. This works very well when the cold finger tip is a bit colder than the room and the reservoir a bit warmer. To explore the surface tension for other temperatures one problem occurs. The walls of the experimental chamber also have a temperature which, if uncontrolled, could be higher or lower than the tip. For example, to measure the surface tension of a drop at 30 °C the cold finger would have to be set to for example 30 °C and the Reservoir to 31 °C or above. But with the room temperature being in the range of 20 - 25 °C the water would condense at the Chamber walls instead of the cold finger tip. Moreover, for temperatures below room temperature, for example with a cold finger tip at 5 °C and the reservoir at 7 °C, the walls would heat the water in the drop causing temperature gradients and producing very inaccurate results. This not only means we would be unable to properly determine the drop's temperature but also that we limit the maximum size of the drop. If the drop gets warmed above 7 °C in this example the water would get pumped back to the reservoir.

To solve these issues, an environmental box was designed as shown in figure [4.2.24](#). It allows for the temperature of the whole experimental chamber to be controlled and measured. This means the chamber walls can be brought to within +0.5 °C of the water drop, alleviating the previously mentioned problems of the drop being warmed or water condensing on the chamber walls. It consists of a stainless steel structural shell with insulating layers of polyisocyanurate insulation (PIC) foam (ICO-C1) (thermal conductivity =  $0.026 \frac{W}{mk}$ ) placed internal to the shell. Kevlar fabric was then glued to the PIC foam to protect it from damage. To control the temperature inside the box, aluminium sheets with fixed heat exchangers were glued to the kevlar fabric. Heat exchanger fluid flows through these heat exchangers with the temperature of the fluid being controlled by an external heater-chiller (Lauda PRO RP 290 E). This box would be big enough to fit the entire experimental chamber into it except for an opening at the top to keep the cold finger's liquid nitrogen reservoir outside. This heater-chiller combination allows for the temperature of the environmental box to be in the range -50 to +100 °C.

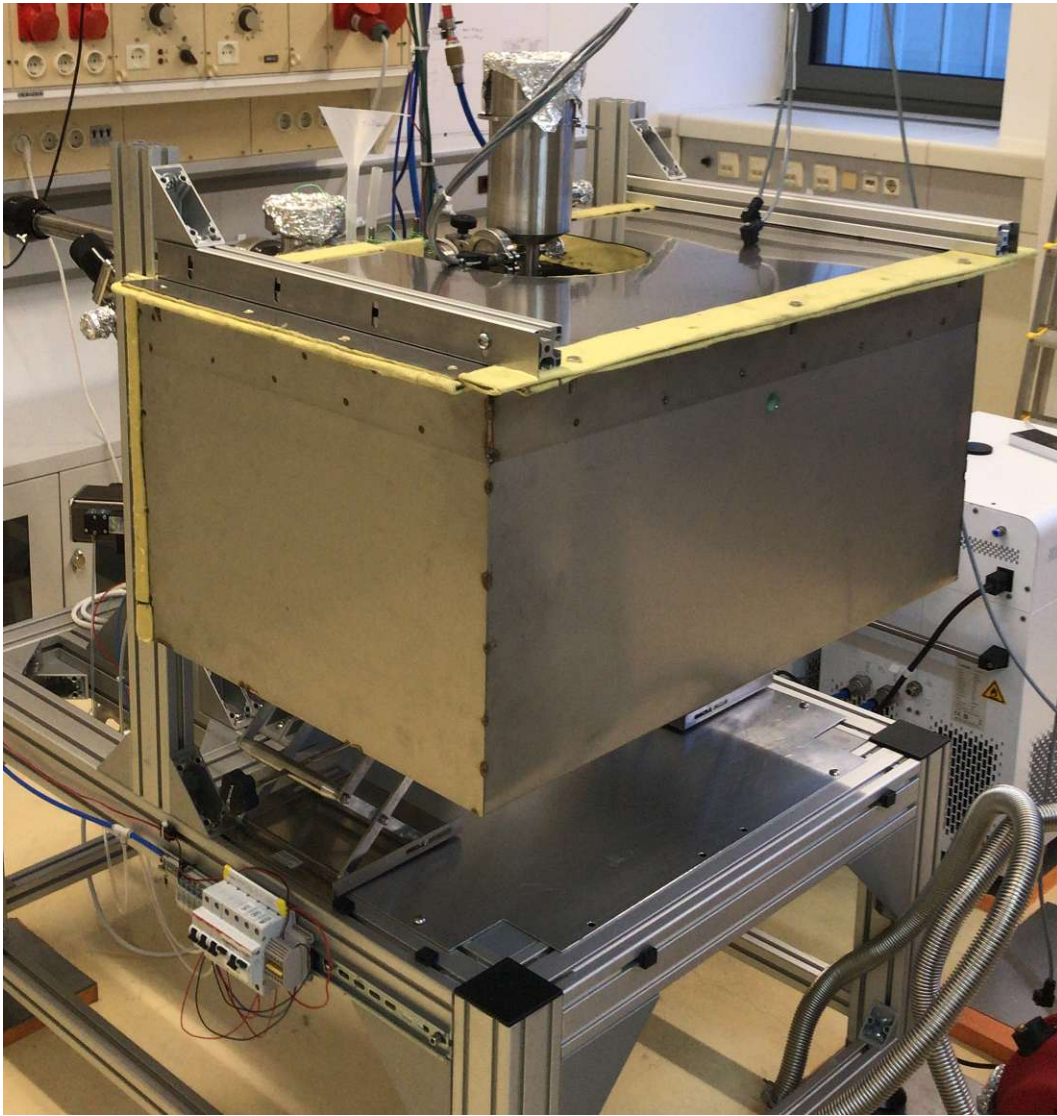


**Figure 4.2.24:** This figure shows the environmental box in its working state. On its top the cold finger liquid nitrogen reservoir sticks out but the rest of the experimental chamber including the optical setup is inside. The hole at the top is closed with a lid during experimentation.

## 4.3 The Drop Chamber Assembly

### 4.3.1 Assembly of the Cold finger

The assembly of the cold finger was done from the inside out. First the heaters themselves were built which meant gluing the heating wire on and bringing the diodes in position. Then O-Rings were placed on the Spine and the wires bundled and put loosely into place before the DIN feed through was assembled and the wires connected to it at the end. In the pre-built state the spine together with the heater was placed in the neck and held in position with a tool that was made to fit into the Exhaust opening

to be able to take it to the experimental chamber where the cold finger tip was already mounted to. The zirconium balls were placed in their slots, the tip Heater slid into the cold finger tip and everything connected by screws. A detailed description of every step follows in this chapter.

First the counter heater was built as it is the bigger of the two and therefore easier to figure out a good process with. As a first step 2 m of 0.14 mm diameter kapton insulated manganin wire and six pieces of 0.25 mm diameter kapton insulated copper wire of 1 m in length were prepared and the ends insulation removed. Then the manganin wire was bent in the middle to run double and the bent end glued on the copper piece right next to the groove for the diode. To fix it in place a small piece of aluminium was put on top and some Teflon tape wrapped around. This was done because the aluminium foil was easy to cleanly remove after curing of the glue while the Teflon tape would leave some small bits behind in previous attempts. The copper piece with the strapped on manganin wire was then put in an oven and left there for 70 minutes at 150 °C. With this anchor point in place the part was placed in a bench vise. Two pieces of the prepared copper wire would be soldered to the ends of the manganin wire and insulated with Teflon tape and UHV shrinktube. The remaining 4 would be evenly positioned on a flattened area in the cylindrical counter heater and secured at the top and bottom with more Teflon tape to keep them temporarily in place. Then the manganin wire was wrapped around the counter heater and gradually covered with more silver epoxy glue. It was taken care that no glue could reach the soldering spot inside the shrink tube and all the manganin wire was covered to ensure good thermal conductivity to the copper and avoid damages to the wire due to overheating. A hot air gun was used to pre-cure the glue far enough so the wires wouldn't come off in the actual curing process and the part was then carefully placed in the oven to be again left for 70 minutes at 150 °C. Figure 4.3.25 shows the counter heater at this time in the process. On the top end of the counter heater one can see 2 pieces of transparent shrink tube. That are the connection points of the manganin wire that acts as heating wire and the copper wire that supplies current for said heating. The copper wires are also glued in place shortly after the connection point to avoid damages due to movement during further assembly. There is also a gap in the copper cylinder that allows the copper wires to go "inside" from where the wires will be lead to a DIN feed through that connects the Lakeshore to the diode and the heating. The other four copper wire pieces are for the diode. The diode is put in its place in this picture but not yet glued on.

After this the diode was glued into the groove. A very small amount of glue was put on the bottom of the diode and gently spread before it was then placed in the groove and secured with Teflon tape. Then it was left in the oven for 70min at 150 °C after which the diode leads were cut and the copper wire soldered onto the connections of the diode. Next the tip heater was done with the exact same procedure. The end result is shown in figure 4.3.26a.

With this done the assembly of the individual parts could begin. First the cold fingers

spine was equipped with O-rings and the springs. Then the tip heater was screwed in with some Teflon tape wrapped around the thread for better sealing. The counter heater adaptor was pushed on with the copper wires first going through its middle and then through the middle of the big spring which spring loads the counter heater. Then all wires run through holes in the spine. A map which wire runs through which hole is shown in figure [4.3.27](#) and the partly assembly pieces in figure [4.3.28](#).

After this the wire would be put through the body of the cold finger that is attached to the liquid nitrogen reservoir. The copper wires were crimped on the connector with shrink tubes of different lengths used to identify wires in case repairs or changes to them are needed later. Figure [4.3.31](#) explains how to identify each wire using the shrink tube identifiers via a picture of the connector from the inside the feed through. The wires coming from the cold finger to this DIN feed through are first separated in 4 bundles. Two of them are in shrink tubes of 3 mm length and come from the tip heater and two of them are in shrink tubes of 10 mm length and come from the counter heater. Each of the two sets contains one bundle with 4 wires and one bundle with two wires. The bundles with 4 contain the diode wires that are again separated in two wires for the positive pole in a shrinktube of 3 mm and a two wires for the negative pole in shrink tube of 7 mm length. The second bundle in each set contains just two wires for the heater wire.

The Lakeshore cable connector was closed and the spine pushed into the body. A pin was then used through one of the openings in the body to keep the spine in position. Next the counter heater was pushed on and 3 screws with some washers were used to keep it in position as well. Also the 3 zirconium balls that isolate the heater against the side walls of the cold finger tip were put in place.

A small piece of gold foil was put into the cold finger tip. It was there to improve thermal contact between the copper of the heater and the stainless steel.

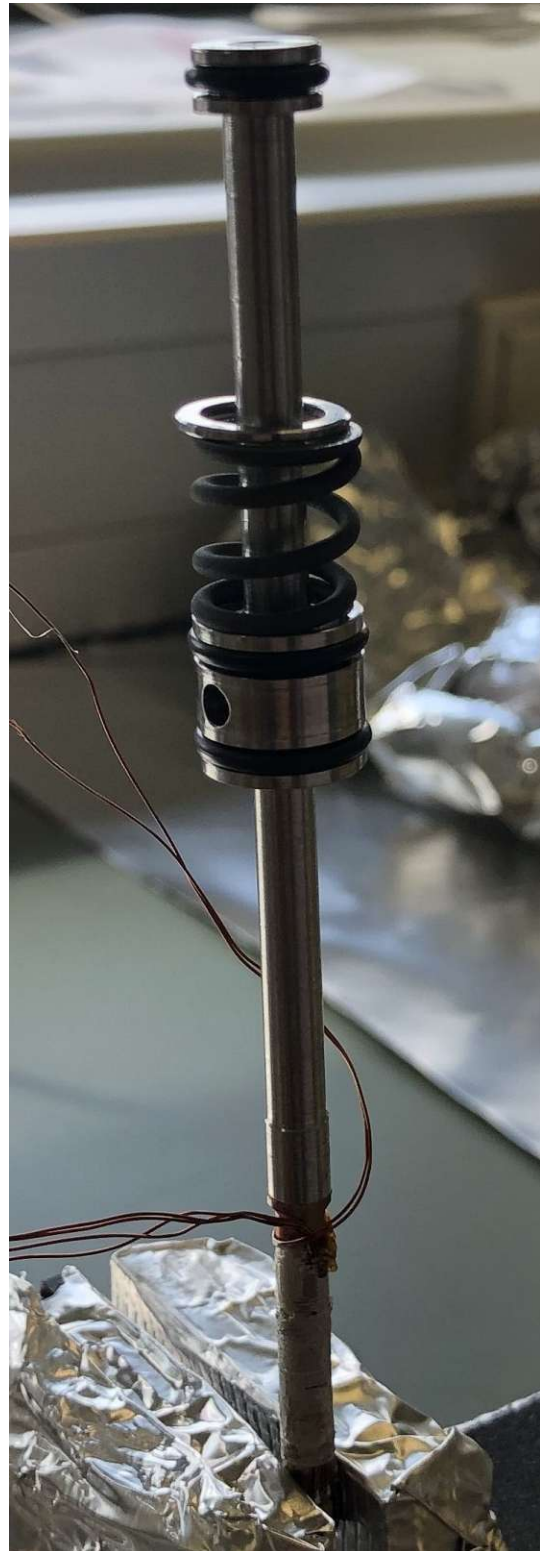
Lastly the cold finger was flipped and placed in the tip. While one person was holding it in position a second would slowly replace the screws and washers and to connect both parts.



**Figure 4.3.25:** The secondary heater in the cold finger with the manganin heating wire already glued on. The bigger picture shows the diode before and the smaller after it was glued into the groove and soldered to its wires. In both there are 2 transparent shrinktube pieces visible. They are the connection point between the 0.14 mm manganin and the 0.25 mm copper wire. The connection is soldered, and then insulated with some Teflon tape and said shrink tube. We tried to have all of the manganin wire covered in silver glue to ensure good thermal contact and avoid damages to the manganin wire due to overheating. Behind the shrink tube also the copper wire was glued onto the copper. This was done to avoid mechanical strain during the further building steps breaking the electrical connection between the wires.



(a) The finished tip heater. Here different to the counter heater the connection between the manganin and the copper wire was insulated by capton tube. The space around the tip heater is more restrictive than around the counter heater and the shrink tube would not fit. Other than that it was done in the same way. 47



(b) The tip heater screwed into the spine. The screwing connection is sealed with a thin Teflon strip since it is a seal between the nitrogen flow and the cold finger insulation vacuum. The spring is there to push the tip heater into the cold finger tip to improve thermal contact. The hole in the side of the spine is for the venturi pump fueled nitrogen exhaust with the 2 O-rings above and below sealing against the cold finger insulation vacuum.

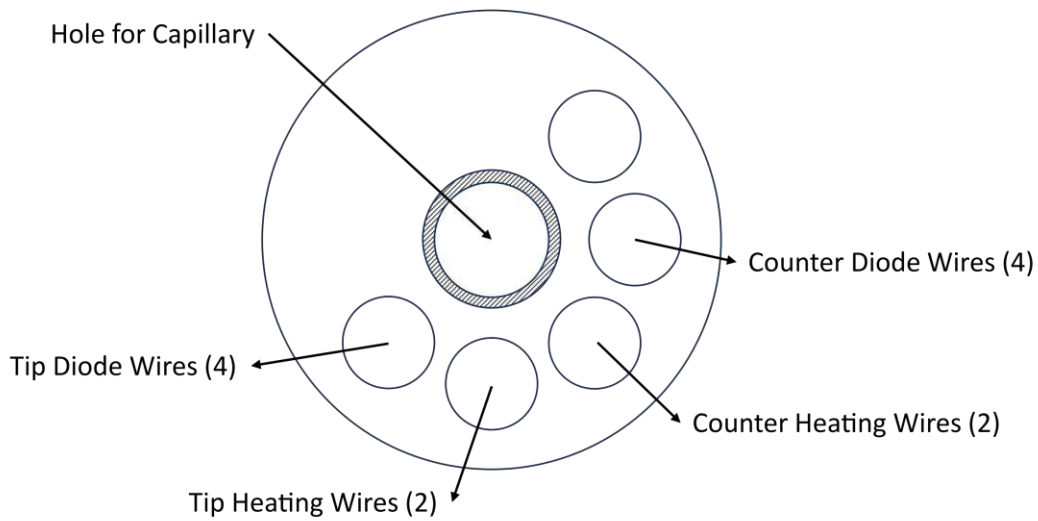


**Figure 4.3.27:** This shows the top view on the spine shown in [4.3.26](#). The 5 holes allow wires from the heaters to pass through the spines thicker portions that acts as nitrogen exhaust. The wires were bundled according to what they are connected to and put through different holes to keep them organised in the building process. The numbers in brackets state how many single 0.25 mm copper wires run through the corresponding hole.



**Figure 4.3.28:** The inside of the cold finger put together. For final assembly of the cold finger the tip heater will be put through the counter heater so that the long spring is compressed by the counter heater adaptor that in this picture is already connected to the counter heater by tight fit on the adaptor. This spring is for spring loading the counter heater to improve thermal contact there to. The wires are put through the holes in the spine according to [4.3.27](#).

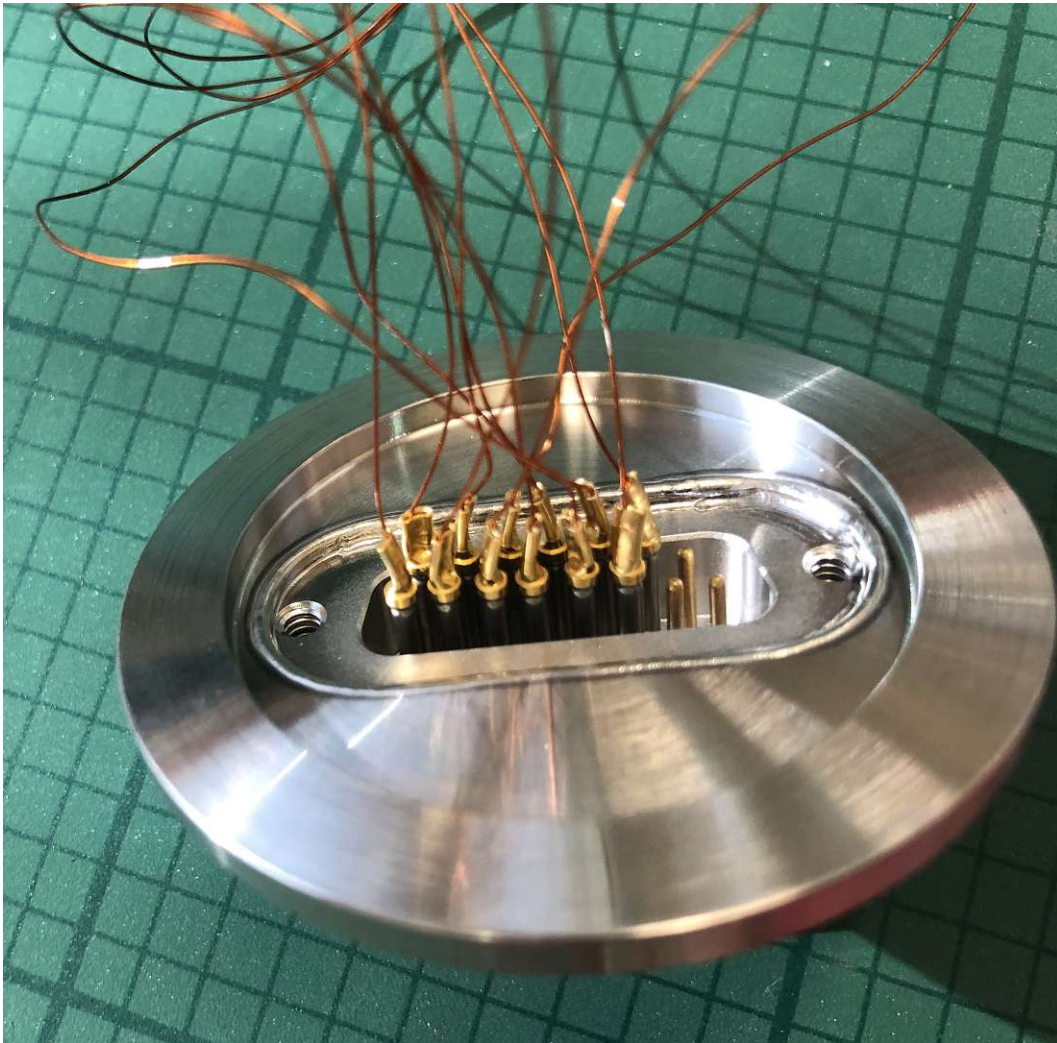


**Figure 4.3.29:** This picture shows the crimped connector that connect the 0.25 mm copper wires to the DIN feed through and therefore to the Lakeshore cable. The connections are done according to figure [4.3.31](#).

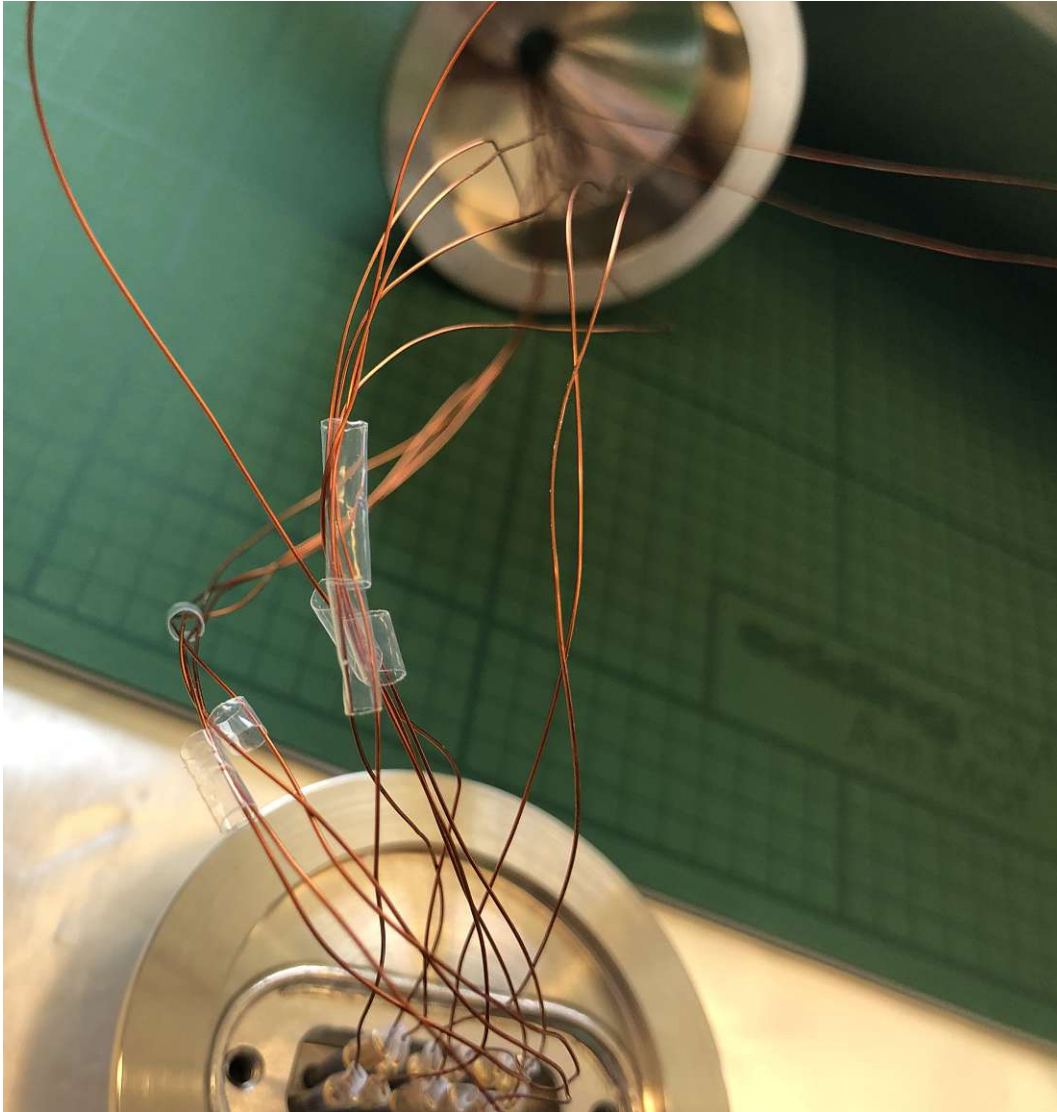
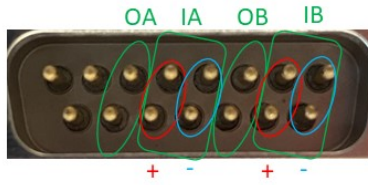


**Figure 4.3.30:** To be able to identify wires during potential repairs or upgrades in the future the wires are bundles in shrink tube pieces of different lengths. The shrink tubes lengths and how to identify each bundle is shown in figure [4.3.31](#).

## Inside The Coldfinger for Internal Repairs! Overview Guide



- OA Connected to the Heater Wires of the Tip Heater (Output A on the Lakeshore)
- IA Connected to the Diode Wires of the Tip Diode (Input A on the Lakeshore)
- OB Connected to the Heater Wires of the Counter Heater (Output B on the Lakeshore)
- IB Connected to the Diode Wires of the Counter Diode (Input B on the Lakeshore)

Shrinktube Length:



The wires are bundled up and marked with shrinktube pieces of different length. The organigram to the left explains which length corresponds to which wirebundle. The number in the brackets corresponds to the amount of wires going through the shrinktube.

**Figure 4.3.31:** This info graphic explains how to identify each wire using the shrink tube identifiers. The picture of the connector is from the inside the feed through.

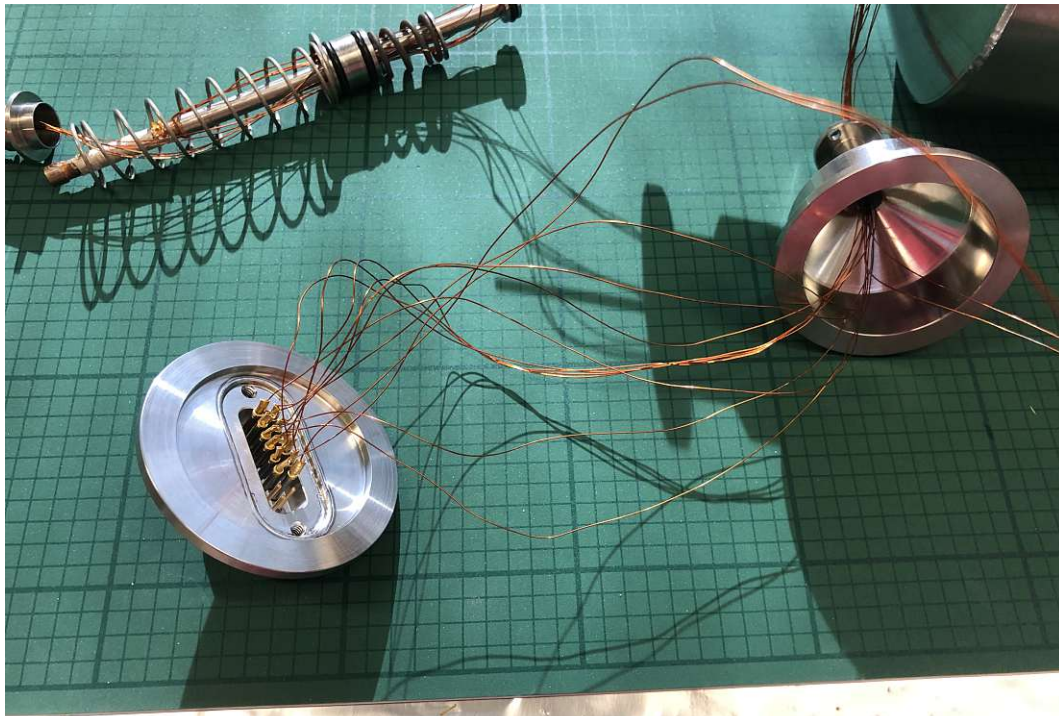


**Figure 4.3.32:** This figure shows the full insides of the cold finger ready for final assembly.



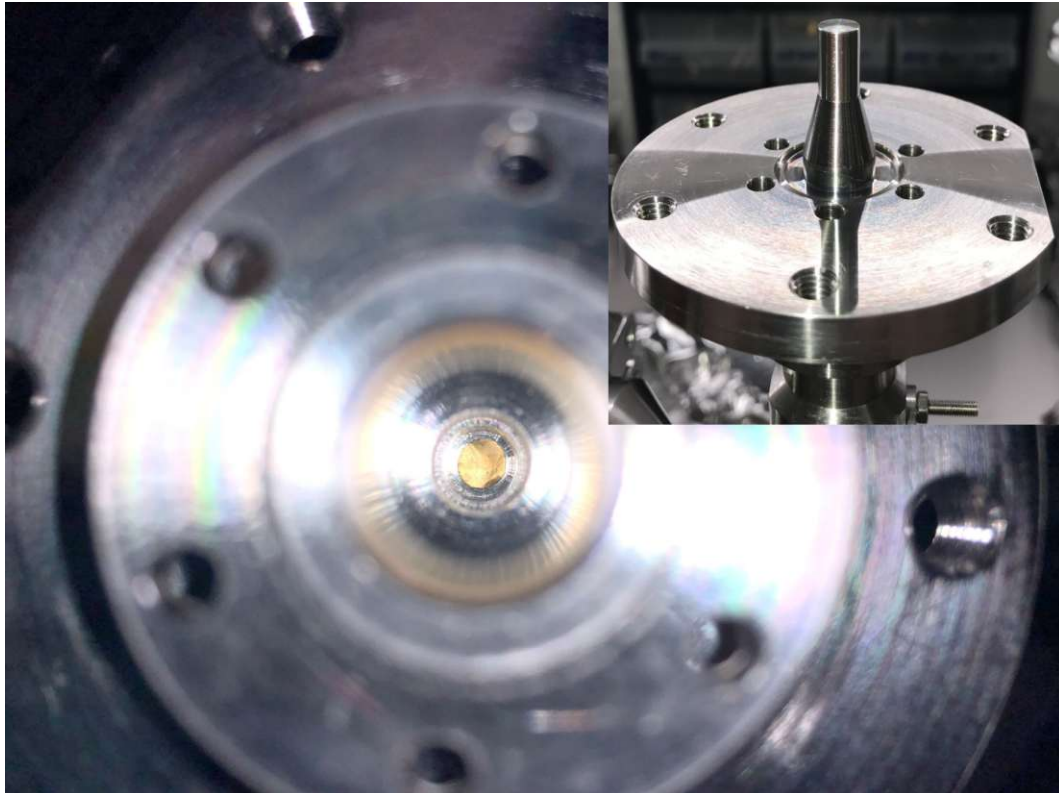


**Figure 4.3.34:** This is the view into the cold finger tip before the heaters that are shown in their pre-assembled state in [4.3.33](#) are put in. On the bottom there is a small piece of gold foil that should improve thermal conductivity. The foil has a thickness of 0.125 mm. In the top right there is a picture of the upside down cold finger tip for reference. The big picture is taken from the bottom in the top right picture and the piece of gold foil is positioned at the very top end in the top right picture inside the cold finger tip.



**Figure 4.3.35:** This picture shows the fully mounted cold finger on the instrument. Below there is one of the windows for the optical setup specifically for the back illumination. Also visible is the DIN feed through on which the Lakeshore cable will be connected to read the diodes signal and control the heating. In the back the silicone hose with the funnel is for filling cryo traps reservoir. The support is front of this reservoir is the last part outside the environmental box. Everything in front of it and below the main liquid nitrogens reservoir will be inside the box.

### 4.3.2 UHV Part Cleaning procedure

After investigating how strongly different materials dissolve in water it was clear that the containers we use for the cleaning process not only have to be clean but also have to be made from a appropriate material. To avoid cross contamination with materials that were previously cleaned in existing containers we decided to purchase new ones and ended up with pots made of LN304 Stainless steel. In total 4 containers were used with each of them having an assigned cleaning step. This was done to avoid contaminants from early cleaning steps getting into later cleaning steps. Also we used a laminar flowhood for some of the steps of cleaning, to store the parts and for assembly. All pots were cleaned themselves in a typical UHV cleaned process of

1. Soap Solvent (Extran)
2. Ultra Pure Water (MilliQ)
3. Isopropanol
4. Acetone
5. Isopropanol
6. Soap Solvent (Extran)
7. Ultra Pure Water (MilliQ)

The same was done to each of the lids. Three of the pots were place next to the sonicator on spots labeled with their respective fluid and the last in the flowhood.

As can be seen in the picture that was taken after most of the cleaning was done the pots while being cleaned properly in the beginning and treated well in the process have lots of stains visible on them. These stains are coming from contact of the pots with wet gloves. In the cleaning process getting ones gloves wet is almost impossible to avoid since we do a lot of rinsing with MilliQ and the sonicator is filled with water in which the pots are partially submerged in the process. Knowing this from previous experience for this reason we decided to not touch the parts at all in the cleaning process. Instead we used some LN316 stainless steel wire that was cleaned in the same process the pots were to handle each of the parts without the need of touching them in the process. A picture of this can be seen in figure [4.3.37](#)

With this in mind the full cleaned process for a part that would be exposed to water in the experiments would be as followed.

01. Rough clean with dishsoap to get rid of metal shavings and heavy oils.
02. Sonication in hot Extran in an extra bucket.
03. Rinsing with MilliQ water.
04. Attaching wire.
05. Sonication in pot A in hot Extran for 20 minutes.
06. Rinsing with MilliQ water.
07. Sonication in pot B in MilliQ for 20 minutes.
08. Sonication in pot C in Acetone for 20 minutes.
09. Rinsing with MilliQ water.
10. Sonication in pot C in Isopropanol for 20 minutes.
11. Rinsing with MilliQ water.
12. Sonication in pot A in hot Extran for 20 minutes.
13. Rinsing with MilliQ water.
14. Sonication in pot B in MilliQ for 20 minutes.



**Figure 4.3.36:** This picture shows the pots with their labels. The visible stains are from touching them with wet gloves, which is why we decided to not touch the parts in the cleaning process but would handle them using stainless steel wire instead. Each part would go through each pot in the order of the cleaning steps with each pot being cleaned itself after each use. This was to not recontaminate parts with stuff that is still floating around in the fluids or stuck to the pots walls. a forth pot was stored in the flowhood and was exclusively used for the boiling step.

15. Rinsing with MilliQ water.
16. Transfer into the flowhood.
17. Boiling inside the flowhood in pot D in MilliQ for 30 minutes.
18. Taking out and drying in the flowhood before removing the wire and covering with aluminum foil to store until assembly.
19. After assembly. Pumping the chamber and a bakeout at 150 °C to reach UHV.



**Figure 4.3.37:** As can be seen in [4.3.36](#) the gloves we use leave stains when wet. To avoid these stains on the parts instead of touching them to move them to other cleaning steps we would use 316LN stainless steel wire that was cleaned itself to handle the parts without touching them. The wire also was cleaned after each part it handled to remove stains it had collected from the gloves. The figure shows a reservoir with wire connected to it inside one of the pots that were used for cleaning.

### 4.3.3 Assembly of Chamber

For assembly of the chamber the needed tools, screws, the sapphire windows and gold plated gaskets were also cleaned in a typical UHV process and placed inside the flowhood. The Viton O-rings for the windows were cleaned with the acetone step skipped since acetone might damage them. First the sample holder was put in position inside the experimental chamber and all openings covered with blanks to keep the knife edges safe during all procedures. Then the windows were put in place. We took care to not touch the flat surfaces but only the edges while handling them to ensure a clean view into the chamber. Next the cold finger tip was put on since this is the most sensitive part. After that in no particular order two angle valves, a gate valve, a pressure gauge and a leak valve were mounted followed by the reservoir and the cryopump reservoir. ??? i think this cryo pump reservoir was never mentioned before

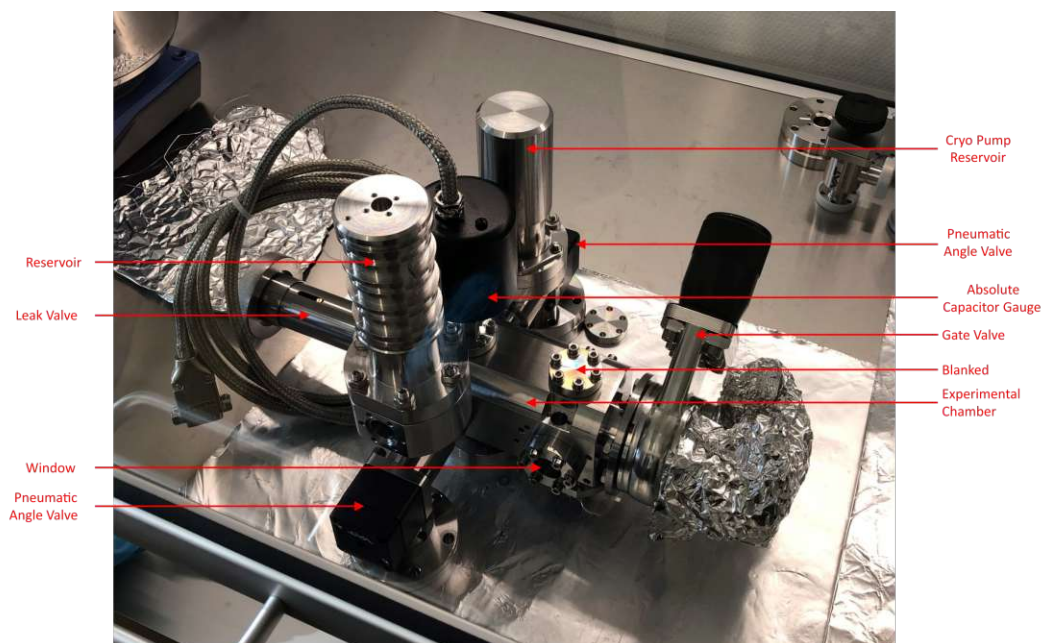


**Figure 4.3.38:** The built chamber in the flowhood. It is upside down so the cold finger tip is mounted on the bottom opposite the blanked unused opening. On the opening on the side of the Reservoir another angle valve was mounted. This was the connection point through which the water will be distilled into the system later.

Still in the flowhood the assembled chamber was then rinsed multiple times with boiling MilliQ water by filling it while moving it to make sure the water reaches everywhere and then emptying it into a waste container. After giving it some time to dry the gate valve was closed to avoid dust entering the chamber during mounting it onto the instrument.

### 4.3.4 Water Cleaning procedure

This process starts with pure water from the MilliQ machine. It is filled into a secondary reservoir which is then sealed with a window. The reservoir is connected via a T-piece

over an angle valve to the experimental chambers reservoir and a scroll pump. Then we use the scroll pump and the window to do freeze-pump-thaw cycles where we freeze the water by dipping the reservoir in liquid nitrogen to pump away everything coming out before turning the pump off, melt the ice and repeat the process. This is done until the ice that is formed does not show any bubbles anymore and grows into homogenous crystals and we are able to reach UHV pressures ( $\sim 10^{-8} \text{mbar}$ ) with the reservoir at liquid nitrogen temperature. With this done the angle valve between the experimental chamber and the reservoir is opened for the water to evaporate into the experimental chamber so experimentation can begin.

## 4.4 Execution

Here it is assumed the instrument was pumped to UHV and then filled with clean water according to section [4.3.4](#). The following is a guide to repeat this measurement with this instrument and software.

### 4.4.1 Getting the Instrument Ready

Turn on all devices (Chillers, Lakeshore, Pfeiffer MaxiGauge)

If the Computer was switched off since the last experiment create the virtual serial port for the Maxigauge

Close the gate valve between the pumping and the experimental chamber

Start pumping the cold fingers and the sold fingers liquid nitrogen reservoirs insulation

Fill the cold fingers liquid nitrogen reservoir

### 4.4.2 Running an Experiment

Start the UI

Click "Init" button and wait for "Done" in the text field

Turn on continuous Temperature measurement

Turn on Logging

Turn on Livestream

Set environmental box temperature to the rough temperature you want to experiment in.

Set reservoir temperature to 1-2 °C above your desired drop temperature

Set cold finger temperature to desired drop temperature or a bit below.

A drop will start to grow.

The drops growth rate can be adjusted but increasing the temperature difference between cold finger tip and reservoir to increase the growth rate or decrease the difference to decrease growth rate.

Stabilize an as big as possible drop by decreasing the temperature difference until the drop is in thermal equilibrium.

Take snapshots whenever you like. They are stored with a timestamp attached. The corresponding temperature and pressure data can be found in the logging files by searching for matching timestamps.

## 4.5 Supporting Measurements

### 4.5.1 Diode Calibrations

The temperature in the instrument is measured using diodes and a Lakeshore controller. The diodes are powered by a  $10 \mu A$  signal from the Lakeshore controller and modify the resulting voltage by changing their resistivity dependant on the temperature. The Lakeshore controller then measures this voltage and uses a set of temperature/voltage values to linearly interpolate a temperature/voltage curve out of. With this curve and the measured voltage a temperature is displayed. Two of the diodes we use for the temperature measurements were bought including a calibrated curve from the company while the other 3 use a standardized curve instead. To improve accuracy we used the calibrated ones to calibrate the others. For this we designed a copper block to mount the diode on one side covered by a cap to avoid temperature gradients in the air around and a heat exchanger from one of our chillers on the other to control temperature. Additionally the setup was placed inside a box that was connected to a nitrogen line to fill the volume and keep a positive pressure to the outside during the experiments to stop ice formation or water condensation depending on the current temperature from influencing the results or damaging the diodes.

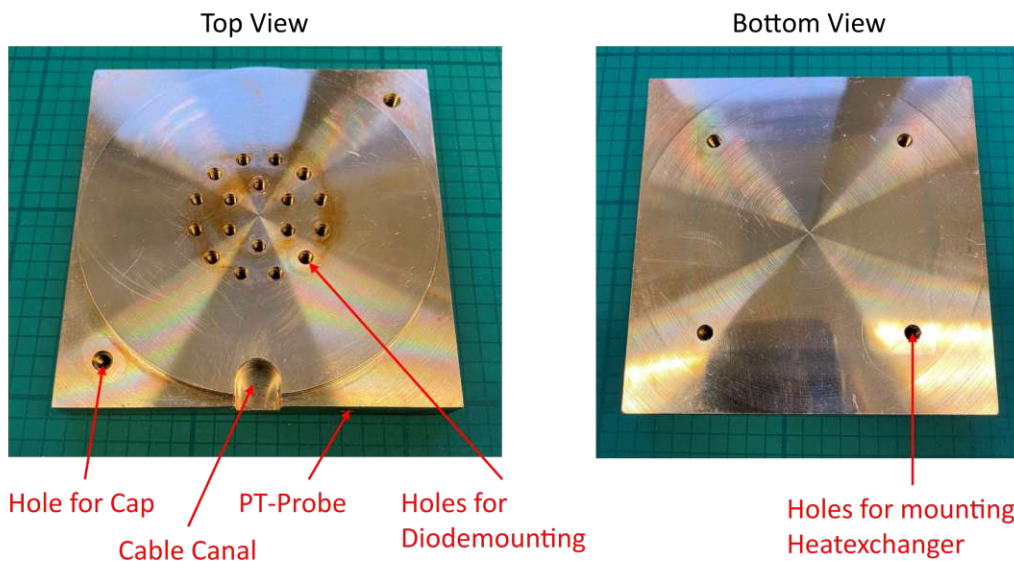
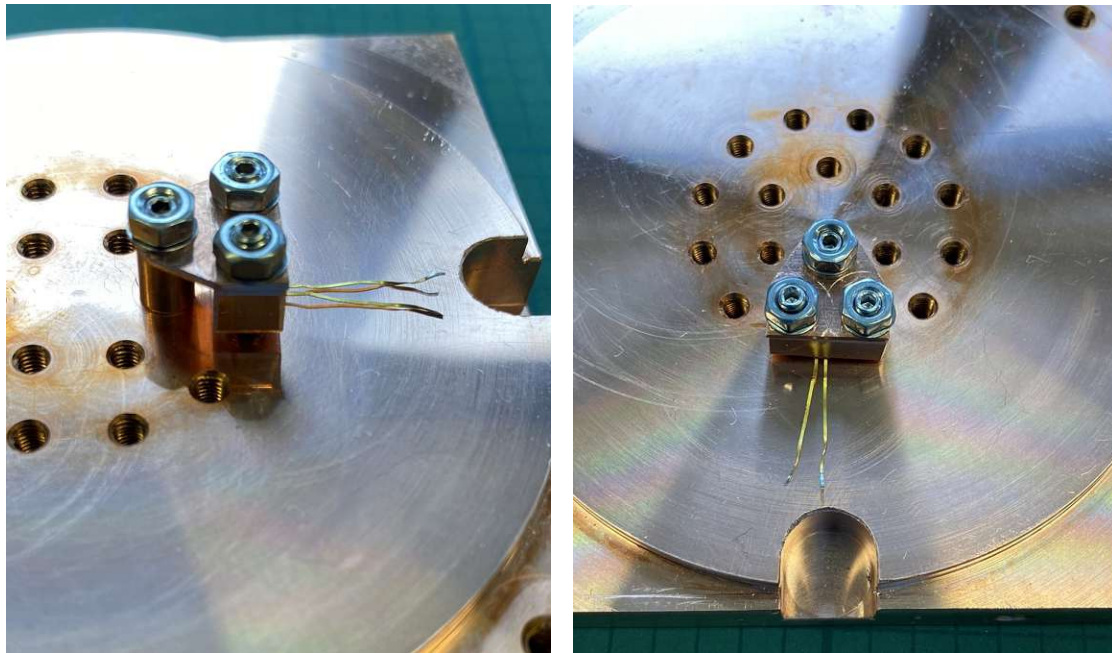


**Figure 4.5.39:** Copper block used for diode calibration. In the top view one can see 6 sets of three holes for mounting diodes (two for the clamp that pushes them down and one for a post that thermally connects the top part of the clamp to the block), holes to mount a cap and the cable canal for the wires the diodes need. On the right in the bottom view there are 4 holes to mount a heat exchanger. Additionally there was an opening on one of the sides for a PT100 Probe to go into. Its position is marked with an arrow and it reaches almost to the other side. The initial idea was to use the measure temperature as a reference point but the PT100 Probe was twice as long as the block was wide so we could not acquire an accurate value with it as it is better suited for measurements of bigger volumes.

The diodes were mounted with a self built copper clamp and had a piece of silver foil underneath and a piece of kapton foil above them. The silver should simulate the silver glue that would later be used to glue the diodes into their final position while the kapton should electrically insulate the top of the diode against the bottom. Since the top clamp part was thermally connected to the bottom by a copper post that can be seen in figure 4.5.40a it is also electrically connected and would short circuit the diode without the kapton in place. The nuts had spring washers underneath and were tightened using a torque wrench to 1 cNm. The 6 positions for diodes are ordered in a circle in case there would be any temperature gradients between the middle and the edged of the block.



(a) Side view of a mounted diode. A small copper block acts as clamp for the diode while a cylinder next to it connects it thermally to the bottom via a copper plate. For the nuts spring washers were used and tightened to 1 cNm using a torque wrench.

(b) Top view of one mounted diode with 5 more empty diode slots. During experiments a second diode was mounted on the opposite position in the circle. For calibration of more diodes the second diode was exchanged and multiple runs of the experiment carried out.

**Figure 4.5.40**

To prepare the experiment first two diodes were mounted like it is shown in figure 4.5.40. One calibrated diode in the position shown in the picture and one to be calibrated diode on the opposing side in the circle. Then 0.25 mm kapton insulated copper wires were soldered between the diodes leads and a Lakeshore input cable. The copper wires were also fixed using another copper clamp to stop unwanted movement that might damage a diode. The cap was put on with the wires reaching outside via the cable canal and the heat exchanger was mounted to the bottom of the copper block. The PT100 Probe was placed in its position and the whole installation put into a box that can be seen in figure 4.5.41. The Box had holes in its side to allow the hoses for the heat

exchanger but also our nitrogen line and cables to enter and the inside was insulated with styrofoam. The box was then filled with nitrogen with some flow kept going to have a positive pressure against the outside and avoid air and therefore water entering the system during experimentation. With this setup one run of the experiment allowed for one diode to be calibrated before the box needed to be opened and the diode exchanged.

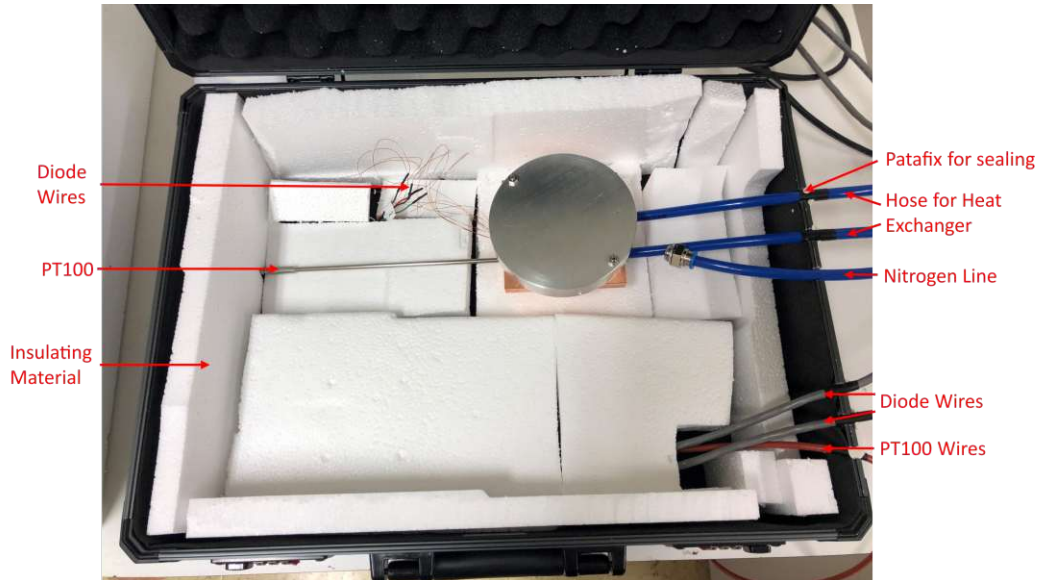


**Figure 4.5.41:** Opened box for the diode calibration. The chiller is connected via two hoses to the heat exchanger on the bottom of the copper block to control the temperature in the box. A nitrogen line to avoid water condensation damaging the diodes and some insulating material to stabilize the temperature and avoid gradients close to the calibrating setup.

To start the experiment the chiller would then be set to different temperature values between  $-50\text{ }^{\circ}\text{C}$  and  $70\text{ }^{\circ}\text{C}$  in steps of  $10\text{ }^{\circ}\text{C}$  with a smaller step size of  $5\text{ }^{\circ}\text{C}$  between  $-10\text{ }^{\circ}\text{C}$  and  $30\text{ }^{\circ}\text{C}$ . Since most of our measurements are taken around room temperature  $17.5\text{ }^{\circ}\text{C}$  and  $22.5\text{ }^{\circ}\text{C}$  were chosen as additional temperature points. For each temperature the system would be given time to reach equilibrium before a measurement was taken. This was done because the drop later will also be photographed in thermal equilibrium. Before showing measured values it should be mentioned that the chillers PID was set to keep the temperature of the chillers internal bath at the set value. The initial idea was to use the PT100 Probe as input for the PID but since it was not possible to have its entire length close to the experiment and instead only a fraction of it was inside the copper the temperature the reference diode and the PT100 would measure were offset substantially. Therefore the exact temperature the chiller would provide was not used as reference but should only supply a stable temperature value for the diodes to measure so offsets between the chiller set temperature and what temperature the diode would be kept at didn't matter for the experiment.

For verification of the method a first measurement was taken using both calibrated diodes (serial numbers D6105593 and D6105595). D6105593 was defined as the "reference" diode and D6105595 was defined as the "test" diode. Using the above procedure



**Figure 4.5.42:** Closed box in the state the Measurement was taken in.

for preparation to each of the 20 chosen temperature values 300 sets of data points were taken with one set containing the temperatures of both diodes, the set temperature, the chillers internal baths temperature, the temperature the PT100 measured, the chillers pumping level and the room temperature that was measured with a second PT100. The pumping speed was saved since we expected it to influence the offset between the chiller internal temperature and the temperature at the heat exchanger. Usually the heat exchanger would be offset toward room temperature since the fluid the chiller uses has to travel through hoses that are exposed to the room temperature. Also the difference between the two values the diodes take were calculated and stored in the same file. Between sets about 1 second would pass. The averages over the 300 data points for each temperature value then was collected in a results file that contained for each of the set temperatures the average reference diode temperature, the average test diodes temperature, the average difference between both, the standard deviation of this difference and the test diodes voltage which was calculated by interpolating the used curve data to the temperature measured by the diode using linear interpolation. Some of the collected data from the initial run can be seen in table 3. The standard deviation of the difference was always of the order of magnitude of  $1e-3$ . Especially in the range that most interests us which is around room temperature the two diodes agree precisely which means the designed device is suitable for calibrating the uncalibrated diodes.

For calibrating the diodes now the calibrated diode with the serial number D6105595 was taken of and replaced with an uncalibrated one and the above process was repeated. Out of the created results file the reference temperature and the test voltage were used to create a custom temperature/voltage curve for the currently mounted test diode. To

Setpoint [°C]	Reference [°C]	Test [°C]	Difference [°C]	Test Voltage [V]
70	69.250	69.275	0.025	0.4611
60	59.449	59.470	0.021	0.4840
50	49.600	49.612	0.012	0.5070
40	39.768	39.773	0.006	0.5298
30	29.916	29.917	0.001	0.5526
25	24.976	24.975	-0.001	0.5640
22.5	22.525	22.523	-0.002	0.5696
20	20.063	20.060	-0.003	0.5753
17.5	17.610	17.607	-0.004	0.5809
15	15.150	15.145	-0.004	0.5865
10	10.261	10.255	-0.006	0.5977
5	5.293	5.284	-0.010	0.6091
0	0.438	0.432	-0.006	0.6202
-5	-4.412	-4.419	-0.007	0.6312
-10	-9.220	-9.228	-0.008	0.6421
-15	-14.026	-14.031	-0.004	0.6529
-20	-18.745	-18.754	-0.008	0.6636
-30	-27.988	-27.996	-0.008	0.6843
-40	-37.175	-37.193	-0.019	0.7048
-50	-46.091	-46.113	-0.022	0.7246

**Table 3:** Temperature data from both calibrated diodes (serial numbers D6105593 and D6105595). The difference between them is noticeably smaller than the error of 35mK claimed by the company. Also the voltage of one of them is shown. This will be used in the actual calibration to create the custom curve for the Lakeshore. The values for Reference, Test and Difference are averages over 300 measurements. The Test Voltage the corresponding single value to the average Test Temperature.

create the curve we took a standard curve, removed the values between  $-50\text{ }^{\circ}\text{C}$  and  $70\text{ }^{\circ}\text{C}$  and added our measured ones. This means the diodes are still usable in their whole temperature range but use a standard curve outside our calibrated range. The custom curves were saved on the Lakeshore as .340 files and are named by their corresponding diodes serial number. The data from these calibrations can be found in the appendix in section [7.1](#). With this method custom curves for the diode serial numbers D6107256, D6107259 and D6107924 were created.

## 4.6 Optics

The optical system is responsible for gathering the actual data the surface tension is derived from. Systematic errors here directly translate to an error in our results, therefore we need to take as much care in the design of it as we did for temperature and purity control. The goal is to be able to extract the shape from any given drop from an image as precisely as possible. To achieve this a few different sources of errors have to be considered. Namely there are distortions caused by the lens, uncertainty of the exact magnification and Fresnel diffraction.

To control these factors the system was designed consisting of a camera using a telecentric lens and a back illuminator made of a uniform light source. Telecentric lenses have the advantages against ordinary lenses that their magnification is constant across their whole depth of field and therefore distort the image less than ordinary lenses would. Additionally we used a micrometer dot grid to create reference images that are used to undistort images of drops programmatically that were caused by the lens. Regarding Fresnel diffraction we built a small test setup where we took images of a calibration ball that is  $6 \pm 0.001\text{ mm}$  in size with different apertures and intensities of the back illuminator to estimate the influence. On one hand we expected a too small aperture to lead to spacial coherent light in the chamber which is beneficial for Fresnel diffraction on the other hand to high intensity could lead to saturation of the cameras sensor which would move the drops edge causing the drop to appear smaller in the resulting image. Therefore we expected decoherent light in frequency and space to be the ideal case.

### 4.6.1 Telecentric Lensing

The constant magnification is achieved by placing an external aperture screen at the front focal point of the lens to create a new principle point for the System

This is achieved by placing an external aperture screen  $A'$  at the front focal point of the lens to create a new principle point for the system. For the conventional lens the principal ray  $R$  goes through the principle point  $O$  of the lens and hits the imagine screen behind. Is the screen in position  $I_f$  the imagine is in focus and if we move the screen to position  $I_2$  the imagine gets out of focus. In this state we can still find the original edge by finding the center of the added blur but the position has changed. This means by moving the imagine screen to a different position in the systems depth of field we change magnification. For the telecentric system on the other hand the principle ray  $R'$  goes through the new principle point  $O'$  and is parallelized against the optical axis. If we now move the Imaging screen away from the focal position again to  $I_2$ , for example, we still have blur added to the image but the center point position does not change anymore.

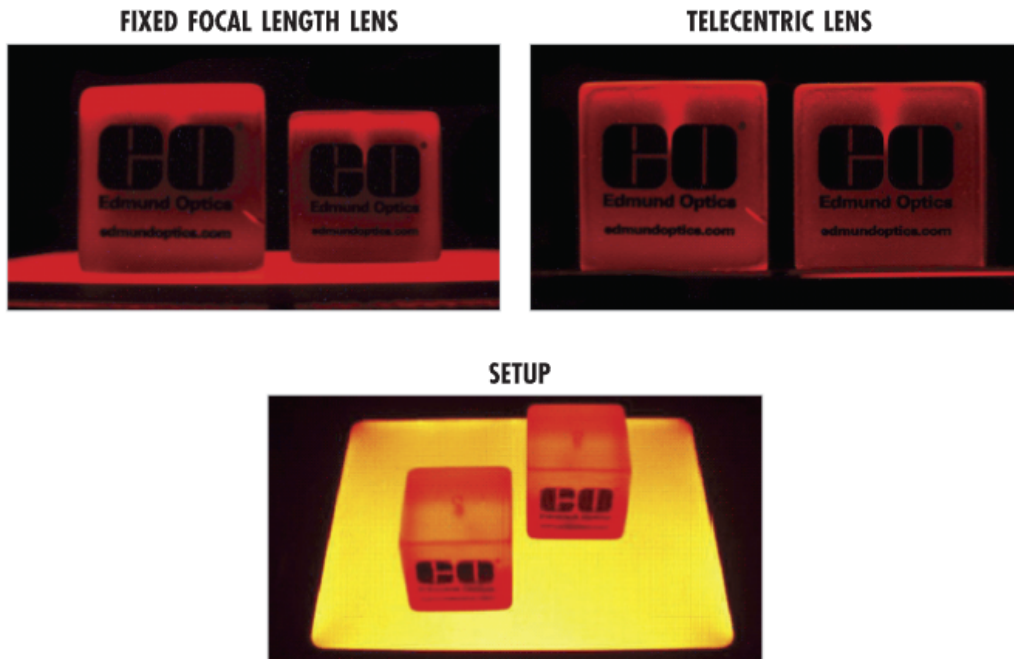


**Figure 4.6.43:** This figure shows the difference in an image taken with a telecentric and an ordinary lens. With the constant magnification across the whole depth of field objects that are in different distances are still the same size in the picture taken of a telecentric lens while being differently sized in a picture taken with a ordinary lens.

We therefore achieved constant magnification across the whole depth of field. [27]. This is visualized in figures 4.6.44 and 4.6.45.

The lens we used is a large format telecentric lens from Edmund optics with a working distance of 111 mm, a primary magnification of  $0.9x$  and  $\pm 0.65\text{ mm}$  depth of field.

#### 4.6.2 Experiment to estimate Fresnel Diffraction effects.

For the optimal light source we did a calibration of the optical system using some item profiles to mount the camera and the light source opposite each other and a calibration ball in between that is  $6[\pm 0.001]\text{ mm}$  in size. Additionally a tube with a hole for the ball and post was positioned on top and the room darkened so that other light sources would not disturb the experiment.

After experimenting with various different voltages for the light sources dimming, pinhole sizes, lens apertures, exposure times and fitting parameters we concluded that an extreme of any of them causes worse results. To low imagine intensity causes the drops profile to be overestimated in size and to high intensity to be underestimated. Intensity was determined by adding up every pixel of the picture and is a result of a combination of the dimming voltage of the light source and the exposure time. We could not find a difference in pictures with high exposure and low voltage vs pictures with high voltage and low exposure if they had the same total intensity value. This demonstrated the importance of keeping reflections in the optical system under control as well as we can, to avoid the edges of the drop to be illuminated from the side by light rays being

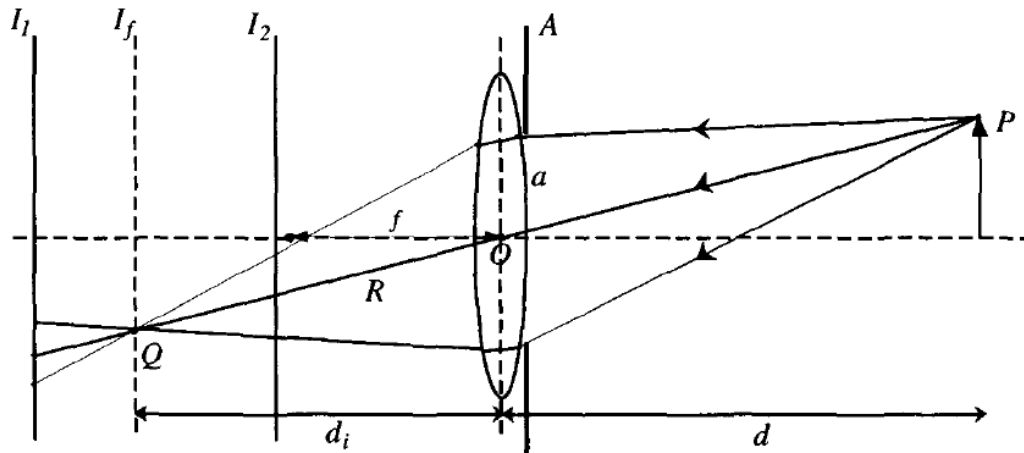


**Figure 4.6.44:** Conventional lensing ray-diagram. Light gets focused by a lens for imagine processes. Moving the imagine plane does not only defocus the imagine but also the magnification changes. This comes with the potential to increase the error of our measurement due to the possibility of inaccuracy in the used magnification value. [27]

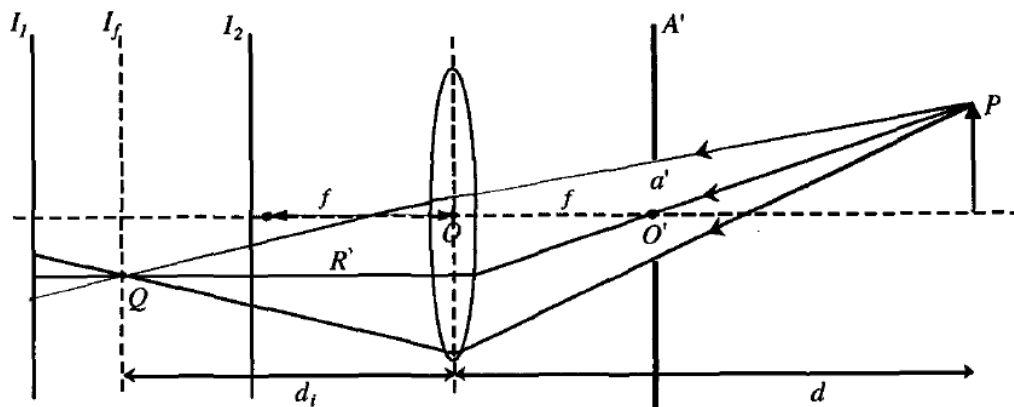


**Figure 4.6.45:** This ray-diagram shows the simplest version of telecentric lensing. An aperture screen  $A'$  is placed at the front focal length of the lens. Like this the principle Ray  $R'$  runs through the middle of  $A'$  and hits the lens in a way so its parallelized with the optical axis of the lens. Moving the imagine plane still causes the image to be defocused but does not change the magnification anymore. Like this we can identify the systems magnification ones and then use the value for the full depth of field without an increased error due to magnification uncertainty. [27]

reflected from the walls of the chamber. This also lead to a optimal pinhole size when it was a bit bigger than the drop itself. Both a too big and too small light source caused similar effects to too high or low intensity values. In the end we managed to fit the calibration balls profile with an error of  $\pm 0.004 \text{ mm}$ . This error likely stems from lens distortions from the telecentric lens. To eliminate it we used a micrometer dot grid to



**Figure 4.6.46:** A picture of the optical calibration setup without the cover. On the left there is the lens with the camera attached to it and on the right the back illumination. In the middle on a small post there is the calibration ball.



**Figure 4.6.47:** A picture of the optical calibration setup with the covers on. The tube has a small hole in the bottom to allow the calibration ball to go in. on the right there is one of the various shutter sheets we produced in position. they were placed there to test the influence of the light sources size on the fitting quality.

take some reference pictures for the Matlab function "undistortImage" to counteract them. The reference images were taken on an optical table with the micrometer grid mounted onto a micrometer board to ensure optimal focus. Additionally we also did a scan over different levels of focus that revealed that the ideal case is perfect focus with as little blur as possible. One example picture taken during any of these experiments is shown in figure [4.6.49](#).

Ultimately however this experiment is not fully finished since it was not conducted in the real chamber. The main take away from it is that our imaging process works as intended but we need to undistort the images. The final calibration of the optical system will be done on the finished machine and happens outside this thesis.

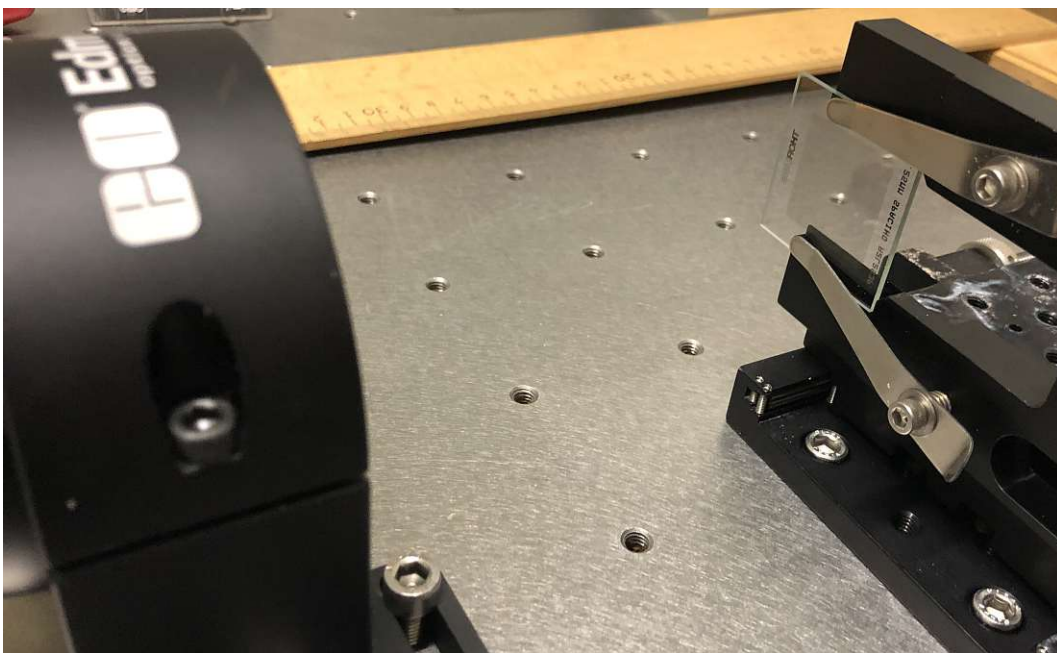


**Figure 4.6.48:** This picture shows how the reference images for undistortion have been acquired. A grid made of  $1\mu\text{m}$  in size in regular distances was mounted on a micrometer board on an optical table to be able to perfectly adjust the grids position to be in focus for the telecentric lens. The images were then used as reference pictures for the Matlab function "undistortImage". ??? are the dots that size or the distances?

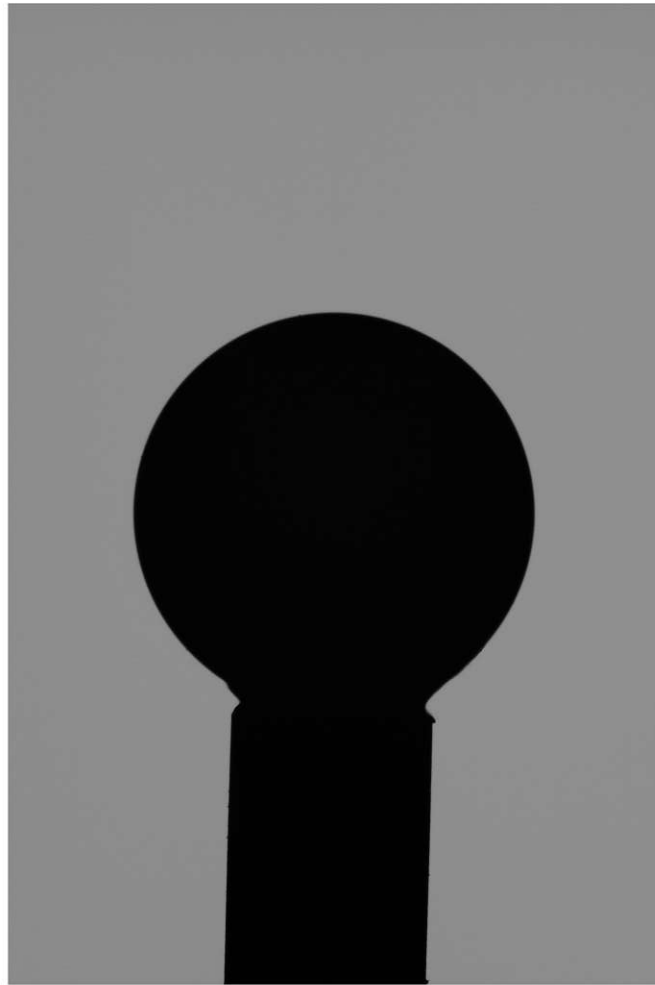


**Figure 4.6.49:** One image from the initial calibration experiment for the optical setup. The ball used is certified to be  $6[\pm 0.001] \text{ mm}$  in size and was mounted by glueing it with a post. It was taken great care to avoid glue anywhere but the connection spot to not alter the precise size with it.

## 5 Results and Discussion

In this chapter results of some initial measurements will be presented and discussed with a focus on how the measurements can be improved for the future. First though, we will discuss the drop creation process and what shortcomings we found that need to be worked out.

### 5.1 Drop creation

Ultimately the drop creation process via condensation from the gas phase was successful. The chamber can be pumped to UHV and the water inserting process worked as intended. We are also able to grow drops on the cold finger tip in a controlled manner and reverse the process to bring the water back to the reservoir. The optical system is capable of taking in focus pictures of the drop with high enough frame rate to use it as a live view in the growth process. However a few improvements are still worked on.

The problem was that in this initial measurements we had to cool the cold finger to  $-140\text{ }^{\circ}\text{C}$  for water to condense at the cold finger tip and a drop to form. The gold foil likely was too thin to fully fill the gap between the cold finger tip and the tip heater which due to the surfaces being not perfectly parallel. This lead to thermal contact only on a tiny fraction of the total surface. The issue was fixed later by replacing the gold foil with a small amount of indium that was molten for a short time to ensure good thermal connection. However, this change is not included in the data in this thesis. Certainly,  $-140\text{ }^{\circ}\text{C}$  is no accurate value for the temperature of the drop itself as the drop was still observed to be liquid; oscillations of the drops surface were observed. That's why for the following discussion for the temperature of the tip a value was used that was measured on the reservoir. Since the images were taken with the drop in equilibrium and not growing or shrinking we assume the temperature difference between the water of the drop and the water in the reservoir to be small.

While we were able to form a drop it can only do so in a very slow process. Further investigation showed that the water condenses on tip's bottom surface first as intended but after further condensation, water growth shifts to the sidewalls of the cold finger tip. From there the droplets cannot pass the sharp edge between the bottom surface and the sidewall to join the main drop until they reach a certain size. In some cases the droplets get so big that instead of merging with the main drop on the bottom surfaces a droplet falls and takes the main drop with it. This causes failed growth attempts that slow down the experiment. A solution to this would be to change the sharp edge of the tip to a radius to alone droplets collected on the sidewalls slide into and merge with the main drop more easily.

A series of figures showing a successful drop growth process can be found in figure [5.1.50](#) where (a) shows the tip with some water already collecting on the bottom surface of the cold finger tip. (b) shows the drop after the first growing phase on the bottom surface has reach its maximum and growth on the sidewalls has already collected rather large amounts of water. In (c) one can see that the droplets on the sides merged with the main drop successfully. From there it was possible to grow the drop to a maximum

volume that is visible in (d).

## 5.2 Water surface tension in its pure vapour

Figure 5.1.51 shows one example picture out of 43 that were taken in the first session with the instrument and have a big enough drop to use them as an input for fitting the surface tension. Measurements were undertaken for one drop at approximately three different temperatures: 15.0 °C, 20.1 °C and 21.0 °C. The exact values can be found in table 4. The acquired surface tension values are shown plotted against their corresponding temperature values in figure 5.2.52. It is clear that for the temperature around 20.1 °C we have a rather large statistical spread, while for those around 15.0 °C and 21.0 °C the spread is smaller. Generally, we can attribute this to larger instrument vibrations for the 20.1 °C drop. To demonstrate this we can plot the surface tension values chronologically against the index number of the corresponding image as seen in figure 5.2.53. We can see that the biggest spread is coming from the first 8 images when vibrations in the instrument were largest. As the vibrations dampen out over time, the surface tension values settle to a tighter spread of values. We can also identify the 5 images that were taken at around 15.0 °C since the surface Tension values of them are all higher compared to the rest of the data. Also the last three images being a bit lower is expected since they were taken at about 21.0 °C. Both shifts are reconfirmed in figure 5.2.54.

This can be further investigated via analysis of the behaviour of the Bond number and the apex radius. The Bond number for each image is plotted chronologically in 5.2.55 and shows that while we can see bigger deviations in the first 8 pictures, later images show a tighter spread of values. There seems to be a slight decrease in the Bond number for the first 20 images, though this can be attributed to a slow growth of the drop and a subsequent change in its shape and generally this shouldn't affect the final conclusions. Similar analysis and conclusions for the behaviour of the apex radius are shown in figure 5.2.56. Again, for the first 10 images or so there is a large spread in apex radius values on the order of 10s microns.

The source of the vibrations is likely from human activity in the lab during the experiment. The first 8 images taken were the first drops ever formed with the instruments with three experimentalists in the lab trying to grow drops as large as possible. This includes first attempts on how to operate the leak valve for the liquid nitrogen cooling, which is directly connected to the cold finger tip, and through which vibrations can be easily imparted into the drop. With the drop "bouncing" up and down the measured apex radius would alternate between a too large a value when the drop is at the top of its amplitude or to small of a value when the drop would be stretched to the minimum of its amplitude. With more experiments on how to operate the instrument people walked around less which reduced the impact of vibrations which leads to a smaller statistical spread in the data and an improvement in the accuracy of the measurement.

The most important take away from this set of measurements is that controlling vibrations is of big importance for this experiment. Aside from handling the instrument with more care and turning off pumping during experimentation a possible solution would be pneumatic legs to decouple the chamber from vibrations in the floor. This is

Surface Tension (mN/m)	Pressure (mbar)	Temperature (°C)	Radius (mm)
72.693	22.57	20.2	2.298
72.894	22.57	20.2	2.288
71.936	22.57	20.2	2.366
74.252	22.57	20.2	2.372
72.988	22.57	20.2	2.294
72.925	22.57	20.2	2.247
73.691	22.57	20.2	2.213
72.032	22.57	20.2	2.316
72.785	21.77	20.15	2.245
73.107	21.77	20.15	2.249
73.15	21.77	20.15	2.242
73.01	21.77	20.15	2.236
72.943	21.77	20.15	2.233
72.895	21.77	20.15	2.228
72.641	21.77	20.15	2.218
72.957	24.056	20.1	2.268
72.573	24.056	20.1	2.191
72.607	24.056	20.1	2.189
73.005	24.056	20.1	2.189
73.132	24.056	20.1	2.187
72.576	24.056	20.1	2.183
72.693	24.07	20.15	2.162
72.87	24.07	20.15	2.157
73.44	22.35	20.06	2.203
73.014	23.67	20.1	2.172
72.958	23.72	20.1	2.164
73.032	24.01	20.17	2.216
73.028	23.99	20.17	2.213
73.015	24.03	20.18	2.191
73.004	23.96	20.17	2.176
72.986	23.98	20.17	2.179
72.876	23.94	20.17	2.18
72.91	23.95	20.17	2.175
72.92	23.97	20.17	2.171
72.915	23.98	20.17	2.171
73.76	17.63	15.34	2.218
73.532	17.63	15.33	2.216
73.364	17.66	15.31	2.216
73.677	17.65	15.31	2.221
73.902	16.21	14.45	2.231
72.827	25.22	21.094	2.19
72.793	25.33	21.1	2.182
72.62	25.5	21.103	2.162

**Table 4:** Data from the drops we measured. The first column shows the surface tension values we calculated using pendant drop tensiometry after fitting a bond number to an image of the drop using our fitting script. The pressure is measured inside the experimental chamber and represents the vapour pressure. The temperature is taken from the reservoir. As discussed we had problems with the thermal conductivity in the cold finger tip. Since the drop and the reservoir are in equilibrium during experimentation we expect only a very little temperature difference between them. So using the reservoirs temperature as input for our calculations on these initial measurements adds only a small error. The radius value is the radius of the drop that we extracted with our fitting script.

consistent with a group in Mexico that tried to quantify the influence of vibrations on the resulting surface tension measurement in this paper [25].

In light of this discussion, the measurements from picture 30 onwards show a smaller spread of results and thus can be readily compared to previous literature results for the surface tension with air. However the data from literature was taken with various different experimental techniques. Notably the capillary rise method is prominently represented but this technique requires a number of assumptions and corrections. Some example assumptions are the capillary radius and the contact angle between the capillary and the fluid which are both typically assumed to be uniform along the full length of the capillary which is likely not true down to a micron. Also the exact shape and volume of the meniscus in capillary rise experiments are often subject to assumptions and corrections. In our pendant drop experiments, on the other hand, we apply an accurate correction for the full field of the lens used in the optical setup but otherwise no assumptions or corrections are necessary. For this reason we decided to compare our results not to the total of all studies in the literature but only with other pendant drop experiments. As such, in figure ?? is plotted the literature line from the international standard, our measured data points and data points taken from 4 other literature studies that also used the pendant drop method [4] [23] [11] [19].

Both our experiments and the experiments with the pendant drop method in literature produce surface tension values higher than the international standard. This hints to the fact that different methods of measuring surface tension produce different results. The average offset of one of our measurements comes out to +0.195 while the average offset from pendant drop literature is +0.139. The data support these numbers can be found in table 5 and table 6. Considering that the literature measurements have been measured in air this is consistent with the work of Massoudi et al. [16] that shows that the presence of any gas reduces the surface tension. Specifically Nitrogen and CO<sub>2</sub> have large impact while also taking the largest share of the composition of our normal air. Therefore after removing contact of the water to air we expect the surface tension to increase.

This means while prior experiments presumed pristine water this is potentially not true under ambient conditions. After removing air from the experiments we see an increase in surface tension like one would expect when removing Nitrogen or CO<sub>2</sub> from the water. The many gas components and contaminants in air therefore change the surface tension of the water-air interface via some mechanism(s). This means that, when discussing the Jones-Ray effect for example, contamination via the atmosphere has to be considered. In particular, the added salt could be changing how these mechanisms change the water-air surface tension. The same might be true for contact angle experimentation like it is mentioned for graphite in section 2. The contaminants in the air are readily adsorbing at the graphite interface affecting all the interfacial phenomena. However air consists of more species of contaminants than Nitrogen and CO<sub>2</sub> and more work is needed to assess the influence of the individual components.

In the end, these results show that for accurate and representative surface tension results, measurements really need to be conducted in a clean and controlled environment.

Description	Temperature [°C]	Surface Tension [mN/m]	Diff. to Literature	Error
Cheng 1990	21.5	72.75	0.245	±0.06
Pallas 1990	20	72.869	0.129	±0.035
Pallas 1990	25	71.989	0.019	±0.035
Jennings 1988	25	72.1	0.130	±0.32
Semmler 1996	25	72.14	0.170	±0.05
Average			0.139	
Standard Deviation			0.073	

**Table 5:** Data from pendant drop experiments in literature that was used to compare to.

Index	Temperature [°C]	Surface Tension [mN/m]	Diff. to Literature
30	20.17	73.004	0.291
31	20.17	72.986	0.273
32	20.17	72.876	0.163
33	20.17	72.910	0.197
34	20.17	72.920	0.207
35	20.17	72.915	0.203
36	15.34	73.759	0.311
37	15.33	73.532	0.082
38	15.31	73.364	-0.089
39	15.31	73.677	0.225
40	14.45	73.902	0.321
41	21.094	72.827	0.261
42	21.1	72.793	0.228
43	21.103	72.620	0.055
avg			0.195
std			0.109

**Table 6:** Our data that was considered for the comparison

Temperature (°C)	Surface Tension (mN/m)	Pressure (mbar)	Radius (mm)
14.45	73.902	16.21	2.233
15.33(1)	73.6(2)	17.64	2.218(2)
20.14(5)	72.9(4)	23.17	2.22(6)
21.100(4)	72.75(9)	25.35	2.18(1)

**Table 7:** In this table the data from table 4 is combine into 4 temperature points over which we averaged. The errors are created from the standard deviation. In the first row its missing since we only had one data point at this temperature and therefore no standard deviation.

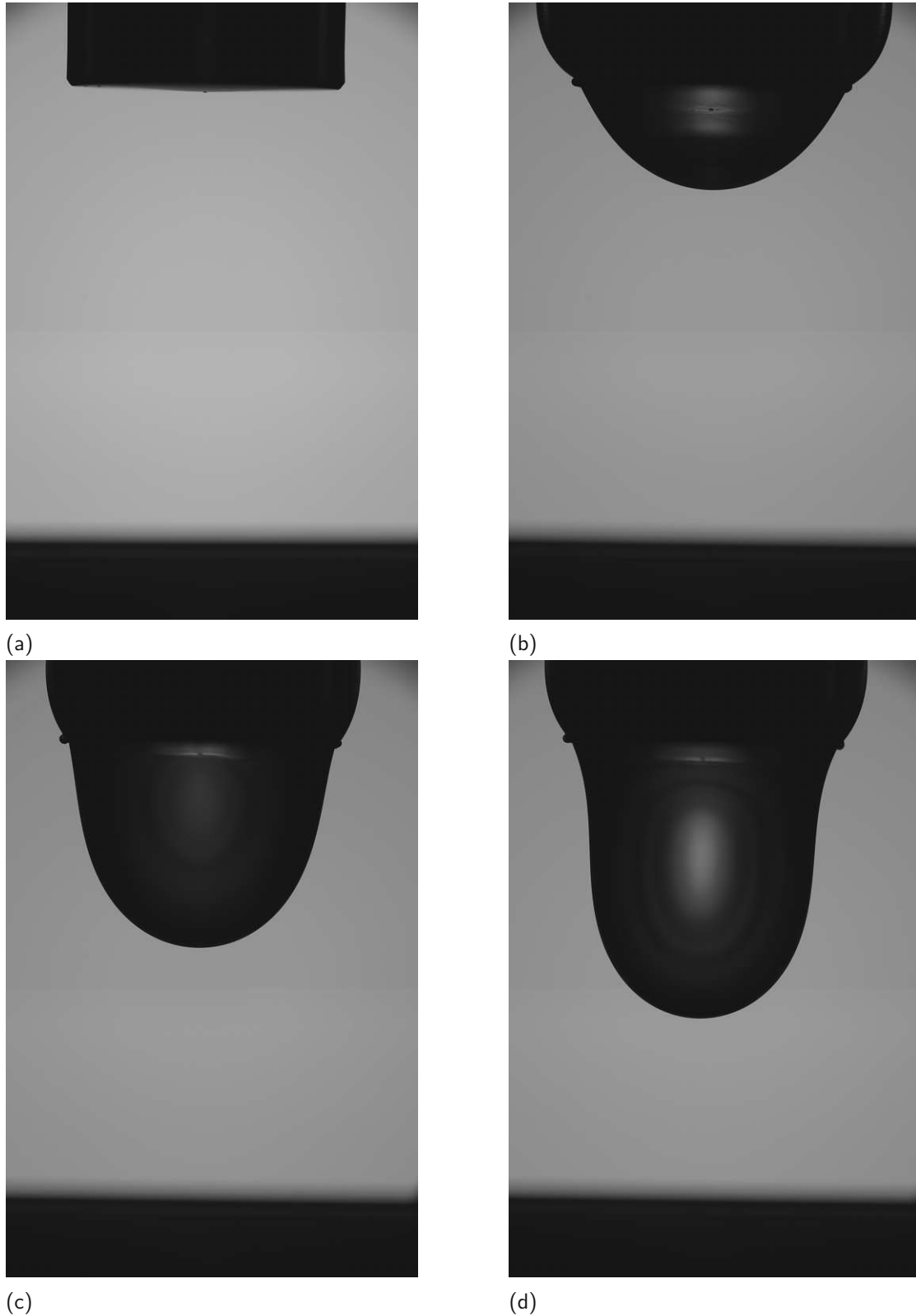


**Figure 5.1.50:** Drop growth process starting from the top left we can see the bare tip. The drop grows on the bottom surface of the tip until it reaches the size shown in (b). At that point the condensation process switches to the sidewalls of the cold finger which is also shown in (b) until the side drops grow big enough to slip over the edge of the tip visible in (a) and merge with the main drop after which a new sub-drop grows on the sidewall. In (d) we can see a drop close to the maximum volume achievable with the setup.

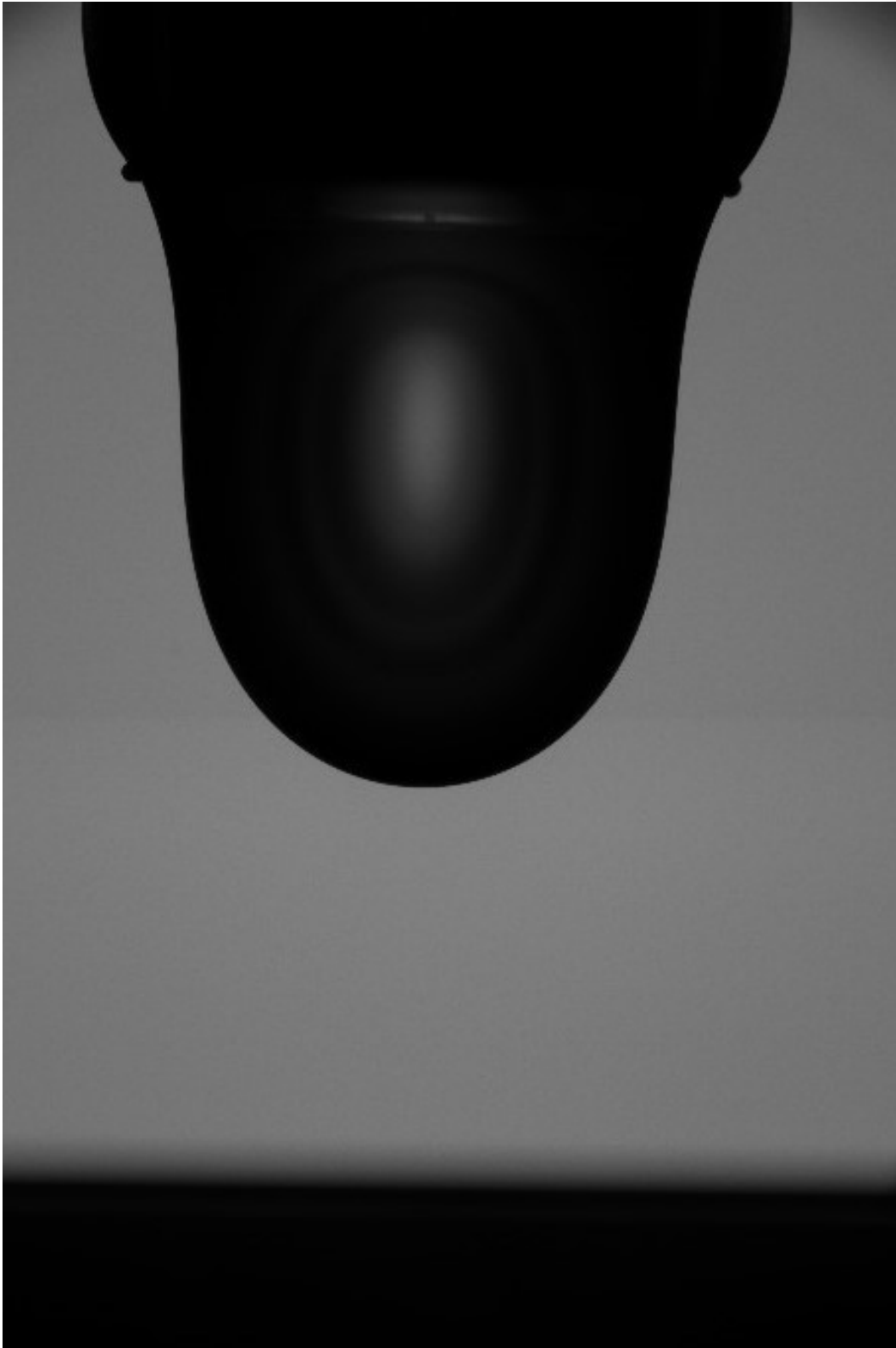
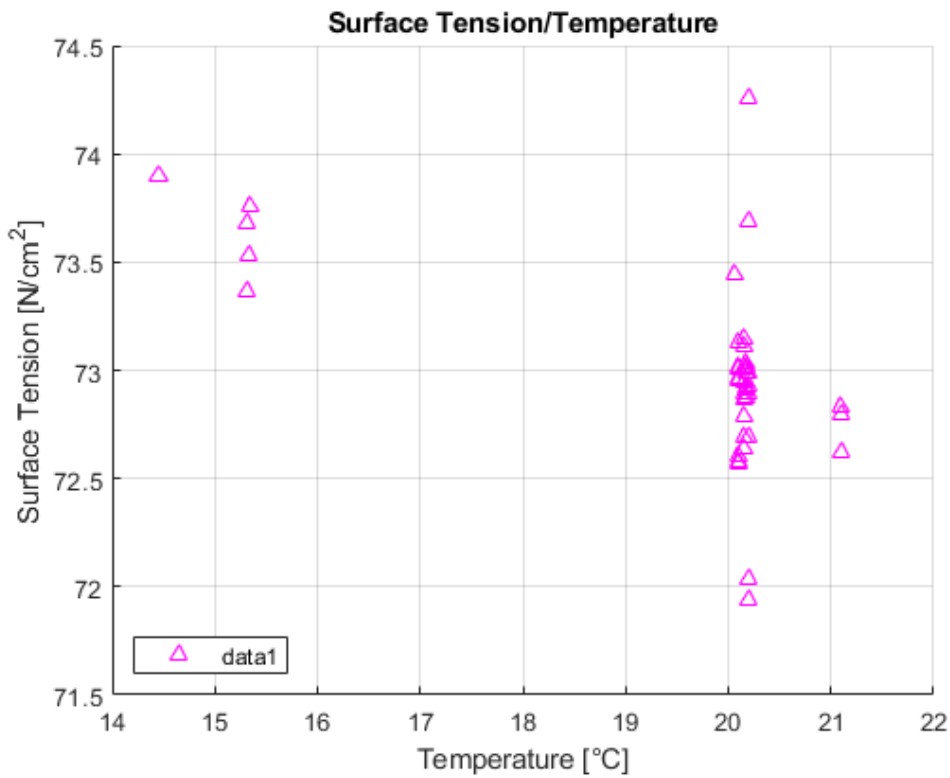
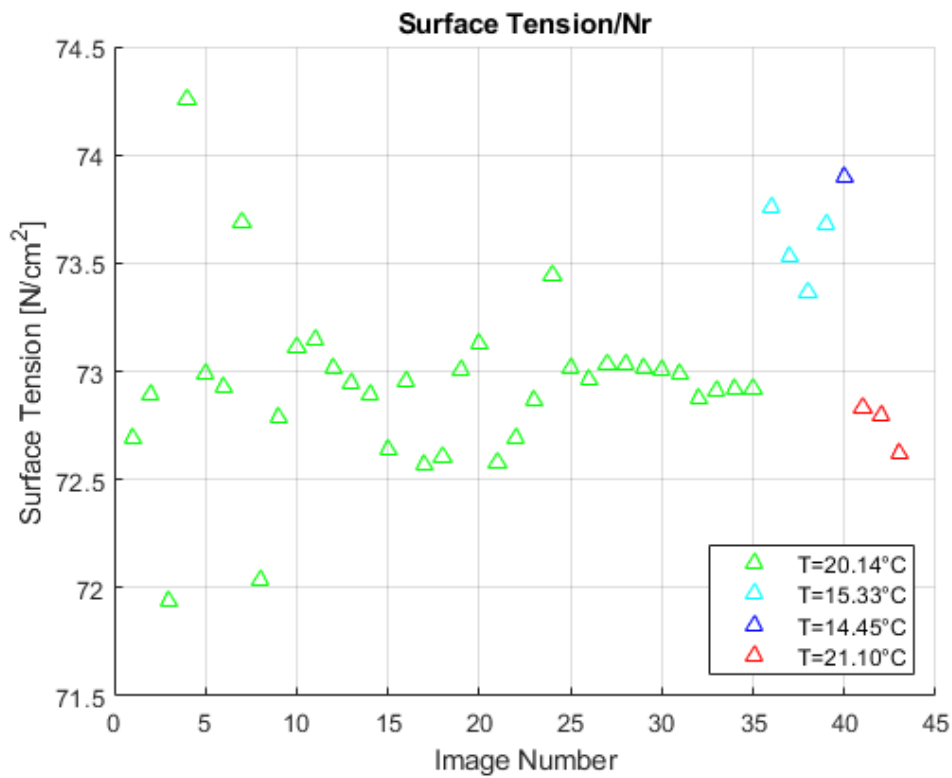


Figure 5.1.51



**Figure 5.2.52:** This graph shows the surface tension plotted against the temperature. Due to the mentioned problem with thermal conductivity in the cold finger tip the temperature was taken from the reservoir which since our experiments take place in thermal equilibrium should be very close to the actual temperature of the drop. The results show a big spread in our results for those around 20.1 °C which should turn out to be caused in part by vibrations.



**Figure 5.2.53:** This graph shows the surface tension plotted against the image number which corresponds to a chronological order for the images. The differing colors represent different average temperature values.

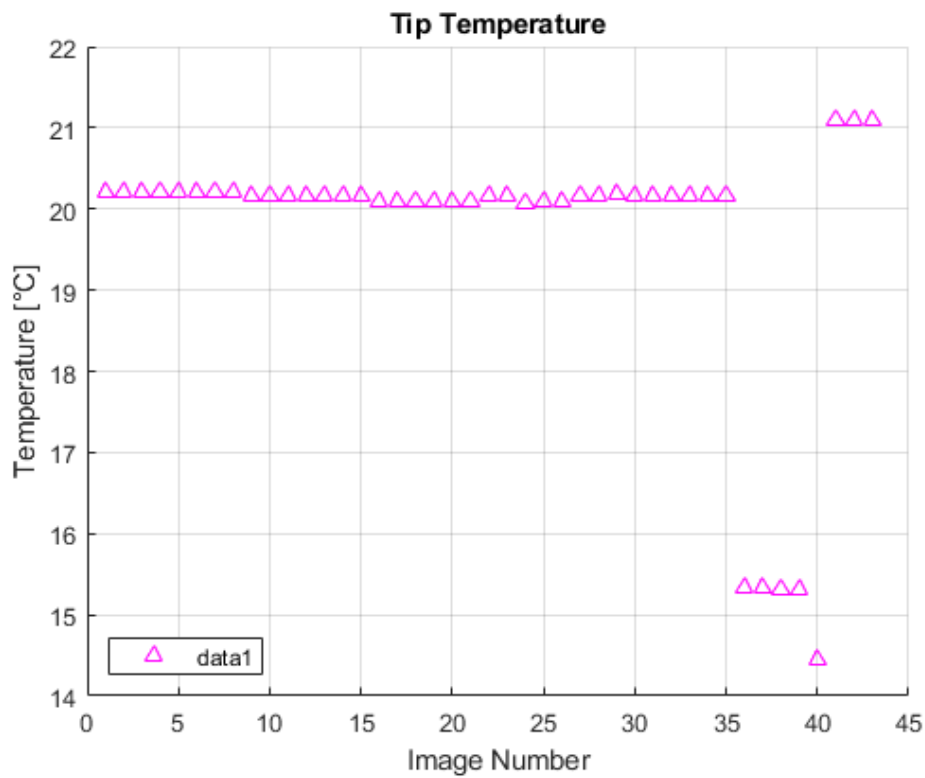


**Figure 5.2.54:** This graph shows the tip temperature plotted against the image numbers. Initially room temperature was chosen as working point but later other temperatures were tested.

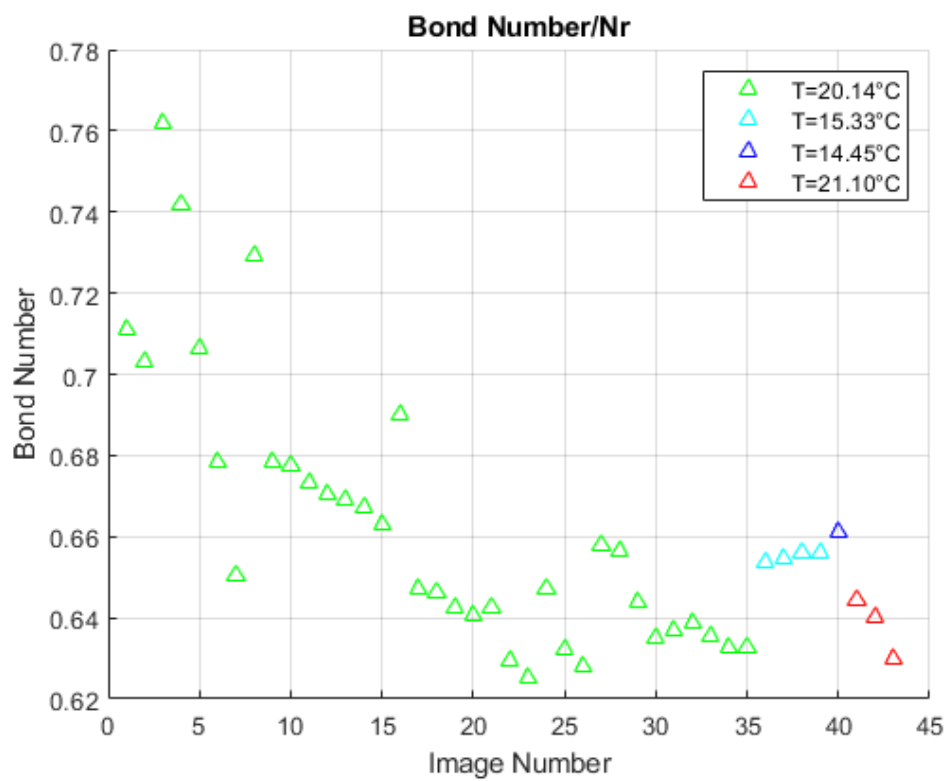


**Figure 5.2.55:** This graph shows the bond number plotted against the image number which corresponds to a chronological order for the images.

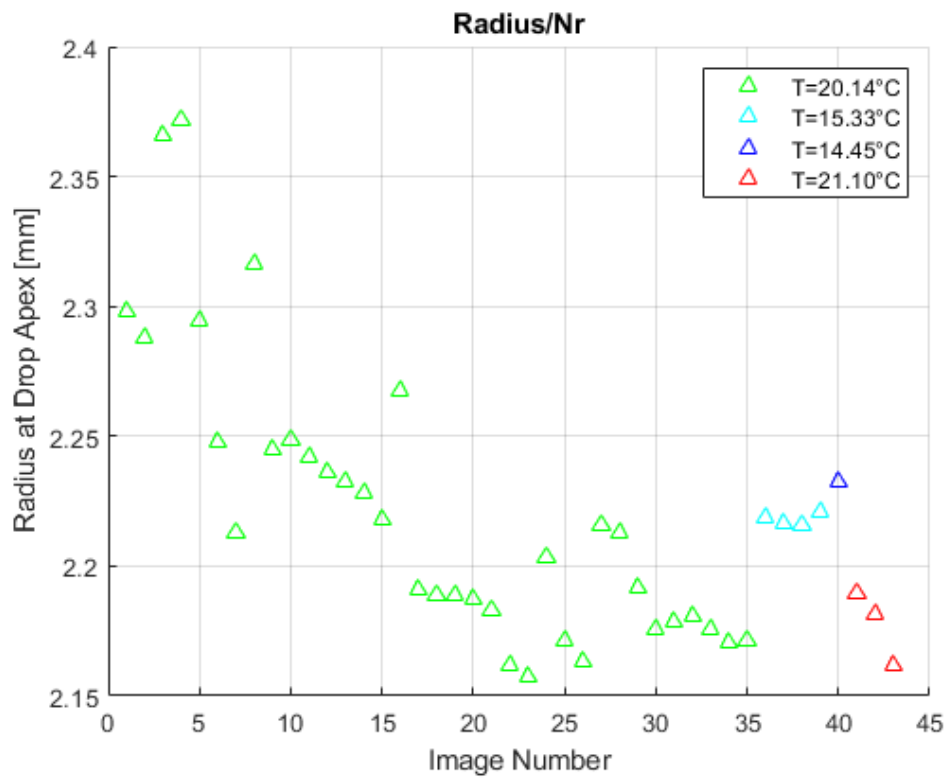


**Figure 5.2.56:** This figure shows the drop radius plotted against the image number. It was created to further investigate the effect of vibrations. The colours differentiate between the average reservoir temperatures.

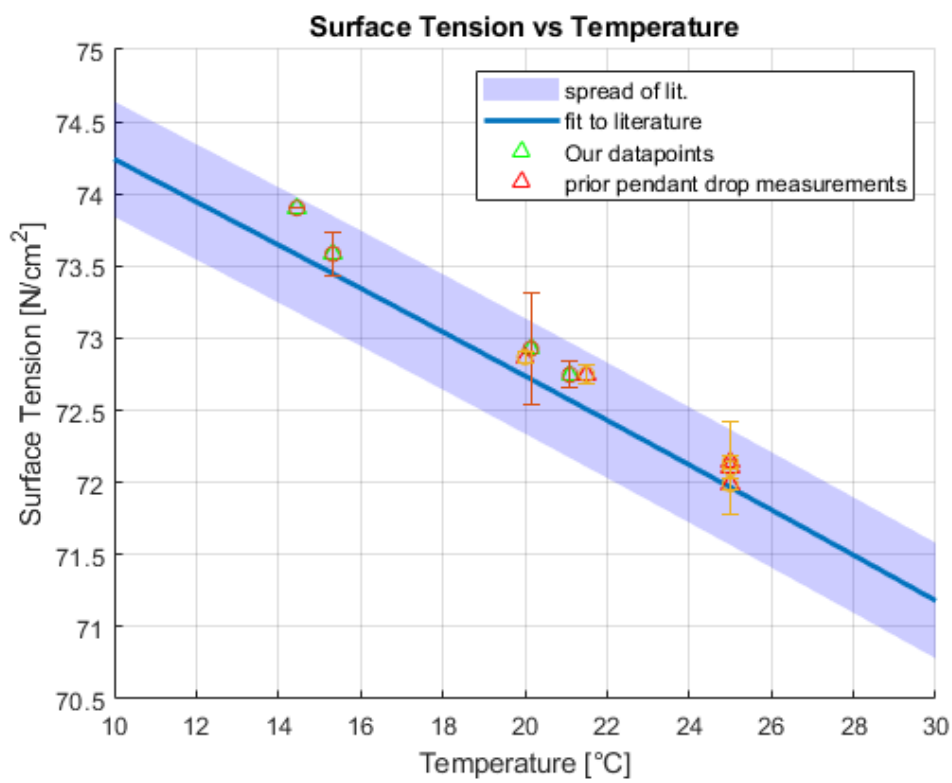


Figure 5.2.57

## 6 Summary and Outlook

The surface tension of water is not only an important property for many scientific fields but also in nature. However there are still unanswered questions surrounding it and the exact value while being measured many times in the literature has a rather large statistical spread to it. This is likely due to differences in experimental conditions between all the ambient pressure studies. This includes differing levels of contamination via differing gas phase compositions. That is why we have built an instrument to attempt to measure the surface tension of water without the effects of other gas phase species or contaminants, not only as accurately as possible but for a broad temperature range. To achieve this we designed a custom UHV chamber that has a cold finger attached to it. On the cold finger tip we control the temperature with a combination of cooling using liquid nitrogen and heating using two specially designed heater elements. This allows us to grow a pure water drop in its own pure vapour before taking a picture using a back illuminator and a telecentric lens. From this picture we can fit the drop's Bond number, a dimensionless property that describes the drop's shape from which we can directly calculate the surface tension. With this approach of having as accurate temperature control as possible and as low contamination levels as possible we hope to add valuable data to many ongoing discussions within water interfacial science. For example, discussions concerning the contact angle measurements of water on various surfaces and the fundamental causes of the Jones-Ray-Effect.

In this thesis we discussed not only the theory behind the thermodynamics of a surface and how we are able to measure surface tension but also described the experimental setups design, how it was built and how our experiments are executed in detail. We were able to grow and fit some first drops. Though, there were some teething problems. Notably, the temperature control of the tip was not ideal due to poor thermal contact inside parts of the cold finger. This did not stop large, maximal volume drops from being created, however, and the first surface tension measurements of water in its pure-vapour were undertaken. While in literature water in ambient conditions is assumed to be pristine this might not be true. We find that water in its pure-vapour has a higher surface tension than one would expect from the available literature. This is even true if one compares the results specifically with other pendant drop experiments. When discussing the Jones-Ray effect or contact angle measurements contamination of interfaces by species found in the experiments ambient have to be considered.

For the future more experiments are planned. We included a leak valve to be able to reintroduce contaminants in a controlled manner to explore more details about the mentioned Jones-Ray effect. We are also equipped with everything we need to do contact angle measurements in this ultra pure environment. Additionally our precise control of all parameters will allow us to experiment on super cooled water. Also some upgrades of the system are planned. Most notably the tip itself currently is made of LN316 Stainless steel. Tests showed that contact of the water with this material causes contamination an order of magnitude higher than contact to sapphire would, so exchanging the tip in favour of sapphire is planned. Also the cold finger tip's shape is in revision. We discovered that the drop grows by condensing water on its bottom like planned but as soon as

some water collected there the condensation shifts to the tips sidewalls. From there the smaller droplets have to pass an edge to enter the main drop which oftentimes does not happen until the small droplets grew big enough to fall off entirely and take the main drop with them. While it is possible to grow drops currently rounding that edge could improve the performance significantly.

While this thesis is motivated by the Ray-Jones-Effect at this point in time we are not ready to claim any discovery in that direction. However we do claim to successfully designed and build a system that is capable of executing precise measurements on ultra pure water in its pure vapour.

## References

- [1] Emerson Y. Arashiro and Nicole R. Demarquette. Use of the pendant drop method to measure interfacial tension between molten polymers. *Materials Research*, page 23–32, 1999.
- [2] Jan Balajka, Jiri Pavelec, Mojmir Komora, Michael Schmid, and Ulrike Diebold. Apparatus for dosing liquid water in ultrahigh vacuum. *Review of Scientific Instruments*, 89(8):083906, 08 2018.
- [3] Joseph D. Berry, Michael J. Neeson, Raymond R. Dagastine, Derek Y.C. Chan, and Rico F. Tabor. Measurement of surface and interfacial tension using pendant drop tensiometry. *Journal of Colloid and Interface Science*, 454:226–237, 2015.
- [4] P. Cheng, D. Li, L. Boruvka, Y. Rotenberg, and A.W. Neumann. Automation of axisymmetric drop shape analysis for measurements of interfacial tensions and contact angles. *Colloids and Surfaces*, 43(2):151–167, 1990. Selected Papers from a Symposium on Recent Progress in Interfacial Tensiometry, held at the Third Chemical Congress of North America.
- [5] Mark Denny. Tree hydraulics: how sap rises. *European Journal of Physics*, 33(1):43, oct 2011.
- [6] Jaroslaw Drelich, Ch Fang, and Calvin White. Measurement of interfacial tension in liquid-liquid systems. *Encyclopedia of Surface and Colloid Science*, pages 3152–3166, 2002.
- [7] N. H. Fletcher. *The Physics of Rainclouds*. Cambridge University Press, 1966.
- [8] F. Gonçalves, A. Trindade, C. Costa, J. Bernardo, I. Johnson, I. Fonseca, and A. Ferreira. Pvt, viscosity, and surface tension of ethanol: New measurements and literature data evaluation. *The Journal of Chemical Thermodynamics*, pages 1039–1049, 2010.
- [9] Bing He, Sucui Yang, Zhangrong Qin, Binghai Wen, and Chaoying Zhang. The roles of wettability and surface tension in droplet formation during inkjet printing. *Scientific Reports*, 7, 09 2017.

- [10] Thorfin R. Hogness. The surface tensions and densities of liquid mercury, cadmium, zinc, lead, tin and bismuth. *J. Am. Chem. Soc.*, pages 1621–1628, 1921.
- [11] James W Jennings Jr and NR Pallas. An efficient method for the determination of interfacial tensions from drop profiles. *Langmuir*, 4(4):959–967, 1988.
- [12] T. Klein, S. Yan, J. Cui, J. Magee, K. Kroenlein, M. Rausch, T. Koller, and A. Froeba. Liquid viscosity and surface tension of n-hexane, n-octane, n-decane, and n-hexadecane up to 573k by surface light scattering. *J. Chem. Eng.*, pages 4116–4131, 2019.
- [13] M. Krenko and TRantisek. Measurement of interfacial tension in liquid-liquid high-temperature systems. *J CHEM ENG DATA*, 55, 2010.
- [14] Z Li, Y Wang, A Kozbial, G Shenoy, and F Zhou. Effect of airborne contaminants on the wettability of supported graphene and graphite. *Nat. Mater.*, pages 925–931, 2013.
- [15] Philip E. Mason, Frank Uhlig, Vaclav Vanek, Tillmann Buttersack, Sigurd Bauerecker, and Pavel Jungwirth. Coulombg explosion during the early stages of the reaction of alkali metal with water. *NCHEM*, pages 250–254, 2015.
- [16] R Massoudi and AD King Jr. Effect of pressure on the surface tension of water. adsorption of low molecular weight gases on water at 25. deg. *The Journal of Physical Chemistry*, 78(22):2262–2266, 1974.
- [17] Halil I. Okur, Chad I. Drexler, Eric Tyrode, Paul S. Cremer, and Sylvie Roke. The jones–ray effect is not caused by surface-active impurities. *The Journal of Physical Chemistry Letters*, 9(23):6739–6743, 2018. PMID: 30398354.
- [18] Lars Onsager and Nicholas N. T. Samaras. The surface tension of debye-hückel electrolytes. *The Journal of Chemical Physics*, 2(8):528–536, 08 1934.
- [19] N.R. Pallas and Y. Harrison. An automated drop shape apparatus and the surface tension of pure water. *Colloids and Surfaces*, 43(2):169–194, 1990. Selected Papers from a Symposium on Recent Progress in Interfacial Tensiometry, held at the Third Chemical Congress of North America.
- [20] Jaroslav Pátek, Monika Součková, and Jaroslav Klomfar. Generation of recommendable values for the surface tension of water using a nonparametric regression. *Journal of Chemical & Engineering Data*, 61, 02 2016.
- [21] J. S. Rowlinson. *Molecular Theory of Capillarity*. Dover Publications, 1982.
- [22] A. C. Oates S. R. Naganthan, M. Popovic. Left-right symmetry of zebrafish embryos requires somite surface tension. *Nature*, pages 516–521, 2022.
- [23] A. Semmler, R. Ferstl, and H. Kohler. New laser technique for automatic interfacial tension measurements: Laser scanning drop shape analysis (lasda). *Langmuir*, 12:4165–4172, 1996.

- [24] Yuki Uematsu, Douwe Jan Bonthuis, and Roland R. Netz. Impurity effects at hydrophobic surfaces. *Current Opinion in Electrochemistry*, 13:166–173, 2019.
- [25] Álvarez Valenzuela, JA Díaz García, and JL Pérez Díaz. Análisis de la sensibilidad a las vibraciones del método de medición de tensión superficial mediante gota suspendida. *Revista mexicana de física*, 56(4):334–338, 2010.
- [26] N. B. Vargaftik, B. N. Volkov, and L. D. Voljak. International tables of the surface tension of water. *Journal of Physical and Chemical Reference Data*, 12(3):817–820, 07 1983.
- [27] M. Watanabe and S. Nayar. *Telecentric optics for computational vision*. Springer Berlin Heidelberg, 1996.
- [28] D. Phil Woodruff. *Introduction and General Background Concepts*, page 1–34. Cambridge University Press, 2016.

## 7 Appendix

### 7.1 Diode Calibration Data

Setpoint [°C]	Reference [°C]	Test [°C]	Difference [°C]	Test Voltage [V]
-50	-46.070	-45.956	0.113	0.724
-40	-37.202	-37.113	0.089	0.705
-30	-27.962	-27.840	0.121	0.684
-20	-18.568	-18.456	0.112	0.663
-15	-13.831	-13.708	0.124	0.652
-10	-9.055	-8.934	0.121	0.641
-5	-4.273	-4.147	0.126	0.631
0	0.498	0.631	0.133	0.620
5	5.330	5.484	0.154	0.609
10	10.219	10.372	0.153	0.597
15	15.124	15.276	0.152	0.586
17.5	17.545	17.685	0.140	0.581
20	20.013	20.160	0.146	0.575
22.5	22.476	22.638	0.162	0.569
25	24.942	25.120	0.178	0.564
30	29.880	30.048	0.168	0.552
40	39.722	39.901	0.179	0.529
50	49.565	49.771	0.206	0.507
60	59.410	59.634	0.223	0.484
70	69.261	69.551	0.291	0.460

**Table 8:** Data acquired during the calibrating measurement with the diodes D6105593(Reference) and D6107256(Test). Set point is the temperature the Lauda chiller was set to. Reference is the temperature measured with the calibrated diode with each value being an average over 300 measurements. Test refers to the temperature measured with the uncalibrated diode with each value being an average of 300 measurements. Difference shows the average of the difference between the 2 and the value shown is created as an average of 300 difference values. Test Voltage is a single value interpolated using the diodes standard curve from the Test Temperature value and will be used to create the costum curve for the tested diode.

Setpoint [°C]	Reference [°C]	Test [°C]	Difference [°C]	Test Voltage [V]
70	69.305	69.402	0.097	0.461
60	59.483	59.525	0.042	0.484
50	49.646	49.678	0.032	0.507
40	39.794	39.804	0.0102	0.530
30	29.929	29.934	0.005	0.553
25	24.931	24.945	0.013	0.564
22.5	22.477	22.479	0.001	0.570
20	20.022	20.010	-0.012	0.575
17.5	17.570	17.554	-0.016	0.581
15	15.115	15.103	-0.012	0.587
10	10.229	10.226	-0.003	0.598
5	5.368	5.369	0.001	0.609
0	0.510	0.494	-0.016	0.620
-5	-4.345	-4.362	-0.017	0.631
-10	-9.176	-9.193	-0.017	0.642
-15	-13.942	-13.952	-0.010	0.653
-20	-18.687	-18.704	-0.017	0.663
-30	-28.066	-28.066	-0.001	0.685
-40	-37.279	-37.307	-0.029	0.705
-50	-46.170	-46.175	-0.005	0.725

**Table 9:** Data acquired during the calibrating measurement with the diodes D6105593(Reference) and D6107259(Test). Set point is the temperature the Lauda chiller was set to. Reference is the temperature measured with the calibrated diode with each value being an average over 300 measurements. Test refers to the temperature measured with the uncalibrated diode with each value being an average of 300 measurements. Difference shows the average of the difference between the 2 and the value shown is created as an average of 300 difference values. Test Voltage is a single value interpolated using the diodes standard curve from the Test Temperature value and will be used to create the costum curve for the tested diode..

Setpoint [°C]	Reference [°C]	Test [°C]	Difference [°C]	Test Voltage [V]
-50	-46.39	-46.713	-0.318	0.726
-40	-37.347	-37.693	-0.346	0.706
-30	-28.056	-28.393	-0.337	0.685
-20	-18.641	-19.006	-0.366	0.664
-15	-13.897	-14.264	-0.367	0.653
-10	-9.112	-9.488	-0.376	0.643
-5	-4.324	-4.705	-0.381	0.632
0	0.469	0.082	-0.388	0.621
5	5.298	4.920	-0.378	0.610
10	10.169	9.785	-0.384	0.599
15	15.068	14.658	-0.410	0.588
17.5	17.509	17.092	-0.418	0.582
20	20.005	19.588	-0.417	0.576
22.5	22.471	22.063	-0.408	0.571
25	24.937	24.538	-0.399	0.565
30	29.874	29.457	-0.417	0.554
40	39.732	39.299	-0.433	0.531
50	49.590	49.158	-0.432	0.508
60	59.451	59.002	-0.449	0.485
70	69.296	68.869	-0.427	0.462

**Table 10:** Data acquired during the calibrating measurement with the diodes D6105593(Reference) and D6107924(Test). Set point is the temperature the Lauda chiller was set to. Reference is the temperature measured with the calibrated diode with each value being and average over 300 measurements. Test refers to the temperature measured with the uncalibrated diode with each value being an average of 300 measurements. Difference shows the average of the difference between the 2 and the value shown is created as an average of 300 difference values. Test Voltage is a single value interpolated using the diodes standard curve from the Test Temperature value and will be used to create the costum curve for the tested diode.

## 7.2 Diode Costume Curve Data

Set Point [°C]	Reference [°C]	Test Voltage [V]
70	69.261	0.4605
60	59.410	0.4836
50	49.565	0.5066
40	39.722	0.5295
30	29.880	0.5523
25	24.942	0.5637
22.5	22.476	0.5693
20	20.013	0.5750
17.5	17.545	0.5807
15	15.124	0.5862
10	10.219	0.5975
5	5.330	0.6087
0	0.498	0.6197
-5	-4.273	0.6305
-10	-9.055	0.6414
-15	-13.831	0.6522
-20	-18.568	0.6629
-30	-27.962	0.6840
-40	-37.202	0.7046
-50	-46.070	0.7243

**Table 11:** Data from the first calibration. The Reference Temperature is an average over 300 measurements and the Test Voltage a value corresponding to an average of 300 measurements with the Test diode. Serial numbers D6105593 and D6107256.

Set Point [°C]	Reference [°C]	Test Voltage [V]
70	69.305	0.4608
60	59.483	0.4839
50	49.646	0.5068
40	39.794	0.5297
30	29.929	0.5525
25	24.931	0.5641
22.5	22.477	0.5697
20	20.022	0.5754
17.5	17.570	0.5810
15	15.115	0.5866
10	10.229	0.5978
5	5.368	0.6089
0	0.510	0.6200
-5	-4.345	0.6310
-10	-9.176	0.6420
-15	-13.942	0.6528
-20	-18.687	0.6635
-30	-28.066	0.6845
-40	-37.279	0.7051
-50	-46.170	0.7248

**Table 12:** Data from the second calibration. The Reference Temperature is an average over 300 measurements and the Test Voltage a value corresponding to an average of 300 measurements with the Test diode. Serial numbers D6105593 and D6107259.

Set Point [°C]	Reference [°C]	Test Voltage [V]
70	69.296	0.4621
60	59.451	0.4851
50	49.590	0.5080
40	39.732	0.5309
30	29.874	0.5536
25	24.937	0.5650
22.5	22.471	0.5707
20	20.005	0.5763
17.5	17.509	0.5821
15	15.068	0.5877
10	10.169	0.5988
5	5.298	0.6100
0	0.469	0.6209
-5	-4.324	0.6318
-10	-9.112	0.6427
-15	-13.897	0.6535
-20	-18.641	0.6641
-30	-28.056	0.6852
-40	-37.347	0.7059
-50	-46.395	0.7259

**Table 13:** Data from the third calibration. The Reference Temperature is an average over 300 measurements and the Test Voltage a value corresponding to an average of 300 measurements with the Test diode. Serial numbers D6105593 and D6107924.

### 7.3 Disolution Measurement

The goal of this experiment was to investigate the rate at which different materials contaminate water due to corrosion during direct contact. For this we placed samples of 4 different materials (LN316 stainless steel, Oxidized LN316 stainless steel, copper, sapphire and a control container without sample) inside containers with ultra pure water (MilliQ) and took water samples after set periods of time. The water was degased with nitrogen for half an hour before the experiment and after each water sample was taken to reduce the influence of contaminants from air. The water samples were taken after 24 h and 218 h with the leftover being analysed after 240 h. The results very clearly showed that copper reacted very strongly with water. This was expected and verified our decision to use gold plated gaskets on the experimental chamber. Between LN316 and Sapphire there was a difference of about one order of magnitude in contamination levels with oxidized LN316 in between the two. The biggest contributor in the case of both kinds of stainless steel was ferrite which was the primary cause of the big difference to sapphire. Figure 7.3.59 shows the biggest contributor of each material sample. All values are adjusted according to the control water sample.



**Figure 7.3.58:** This figure shows the 4 material samples after the experiments.

In conclusion the decision to use gold plated gaskets for the experimental chamber is justified. However the main motivation of the experiment was to estimate the contamina-

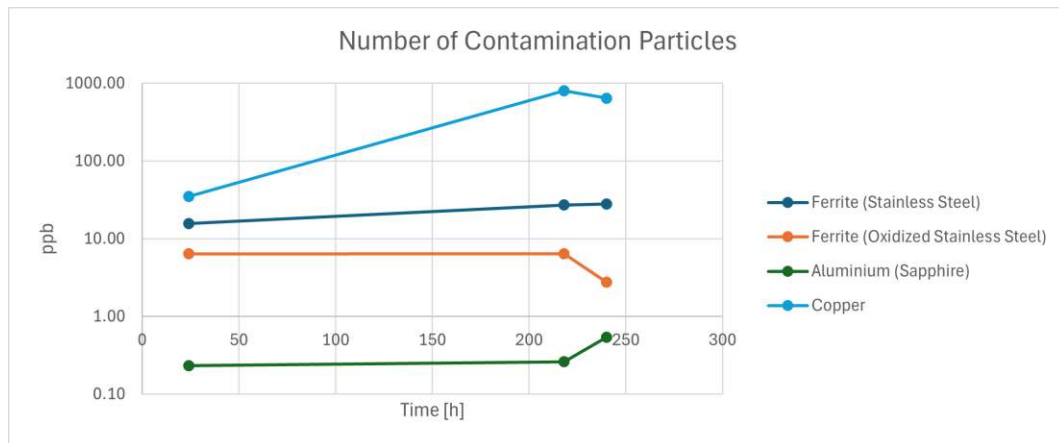


**Figure 7.3.59:** This graph shows the biggest contamination contributor from each of the samples. Copper causes the biggest amounts which verifies the decision to use gold plated gaskets in the experimental chamber. Blank LN316 stainless steel introduces less particles but this can be improved by an oxidation layer that protects the surface as was the case for the oxidized LN316. Sapphire however showed the best results. The error for each material due to the calibration of the device used for measuring is  $\pm 8$  ppb for Ferrite,  $\pm 4$  ppb for Copper and  $\pm 10$  ppb for Aluminum. The last data point of the Copper and oxidized stainless steel series show a drop. This likely comes from cross contamination of the control water sample via the degassing tube since all values are adjusted according to the contamination levels of the control sample.

tion of the water drop due to contact with the cold finger tip. We found that a protective oxidative layer improves the results compared to blank stainless steel. In the current version of the system the cold finger material is somewhere in between the 2 material samples from this study. The oxidized sample was treated with heat to form the layer while the blank was freshly cut. Our cold finger tip was not heated but cleaned and left in air so that a certain oxidative process could occur naturally over time. For the future a sapphire tip is planned to further improve the system towards as little contamination as possible.